Université Mohamed Khider – Biskra

Faculté des Sciences et de la Technologie

Département : Génie Electrique

Ref :………….……

جامعة محمد خيضر بسكرة
كلية العلوم و التكنولوجيا
قسم: الهندسة الكهربائية
المرجع:...............

جامعة محمد خيضر بسكرة

Thesis is submitted for the fulfillment of
the degree of
Doctorate in LMD

Option : **Control of electrical systems**
Thesis has been prepared in the Electrical Engineering Laboratory of Biskra LGEB

Contribution to the Control of Doubly Fed Induction Machine DFIM

Presented by :

Mohammed Saci Chabani

The public thesis defense on : 13/ 07/ 2022

Board of Examiners

Dr. SRAIRI Kamel	**Professor**	**Chairman**	**University of Biskra**
Dr. BENCHOUIA. M^{ed}. Toufik	**Professor**	**Supervisor**	**University of Biskra**
Dr. GOLEA Amar	**Professor**	**Co-supervisor**	**University of Biskra**
Dr. ZIDANI Fatiha	**Professor**	**Examiner**	**University of Batna 2**
Dr. BETKA Achour	**Professor**	**Examiner**	**University of Biskra**

Acknowledgements

Acknowledgements

Abstract

Abstract

Currently, doubly fed induction generators (DFIGs) are widely used for wind turbines. Compared to other variable-speed generators; the main advantage of the DFIG is that the power electronic devices must deal with only about a third of the generator power, compared to full power converters used in synchronous generators . This difference reduces the costs and losses in the power electronic components, rather than other solutions, such as fully converting systems; finally, the overall efficiency is improved. Furthermore, among all the induction generator configurations for generation systems the use of (DFIG) configuration with back to back pulse width modulated voltage source converters (VSC) is one of the best topologies available and it is suitable for both grid connected systems as well as standalone systems. Here only stand-alone application of DFIG is considered. In this thesis, mathematical modelling of doubly fed induction machine is presented. Two control approaches are proposed to improve the control of the rotor side converter which give the best solution to overcome the drawbacks of the recent control methods and provide a high performance stator- voltage magnitude and frequency regulation for all possible operation scenarios (voltage magnitude, load, and rotor speed variations). Various aspects of standalone DFIG generation system such as stator-voltage magnitude and frequency regulation, computational requirement minimization, sensors number reduction, from rotor side converter control is carried out. All proposed control methods have been verified in both simulation and 3 kW DFIG laboratory experimental bench.

Keywords – Standalone doubly fed induction generator (DFIG), stator-voltage magnitude and frequency, Rotor side converter (RSC), Hysteresis current control (HCC), FS-PCC Finite state predictive current control, Direct rotor flux vector control DRFVC, Direct torque control DTC.

Résume

Actuellement, les générateurs à induction à double alimentation **(DFIG)** sont largement utilisés pour les éoliennes. Comparé à d'autres générateurs à vitesse variable ; le principal avantage du **DFIG** est que les dispositifs électroniques de puissance ne doivent traiter qu'environ un tiers de la puissance du générateur, par rapport aux convertisseurs à pleine puissance utilisés dans les générateurs synchrones. Cette différence réduit les coûts et les pertes dans les composants électroniques de puissance, plutôt que d'autres solutions, telles que les systèmes entièrement convertisseurs ; enfin, l'efficacité globale est améliorée. De plus, parmi toutes les configurations de générateurs à induction pour les systèmes de génération, l'utilisation de la configuration **(DFIG)** avec des convertisseurs de source de tension à modulation de largeur d'impulsion **(VSC)** dos à dos est l'une des meilleures topologies disponibles et convient à la fois aux systèmes connectés au réseau ainsi qu'aux systèmes autonomes. Ici, seule l'application autonome de **DFIG** est considérée. Dans cette thèse, la modélisation mathématique d'une machine à induction à double alimentation est présentée. Deux approches de contrôle sont proposées pour améliorer le contrôle du convertisseur côté rotor qui offrent la meilleure solution pour surmonter les inconvénients des méthodes de contrôle récentes et fournir une régulation de fréquence et d'amplitude de tension stator haute performance pour tous les scénarios de fonctionnement possibles (amplitude de tension, charge ; et variations de vitesse du rotor). Divers aspects du système de génération **DFIG** autonome, tels que la régulation de l'amplitude et de la fréquence de la tension du stator, la minimisation des besoins de calcul, la réduction du nombre de capteurs, à partir du contrôle du convertisseur côté rotor sont effectués. Toutes les méthodes de contrôle proposées ont été vérifiées à la fois en simulation et sur le banc expérimental du laboratoire **DFIG** de **3 kW**.

Mots-clés - Générateur d'induction autonome à double alimentation (**DFIG**), amplitude et fréquence de la tension du stator, convertisseur côté rotor (**RSC**), contrôle du courant d'hystérésis (**HCC**), contrôle du courant prédictif à l'état fini **FS-PCC**, contrôle vectoriel du flux du rotor direct **DRFVC**, couple direct contrôle **DTC**.

ملخص

حاليًا ، تُستخدم مولدات الحث ذات التغذية المزدوجة (**DFIGs**) على نطاق واسع لتوربينات الرياح. مقارنة بالمولدات الأخرى متغيرة السرعة؛ الميزة الرئيسية لـ **DFIG** هي أن الأجهزة الإلكترونية الكهربائية يجب أن تتعامل فقط مع حوالي ثلث طاقة المولد ، مقارنة بمحولات الطاقة الكاملة المستخدمة في المولدات المتزامنة. يقلل هذا الاختلاف من التكاليف والخسائر في مكونات الطاقة الإلكترونية، بدلاً من الحلول الأخرى، مثل أنظمة التحويل الكامل. أخيرًا، تم تحسين الكفاءة الإجمالية. علاوة على ذلك ، من بين جميع تكوينات المولدات الحثية لأنظمة التوليد ، يعد استخدام التكوين (**DFIG**) مع محولات مصدر الجهد المعدل بعرض النبضة المتتالية (**VSC**) أحد أفضل الهياكل المتاحة وهو مناسب لكل من الأنظمة المتصلة بالشبكة وكذلك أنظمة قائمة بذاتها. هنا يتم النظر فقط في التطبيق المستقل لـ **DFIG**. في هذه الأطروحة ، يتم تقديم النمذجة الرياضية لآلة الحث ذات التغذية المزدوجة. تم اقتراح طريقتين للتحكم لتحسين التحكم في المحول الجانبي الدوار مما يوفر أفضل حل للتغلب على عيوب طرق التحكم الحديثة ويوفران قدرًا عاليًا من الجهد الثابت والجهد وتنظيم التردد لجميع سيناريوهات التشغيل الممكنة (مقدار الجهد والحمل ، واختلافات سرعة الدوار .(يتم تنفيذ جوانب مختلفة من نظام توليد **DFIG** المستقل مثل حجم الجهد الثابت وتنظيم التردد ، وتقليل المتطلبات الحسابية ، وتقليل عدد أجهزة الاستشعار ، من التحكم في محول الجانب الدوار. تم التحقق من جميع طرق التحكم المقترحة في كل من المحاكاة و 3 كيلوواط من مقاعد المختبر التجريبية **DFIG** .

الكلمات المفتاحية ـ مولد الحث المستقل ذو التغذية المزدوجة (**DFIG**) ، محول الجانب الدوار ، حجم وتردد الجهد الثابت ، التحكم في التيار التنبئي بالحالة المحدودة ، التحكم المباشر في **FS-PCC** ، (**HCC**) ، التحكم في تيار التخلف (**RSC**) الدوار   التدفق   **DRFVC** التحكم   المباشر   الدوران   عزم   ، DTC

Table of Contents

Table of Contents

Chapter 3: Improved RSC of standalone DFIG: Approach-1.

Chapitre 4: Improved RSC of standalone DFIG: Approach-2.

List of figures

List of figures

General Introduction

Chapter 1

Chapter 2

Chapter 3

List of tables

List of tables

Nomenclature

Nomenclature

List of symbols

X^* : Reference value.

$\widehat{X}$: Estimated value.

$|X|$: Magnitude value.

R_s, R_r : [Ω] Stator and rotor resistance.

L_s, L_r : [H] Stator and rotor inductance.

L_m : [H] Magnetizing inductance.

L_{ls} : [H] Stator leakage inductance.

L_{lr} : [H] Rotor leakage inductance

$\vec{\psi}_s$: Stator flux vector

$\vec{\psi}_r$: Rotor flux vector

$\vec{v}_r, \vec{v}_s$: Stator and rotor voltage vector.

p : number of pole pairs.

Ω : [rad/s] vitesse mécanique.

$\omega_m = p\Omega$: [rad/s] Rotor angular speed (rad/s).

ω_r : [rad/s] slip speed.

ω_s : [rad/s] Synchronous speed (rad/s).

$\sigma = 1 - \frac{L_m^2}{L_s L_r}$: Coefficient de dispersion ou de Blondel.

T_e : [N.m] Electromagnetic torque.

f_s, f_r : [Hz] Stator and rotor frequency.

δ : Angle between the rotor and stator flux linkage vector, rad or degree

List of Abbreviations

DFIG: Doubly Fed Induction Generator

RSC: Rotor Side Converter

PLL: Phase locked loop

PI: proportional and integral.

PWM: Pulse Width Modulation.

SVM: Space Vector Modulation.

FOC: Field Oriented Control.

HCC: Hysteresis Current control.

FS-PCC: Finite State Predictive Current Control.

DRFVC: Direct Rotor Flux Vector Control.

DTC: Direct Torque Control.

General introduction

General introduction

Energy is the most essential factor in the social and economic growth of the modern world. The environmental hazards and the scarcity of the nonrenewable source of energy has created a global concern on the existing energy sources. The lack long term replacement for the fossil fuels has enriched the interest in the renewable energy sources. For about two decades, two trends in power systems have been observed: a rapid increase in the use of renewable energy sources and distributed generation of electrical energy. They are caused by both ecological concerns and increasing costs of fossil fuels (in the long-termperspective). The wind energy is one the most favorable long-term solution for the energy concern over the fossil fuel. The concern The wind energy is one of the most competitive and viable energy sources due to several advancement in the wind turbine system [16]. The review paper [17], historical development of the wind energy is presented. In [18] the current scenario of the wind energy in the world, and the advancement in the wind turbine design is discussed. The inclusion of the wind power in the grid increases the fluctuation and randomness in the power. The high penetration of the wind farm can lead to the power system oscillation [19].

Synchronous generators under fixed-speed conditions produce constant-frequency voltage, which is why they are used as main generators in power grid systems. Squirrel-cage induction generators are sometimes used in medium-power generation units due to their simple and robust construction and no need of precise synchronization. They are used, for example, in small hydropower plants as fixed-speed uncontrolled generators. They are also installed in wind farms, which use either turbine mechanical characteristic or pitch control in order to maintain rotor speed close to grid synchronous pulsation and to keep the generator in the stable part of its mechanical characteristic. Unfortunately, this topology does not allow to obtain maximal available power from the wind turbine under low-speed wind, because rotor speed depends on grid frequency. On the contrary, variable-speed wind-driven generators are able to adjust their rotor speed to wind conditions, thus they show superior power conversion efficiency. It has been described in many publications (e.g. [1,40]) that variable-speed generators increase efficiency of wind energy conversion systems in relation to fixed-speed solutions. Maximum Power Point Tracking MPPT algorithms [51,115] allow to harvest more wind energy using a variable-speed generator. Besides wind energy conversion systems, variable-

speed generators show their advantages in combustion engine (mostly diesel) generation systems, popularly used in mobile generators and as uninterrupted power sources. Although diesel generators can operate with a fixed speed, their variable-speed operation reduces engine fuel consumption significantly, as shown in [56]. The worldwide scale of combustion engines utilization in electrical power generation implies that development of variable-speed generators can considerably reduce fuel consumption. Wind-diesel hybrid generator systems [69,75] use the advantages of these two different energy sources and mitigate their drawbacks as well. The diesel engine provides controllable power supply, whereas the wind turbine reduces fuel consumption of the power system thanks to wind energy. Thus, these hybrid systems can be used in remote and isolated areas, where a controllable energy source is necessary, and at the same time, fuel prices may be high due to logistic costs.

Distributed generation and use of renewable energy sources are complementary trends observed in power generation, which fulfil the idea of sustainable economy. Most renewable energy sources (apart from hydropower) are distributed over large areas, therefore in order to use them, a new model of power grid is required – Smart Grid [71]. Distributed generation significantly decreases transmission losses, which has an indirect impact on fuel consumption and pollution of the environment. Unfortunately, renewable energy sources are unpredictable and uncontrollable. Still, achievements of electrical engineering allow to connect smaller power grids and to stabilize power balance in the grid. Firstly, power electronic interfaces between generators and the grid make it possible to join micropower systems in a common grid [15,23]. Moreover, they enable to control loading of energy sources, which leads to a higher efficiency of energy conversion. Secondly, unpredictable instantaneous power of renewable resources entails the use of energy storage devices in order to stabilize the power system dominated by renewable sources. Many different energy storage devices are used to balance power in microgrids: supercapacitors [7], chemical cells [70], flywheels [26]. Hybrid systems are also used, joining benefits of supercapacitors (high charging and discharging current, number of charging cycles in their lifetime) and energy density of Li-on batteries [68]. A power system designer has to answer the question whether energy storage is economical, based on the knowledge about historical energy prices and power demand [14].

The basic topology of a variable-speed generator is a series connection of either a synchronous generator SG or a squirrel-cage induction generator SCIG, and a power electronic converter (usually in the back-to-back topology), which is depicted in Fig. 1.1. In this topology, the converter has the rated power equal to the generator power, which significantly increases overall costs of the series generator system. This is an expensive topology, but it has an important advantage - separation of the

generator from grid faults and distortions, which would affect the generator unit. Moreover, the generator shaft speed can be adjusted to the loading conditions in a wide operation range.
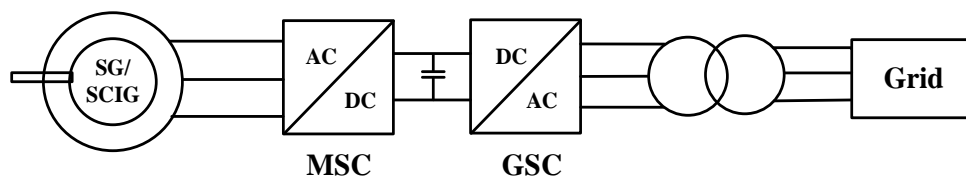
Fig. 1. Series topology of the grid-connected generator.

Due to high costs of power converters in medium- and high-power ranges, and also mechanical characteristics of wind turbines (i.e. turbine torque depends on the square of its speed), another generator topology has been developed based on the wound rotor induction machine - called Doubly Fed Induction Generator DFIG – which is depicted schematically in Fig. 1.2. DFIG is directly connected to the grid from its stator side, but it can operate with a variable speed due to the AC/DC/AC power converter connected to the rotor, which allows to control the active and reactive powers of the machine. The power converter transfers only slip power, which is a fraction of the total generator power (up to 25% of the total power in most wind applications) assuming generator operation close to synchronous speed (easily met in wind, hydro and combustion engine applications). On the other hand, due to lack of an electrical interface between the stator and the grid, the generator is not isolated from grid faults. Therefore, the Low-Voltage Ride-Through is recently one of the biggest research topics concerning DFIG systems.
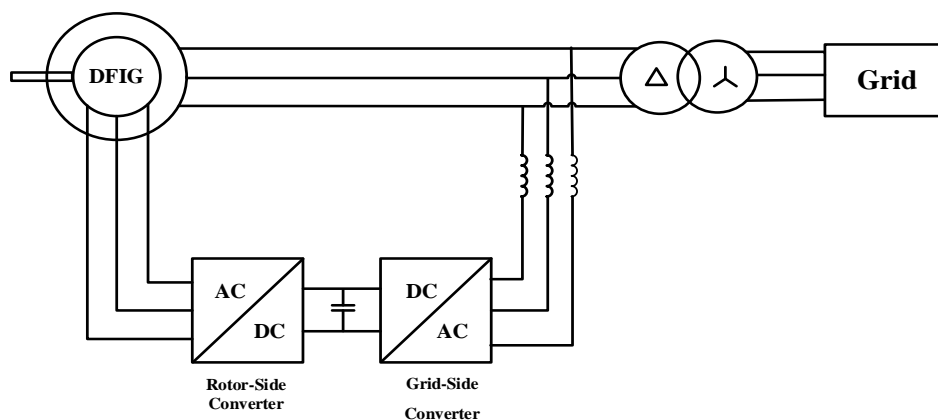
Fig. 2. Parallel topology of the grid-connected generator.

Although grid-connected wind farms are the main application of DFIG, its stand-alone operation also has a wide range of applications. Isolated microgrids in rural areas, high power

uninterruptable power sources, mobile diesel generators, heavy vehicles, ship power systems are only a few possible applications of the stand-alone DFIG, in which reduced costs of the DFIG topology can be of great interest. Topology of the stand-alone DFIG is presented in Fig. 3. The stand-alone DFIG has to provide high-quality voltage even under non-linear and unbalanced loads, the penetration of which in microgrids can be significantly higher than in national power grids. Therefore, active compensation of at least the 5_{th} and 7_{th} harmonics is a necessity in microgrids. Current harmonics compensation should be also realized in such a way that the electromagnetic torque contains as little as possible of high frequency components (ripples) in order not to cause accelerated tear and wear of mechanical components.
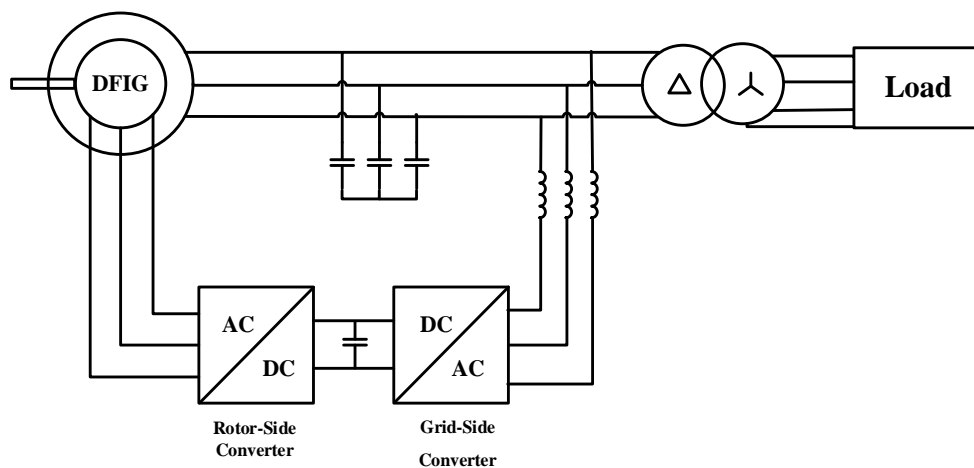
Fig. 3. Parallel topology of the stand-alone generator.

Generator operation without any mechanical sensors is very interesting, due to encoder susceptibility to vibrations. Moreover, using low-cost low-precision encoders often results in worse system performance than under estimated rotor position and speed.

Wind turbine (WT) production has grown in size from some kW to the multi MW power range in last three decades. Since 1990's some manufacturers have replaced in the wind turbine design the asynchronous generator by the synchronous one, while others have introduced the doubly-fed induction machine (DFIM). In this development the pitch control concept, advanced power electronics equipment and control under variable speed have been introduced [28]. Multi MW wind turbines rotates at 10-15 rpm. Hence, a gear-box and a standard fixed speed generator or a multi-pole generator are the possible solutions [37]. A technological roadmap of possible technical solutions for wind turbines is depicted in Fig .4. Taking into account this roadmap, the most common turbine designs can be summarized in four wind turbine schemes:

- **Fixed speed wind turbines:** This scheme is based on a squirrel cage induction machine which is directly connected to the grid. Then, it needs a capacitor bank for reactive power compensation [37], [6]. This scheme is manufactured by NEG Micon, Bonus and Nordex [28].

- **Partial variable speed wind turbine with variable rotor resistance:** This configuration manufactured by Vestas and known as OptiSlip uses a DFIM connected directly to the grid. External resistors are connected to the rotor to control the slip an the power output [37].

- **Variable speed WT with partial-scale frequency converter:** This concept, corresponds to a variable speed DFIM which stator is directly connected to the grid, while a partial-scale power converter (approx. 30% of nominal power) controls the rotor frequency and mechanical speed [37]. The motivation of this concept is a variable speed in a wide range compared with OptiSlip and less expensive compared with full power converter. It is manufactured by Vestas, Gamesa, Enron Wind, Nordex and Dewind [28].
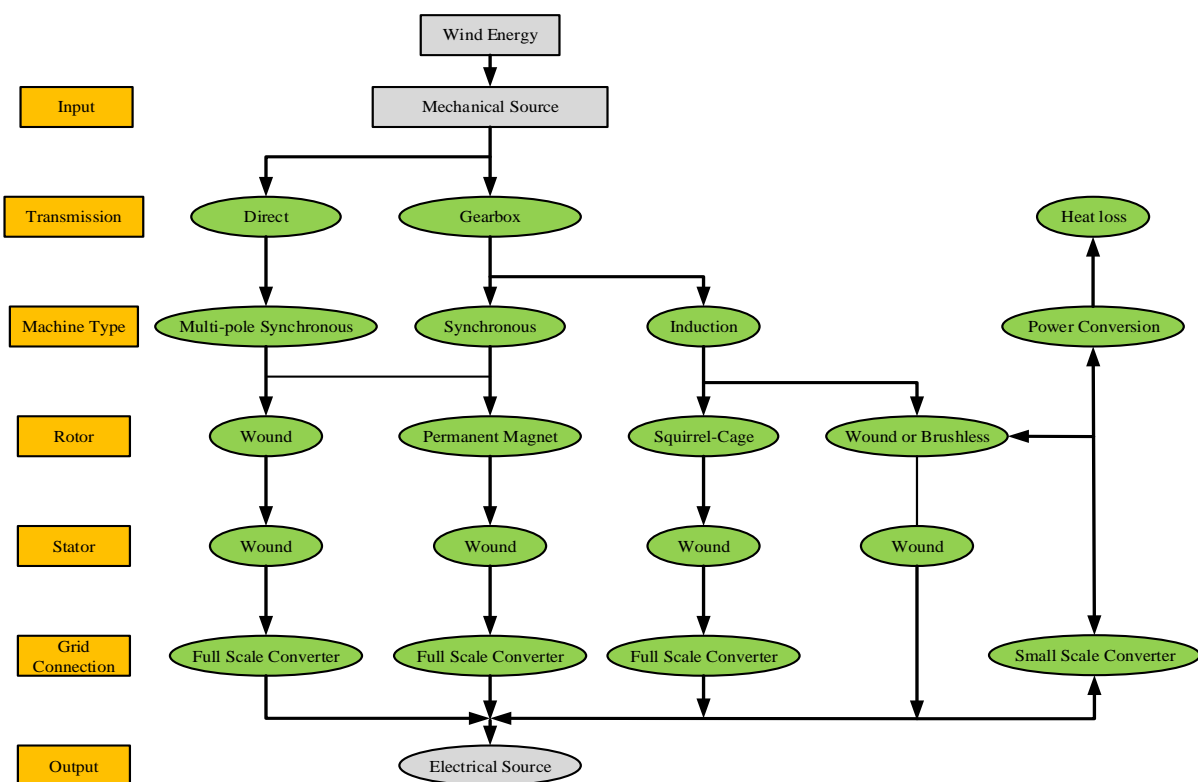
Fig. 4. Technological roadmap for wind turbine's technology [28].

- **Variable speed WT with full-scale power converter:** It corresponds to a full variable speed controlled WT, the generator is connected to the grid trough a fullscale frequency converter. Then,

additional technical performances of the WT can be achieved. The generator can be a DFIM, a PMSM or a WRSG. Some schemes are gearless using a multi-pole machine. Examples of manufacturers are Siemens Wind Power, Made, Lagerway and Enercon. In particular Lagerway and Enercon uses a WRSG [37], [28].

As pointed out above, the DFIG can play and important role for variable speed WT with power converter connected to the stator side, see Figure .3. In this configuration the DFIG is "isolated" from the grid by the power converter. Consequently, the presented control algorithms can help to regulate the stator voltage amplitude and keep the system in the desired operation point.

OBJECTIVE OF THE RESEARCH

The main objective of this research is to contribute to the control method for the standalone doubly fed induction generator. The modelling, analysis and design of the standalone DFIG system without energy storage is carried out. The research also studies the variable speed fixed frequency operation of the standalone DFIG based wind turbine. The thesis aims for improve of the current loops for the filed oriented control of the standalone DFIG. The thesis also aims to develop a novel sensor-less control method for reduce requirement cost for control implementation.

The areas of investigation of the thesis are summarized below :

• Modeling and analysis of the stator flux orientation vector control for rotor side converter.

• Implementation of the hysteresis current control and finite state predictive current control for improve the rotor current control in the rotor side converter.

• Implementation of the direct rotor flux control for rotor side converter.

• Implementing of the direct torque control for rotor side converter.

• Verification of the proposed control methods in simulation tests and in a laboratory set-up under both sub-synchronous, synchronous and the super synchronous speed.

The dissertation consists of four chapters. In the first chapter, DFIG systems and state-of-the-art DFIG control methods are presented. In the second chapter, modeling and basic control of standalone DFIG are presented. The third chapter describes improved rotor current of the RSC control based approach-1. The fourth chapter deals with the used of the direct control method, like DTC and DRFVC based approach-2 .state control. A flux, speed and position observer is designed and analysed. The second and third chapters shows simulation experimental results of proposed control approach. The dissertation ends with some conclusions and some future work.

Chapter 1

Stat of the art: DFIG and multiple generation system topology

Chapter 1

Stat of the art: DFIG and multiple generation system topology

1.1 Chapter introduction

The doubly fed induction generator is a wound rotor induction machine whose stator is directly connected to the grid/load and its rotor is connected to the grid/load via a back-to back power converter (two 3-phase active bridges connected via a DC-link). The major benefit of this parallel topology is reduction of the converter rated power in comparison to the series topology, which gives a lower cost, size and weight of the converter. A smaller power converter in this topology can be used only when the DFIG system operates close to synchronous speed, which is usually the case. This property makes DFIG the most popular generator in wind generator systems. In addition, DFIG can also be applied in hydro plants [1], combustion engine generation units [2, 3] and possibly every energy source whose efficiency depends on generator speed and its operation under very low speeds is either impossible or uneconomical.

The construction of the wound rotor induction machine is well-known and can be found in [4, 5]. A considerable disadvantage of this construction are slip rings, which require frequent service. Thus, a novel concept of a brushless doubly fed induction generator has recently emerged in two variants – with a rotor cage [6] and a reluctant rotor [7, 8]. DFIG is usually designed to have the rotor-to-stator winding ratio of approximately 3, thus rotor voltage is approximately equal to stator voltage under the maximal slip equal to ⅓. This allows to connect the grid-side converter to the grid without an intermediate step-up transformer. The Grid-Side Converter GSC is connected to the stator via an inductor. The Rotor-Side Converter RSC is usually directly connected to rotor windings, because machine inductance is usually sufficient to reduce high harmonics of the rotor current to an acceptable level. However, in [9] it is proposed to use an additional filter on the rotor side in order to obtain a sinusoidal rotor voltage and decrease heating of the machine due to high harmonics and to obtain rotor winding protection against high $\mathrm{d}u/\mathrm{d}t$ of converter voltage.

The first power converters used in DFIG were thyristor-cycloconverters due to lack of high-power fully-controlled switches. The Insulated Gate Bipolar Transistor IGBT technology has enabled to build forced-commutating converters, which deliver high quality currents with Pulse Width Modulation PWM. A classical topology of a frequency inverter is the AC/DC/AC converter, which is also called a back-to-back converter. A great advantage of this topology is that the faults and distortions in one power converter are isolated from the second one by the DC-link, which has big capacitance. Moreover, it enables to easily incorporate energy storage into the DC-link via a DC/DC converter. Matrix converters are a competitive solution, which has emerged recently and they make it possible to remove a DC-link capacitor at the expense of an increased number of power electronic switches. However, the lack of capacitor causes that energy oscillation in one power system cannot be stored in the DC-link due to the absence of an intermediate capacitor. Furthermore, complicated snubbed circuits are often necessary in the matrix converter, which puts into question the advantage of this topology. Another trend in development of power converters emerged when the IGBT technology became unable to provide sufficient voltage levels for medium- and high-power converters. Multilevel converters solve this problem by using a greater number of switches with reduced voltage ratings in comparison to the two-level topology. Therefore, it has become possible to build converters for the highest voltages used in the power grid. Moreover, the shape of voltage generated by the converter consists of less high harmonics, thus inductive filters used in these converters can be reduced. State-of-the-art multilevel converters are of the DC/DC converter type used in High-Voltage Direct-Current transmission lines, which use many converters connected in a cascade [10].

Topologies and properties of power electronic converters used in DFIG systems are not the main topic of this dissertation and due to rich literature; the reader is referred to the following papers:

- AC/DC/AC topologies – general issues [11], application in DFIG [12].
- Multilevel topologies – general issues [13], application in DFIG [14].
- Matrix converter topologies – general issues [15], application in DFIG [16].

1.2 DFIG system topologies

There are four basic DFIG topologies used in generation systems, as presented in Fig. 1.1. In this subsection, these system topologies will be briefly introduced.

Nowadays, the most popular application of DFIG is a grid-connected wind turbine, but stand-alone diesel-driven generators are a promising solution for power systems in remote areas such as ships, islands, small villages in rural areas. High-power wind farms (5-300MW) are connected to the high-voltage power grid with step-up transformers. In power grids with high renewable energy

penetration, behavior of wind farms during grid faults is one of the biggest concerns, because power grid stability cannot be guaranteed without participation of wind farms in reactive power generation. Therefore, special grid codes have been introduced in order to regulate the behavior of grid-connected generators (a brief 16 introduction to grid codes can be found in [17, 18]). Grid codes make wind turbines remain connected to the grid during grid faults, feeding reactive power to help in voltage recovery. A control target in the grid-connected DFIG is usually maximization of energy extracted from the energy source. However, the main target of both controllers under either very low or very

high wind speeds is to stabilize the turbine speed at the maximal/minimal allowed value in order not to exceed the safe operating area of RSC. MPPT methods are activated when the rotor speed is within the limits, and together with pitch-stall control, they maximize turbine power available at the time.
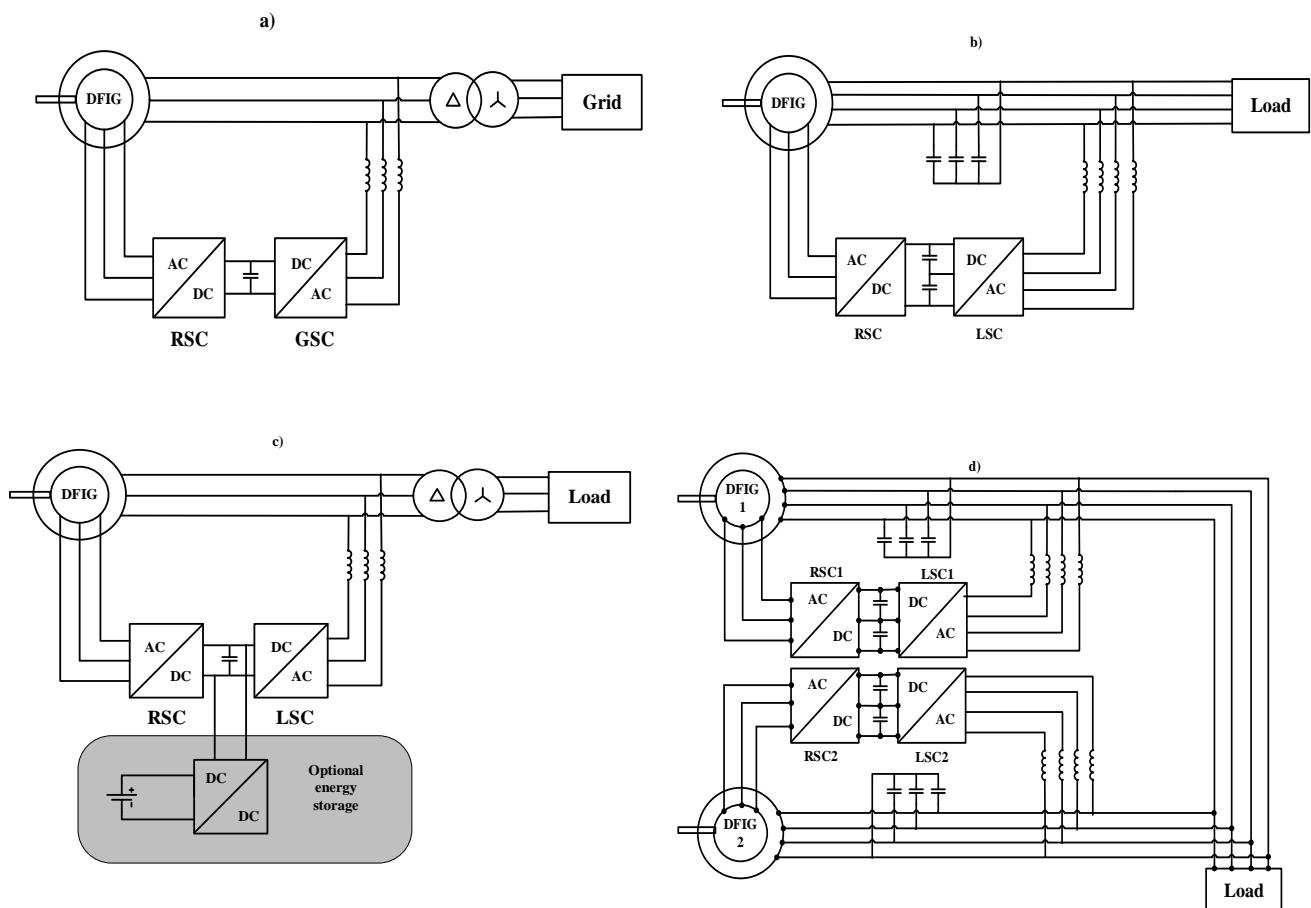
Fig. 1.1. Basic DFIG topologies: a) grid-connected DFIG, b) 4-wire stand-alone DFIG, c) 3-wire stand-alone DFIG with an intermediate transformer, d) parallel operating DFIGs in a microgrid.

Currently, main research subjects in the field of the grid-connected DFIG are:

- Operation under unbalanced grid voltage conditions (different control targets: torque ripples reduction, sinusoidal rotor/stator currents, cancellation of power ripples, symmetriation of the microgrid with high impedance).

- Sustaining either symmetric or asymmetric grid faults (property called Low-Voltage Ride-Through) using crowbar protection and active flux damping when the induced voltage is within control limits.

Currently there are few stand-alone DFIGs used commercially, whereas there are quite a lot of wind applications of the grid-connected DFIG. In stand-alone operation, the main control target is microgrid voltage stabilization. The stand-alone DFIG has to provide sinusoidal constant-amplitude constant-frequency voltage under non-linear and unbalanced loads. Therefore, it has to have an ability to reduce the high harmonics of stator voltage and to symmetries the voltage under a big share of non-linear and unbalanced loads in the standalone microgrid. On the other hand, generating high harmonics of the stator current causes torque ripples, which negatively affect mechanical elements of the generator and prime mover. The harmonics and negative sequence of the load current should be compensated for by the Load-Side Converter LSC as much as it is possible. The function of LSC is to stabilize the DC-link voltage and optionally to reduce the content of load current high harmonics [19], which would cause electromagnetic torque ripples if they are transferred through the generator. However, not always can the total amount of high harmonics and negative sequence be compensated for by LSC due to its current limits. RSC should guarantee sinusoidal stator voltage, whereas LSC should compensate for the high harmonics and negative sequence of the load current as far as its current limits allow. In micro grids, the neutral wire is usually present in order to connect 1-phase loads to the grid. In case of high-power standalone generators, a transformer is often present between generators and the load in order to match voltage parameters of the high power generator and the load. When a low-voltage generator is used, it is possible to eliminate the matching transformer and to use a 4-wire 3-phase LSC.

Major topics concerning DFIG stand-alone operation are:

- Voltage stabilization under rapid load changes,

- Providing symmetrical sinusoidal voltage under non-linear and unbalanced loads,

- Converter current limitations and load current sharing between converters,

- Fault detection and its isolation (providing the short-circuit current for overcurrent protection devices in order to allow them to break the short-circuit loop).

Parallel operation (also called load sharing) of DFIGs can be used in micro grids where there are multiple generators, which provide energy for the load. A popular strategy of load sharing among generators is the master-slave configuration, in which one generator operates as a voltage source (it stabilizes grid voltage), while others operate as current sources. The main problem with the master-slave topology is its vulnerability to failures of the master generator, which leads to a collapse of the whole power system. Moreover, this topology requires signal interconnections among generators, which reduces its robustness and increases the system cost (in many cases building the information infrastructure can be simply unfeasible due to e.g. large distances between the generators).

1.3 Evaluation of control methods for DFIG

Almost all advanced control methods that have been developed for induction motor studying in 1974 can be applied to DFIG [20]. However, control of the DFIG is more complicated than the control of a standard induction motor. It will be shown in the next chapter that any three-phase quantity, whether a voltage, current or flux linkage, can be expressed as a single rotating vector [21]. Therefore, two main methods, namely scalar and VC, can be developed to control the IM. Scalar control, where V/f control is based on the open and closed-loop control system of the IM speed. The V/f control is applied to control the supply voltage magnitude of IMs. It is one of the best choices for variable speed and the frequency applications. Vector control acts to control these space vectors in magnitude and phase [22, 23]. Many different combinations can work and they each have advantages and disadvantages [24, 25]. Fig 1.6. shows the classification of control strategies in DFIG market. Field oriented control (FOC) [26], [27-44], direct torque control (DTC) [44-50] and direct power control (DPC) [41-51] are practical control strategies which have been well developed for DFIG-based wind energy generation systems since 1996. The following subsection discusses more about the evolution of these control methods.
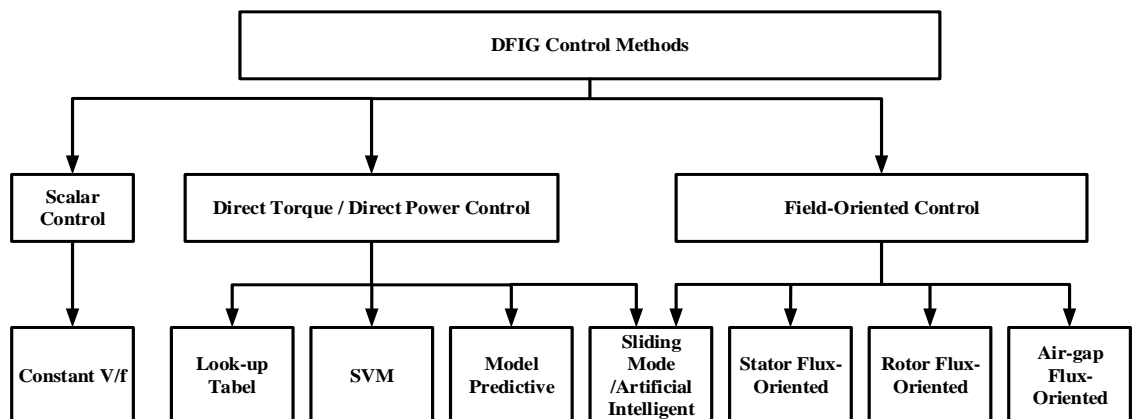
Fig. 1.2. Classification of DFIG control methods.

1.3.1 Field oriented control for grid connected DFIGs

The field oriented control (FOC) was invented on 1970s based on control method of the separately excited DC machine. In a DC machine, the field flux is produced by the field winding is perpendicular to the armature field which is provided by stator windings. Because of decupling relation between stator and field flux space vectors, when torque is controlled the variation of field flux is not affected armature flux. The same concept is extended for induction machine [13] using three-phase (abc) to two-phase (dq-frame) transformation where the sinusoidal variables are projected to DC quantities in rotating direct-axis (d) and quadrature-axis (q). The vector control method that applied for squirrel cage induction motor [13] can be extended to DFIG [8, 14]. In squirrel cage machine, the power electronic converter is connected to the stator windings to control the input currents in dq frame aligned with rotor flux [13]. Similarly as shown in Figure 1.7. , in DFIGs, the rotor side converter connects to the rotor windings; therefore, control strategies are applied on rotor currents using a rotating frame aligned to stator flux known as stator-flux orientation [8],[14-15], or with air-gap-flux orientation [27,30]. The reference rotor current is calculated based on active power P_s^* and reactive power Q_s^* references. The rotor currents can then be separated into two components, the one in line with the stator flux, i_{rd} (direct-axis), which is responsible for contributing to it, and the other, i_{rq} (quadrature axis), which is orthogonal. The power can be controlled by varying the magnitude of i_{rq} while keeping i_{rd}, and the field flux constant. To do this the magnitude and phase angle with respect to the stator flux vector must be controlled. In this way there is a linear relationship between power and the control variable. It can be shown that i_{rq} can further be related to the real power P_s^* and i_{rd} to the reactive power Q_s^*, allowing for decoupled control of these important variables [8]. The flux estimation difficulty in stator-flux orientation method leads researchers to develop orientation based on grid voltage information [18-30]. For grid voltage orientation, all variables need to be transferred from 3-phase ABC to 2-phase dq synchronous reference frame. For the transformation, the shaft rotating angle θ_r and stator voltage phase θ_s are required that can be obtained through encoder and phase lock loop (PLL), respectively.

Artificial intelligence (AI) is advanced controller that is based on expert knowledge (human knowledge) and the implicit inaccuracy [33]. Fuzzy logic controller (FLC) and artificial neural network (ANN) were known as AI controllers which were used extensively in power electronic applications [23-34]. In [34], fuzzy logic controllers are used in place of the PI controller to avoid machine parameters dependency of the controller. The pitch angle control for DFIG wind turbine through neural network was discussed in [34].

Since FOC is based on rotor current vector control which is in stator voltage or flux reference frame, it requires the transformation of stator voltages, currents and control output variable among stationary and synchronous reference frames. Also, FOC requires accurate information of DFIG parameters such as stator, rotor resistor and inductance, and mutual inductance. So, the control performance may be degraded when the actual value of parameters are differ from those values used in FOC control system. Also, the rotor current controllers should be tuned carefully to have good dynamic response [20].
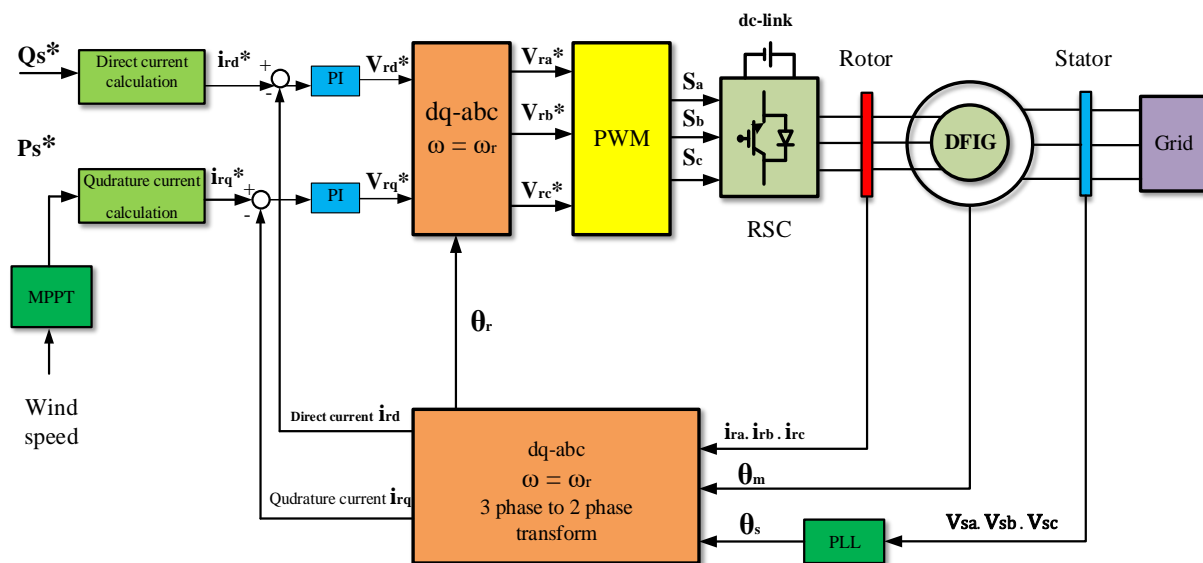
Fig. 1.3. Field oriented control schematic.

These drawbacks of FOC gave a motivation to the researchers to develop a newer control method that had less dependency on the machine parameters and also less compensator tuning efforts. This novel control method was known as direct torque control (DTC) [37].

1.3.2 Direct torque/power control for grid connected DFIGs

For reducing control difficulty and tuning efforts in FOC, the direct torque control (DTC) is developed for squirrel cage induction motor in late 1980's [26,37]. This controller was extended to DFIG in 2002 [37]. The DTC technique is based on a space vector representation of the achievable output AC voltages of the rotor side converter, which is used for a two-level voltage source inverter. Fig 1.4. shows the basic schematic of the DTC method. The control part of DTC consists of three blocks, estimation block, hysteresis-based controllers and DTC switching table. The torque T_{e*} and the rotor flux amplitude ψ_{r*} is primary control variables [37]. The rotor flux and stator flux space vectors rotate clockwise (sub-synchronism) or anticlockwise (sup-synchronism) to a distance known

as the torque angle which is estimated in estimation block using rotor and stator currents. The actual torque is also estimated using stator and rotor currents and voltages measured value. By modifying the angle between stator and rotor flux space vectors, it is possible to control the torque. In order to influence the rotor flux trajectory stator currents. The actual torque is also estimated using stator and rotor currents and voltages measured value. By modifying the angle between stator and rotor flux space vectors, it is possible to control the torque. In order to influence the rotor flux trajectory and amplitude, different voltage vectors from the DTC are injected into the rotor of the machine. The reference torque and rotor flux are compared to their actual values and proceeds through the three-level and two-level hysteresis controllers, respectively to provide error signal status for switching table to select a proper rotor voltage vector. These voltage vectors are provided by the two-level voltage source converter known as rotor side converter that supplies power to the rotor windings. and amplitude, different voltage vectors from the DTC are injected into the rotor of the machine. The reference torque and rotor flux are compared to their actual values and proceeds through the three-level and two-level hysteresis controllers, respectively to provide error signal status for switching table to select a proper rotor voltage vector. These voltage vectors are provided by the two-level voltage source converter, known as rotor side converter that supplies power to the rotor windings.
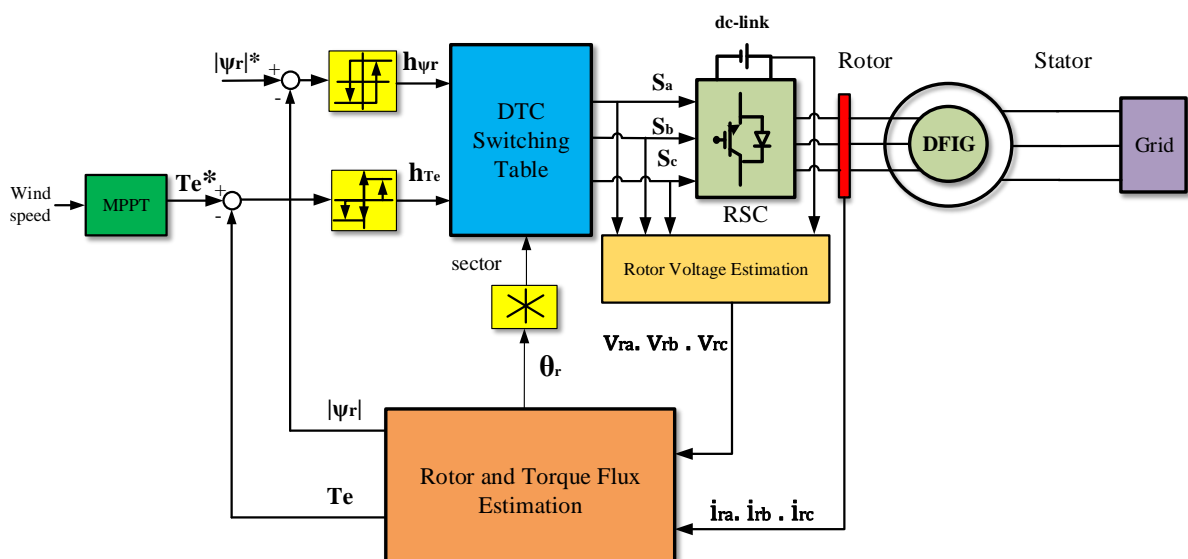
Fig. 1.4. Typical block diagram of direct torque control (DTC).

Based on DTC, the direct power control (DPC) technique was developed about more than a decade ago for controlling three-phase rectifiers [29]. In DPC approach, the primary variable signals are stator active P_s^* and reactive power Q_s^* [39, 40, 41]. Also in DPC, there is a block and no need to estimate the control variables because stator active and reactive power can be calculated using

stator voltages and currents. Fig 1.5. shows the basic schematic of direct power control (DPC). As shown, DPC is based on how the inverter switching vectors were selected from DPC switching table using the rotor or stator flux position, and the errors in the active power and reactive powers. Thus, high performances, robustness and low sensitivity to the system parameter variations can be considered as the main advantages of the DPC method [41].
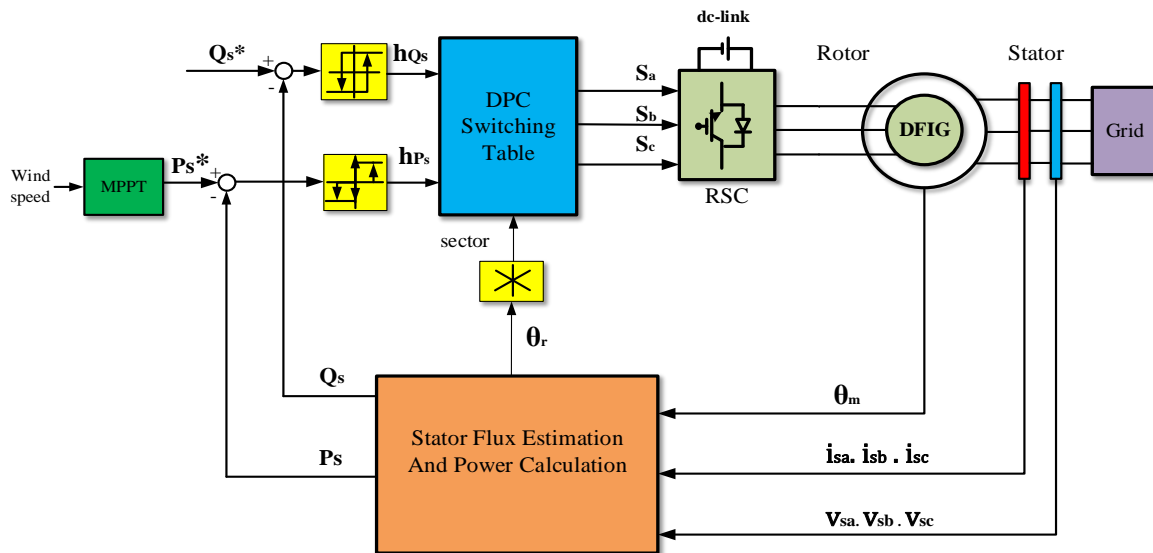
Fig. 1.5. Typical block diagram of direct power control (DPC).

Comparing DTC to DPC, it can be highlighted that the DPC does not require the rotor currents information and control variable estimation block. Both of them have high dynamic performance because of using hysteresis-based controllers. However, using hysteresis-based controllers have a penalty of high ripple in the developed torque or power and also operated at a non-constant switching frequency, which is a source of non-linear behavior. Moreover, the rotor side converter's switching frequency is highly influenced by the shaft speed, which is mainly due to the power slope that depends on the rotor speed. In addition, variable switching frequency may produce significant acoustic noise of variable intensity, a non-uniform distribution of switching losses for each semiconductor switch in the power inverter and currents that have nondeterministic harmonic content [41, 42]. The harmonic in stator currents complicate the design of an AC filter with capability of absorbing a wide range of frequency components, and also complicate the heat-sink design. Hence, a number of researchers have worked on DPC and DTC for DFIG to reduce output ripple and keep rotor side converter switching constant [41-49]. These include the use of space vector modulation (SVM) [41-44], discrete vector modulation technique (DSVM) [45], predictive direct power control scheme (PDPC) [46-48], and sliding-mode control (SMC) [49]. Fuzzy logic was employed in direct power control of DFIG by replacing hysteresis-based controller and conventional switching table with fuzzy based controllers

[33-35]. All these contributions allow the DPC performance to be improved, but at the same time they lead to more complex schemes.

In [41], the required rotor voltage vectors over a constant period are calculated and implemented by space vector modulation. Although this method adds constant switching frequency feature to DPC system, calculating duty ration of each voltage vector in each sample time increases the mathematical calculations. In discrete SVM (DSVM) method [44], the three rotor voltage vectors applied within the switching period are selected using a modified lookup table and a five-level hysteresis comparator.

In model-based predictive direct power control (PDPC), during constant period of time, three sequences of rotor voltage vectors are injected to the rotor windings. These vectors are chosen based on minimizing cost functions of active and reactive power errors. Online calculation difficulties from microprocessor point of view and complexity in control are main disadvantages of PDPC. In [49], the application of sliding-mode control (SMC) strategy for DPC drive was proposed. In SMC strategy, by selecting appropriate quadratic Lyapunov function, the controller is designed to provide the rotor side converter output voltage references as an input to SVM module.

1.3.3   Control methods for stand-Alone DFIGs

As mentioned in literature of grid connected mode of DFIG, the stator is connects to the stiff grid voltage, which provides the power vectors that are used in the feedback superior. However, in the case of grid voltage absence on grid failure or electrification of a remote area with no grid, the grid-connected control strategies are no longer valid. These cases are known stand-alone mode of DFIG where the grid voltage is not connected to the stator. A standalone generating system should provide regulated voltage and frequency to the loads [50]. There are two different control methods for stand-alone system known as indirect stator flux orientation (ISFO) [50-53] and direct voltage control (DVC) based scalar control method [54-55]. Fig. 1.6. shows the diagram block of ISFO and DVC of stand-alone control approaches.

Direct voltage control (DVC) is alternative method which can directly control the voltage and frequency of the stator side of a DFIG as shown in Fig 1.6 (a). In DVC the reference stator space vector is represented in a rotating polar reference frame with desired speed. The rotor current amplitude and frequency are calculated directly from stator voltage regulator. The main advantage of this method is no need to measure the shaft speed. The shaft speed is o measure the shaft speed. The shaft speed is obtained as from output of stator frequency error compensator [55]. In ISFO-controlled DFIG, the voltage and current values are referred to reference frame aligned to the stator flux. The d-

axis of the rotor current is obtained from magnetizing current using a PI controller as shown in Fig. 1.6. (b).
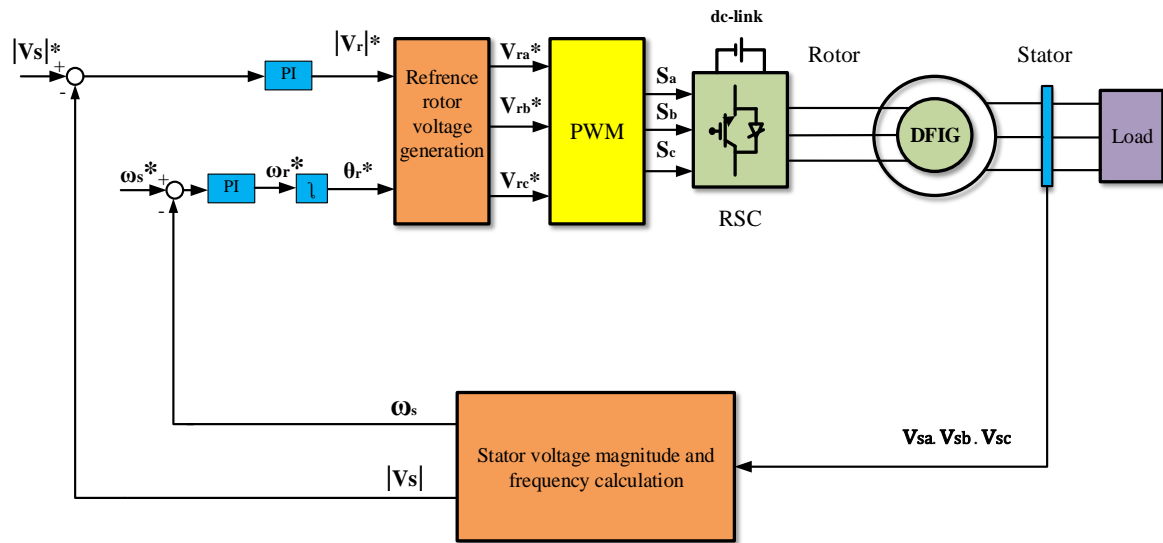
(a) Direct voltage control (DVC)
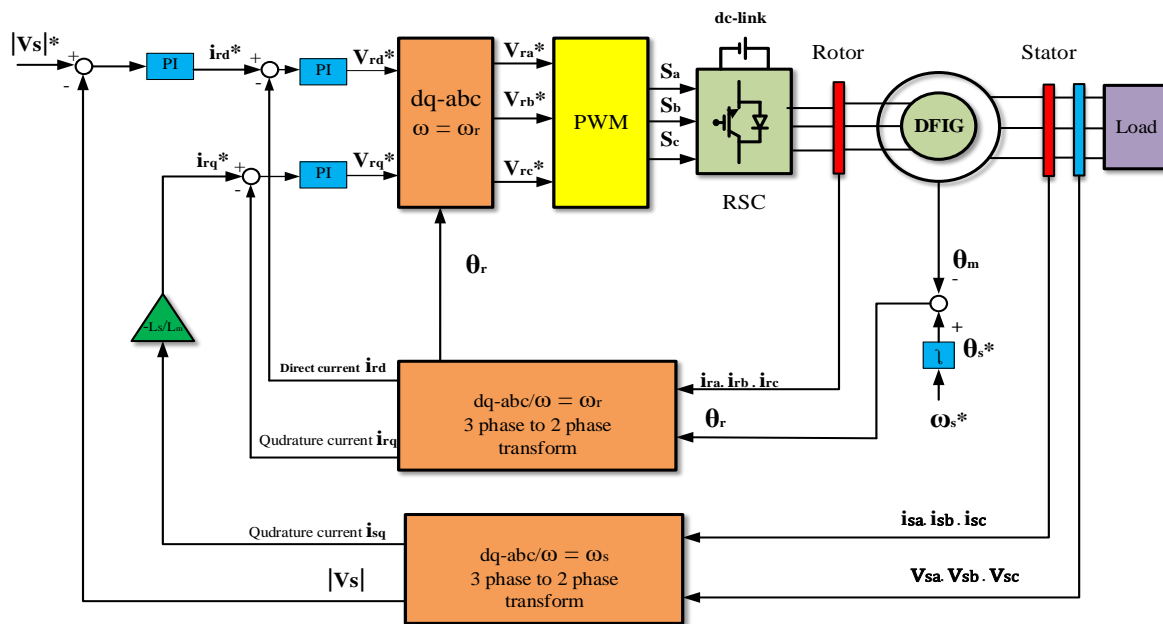
(b) Indirect stator flux oriented (ISFO)

Fig. 1.6. Diagram block of stand-alone control systems.

The main drawback of the ISFO control is the lack of direct electrical torque or active power control of the DFIG. This is because under ISFO control the quadrature component of stator current (i_{sq}) is set by the load, and in order to maintain the field orientation of the DFIG the q-component of rotor current (i_{rq}) must be kept proportional to i_{sq}. Hence, i_{sq} cannot be used to control T_e or P_s. Moreover, using low-cost low-precision encoders often results in worse system performance than

under estimated rotor position and speed. Instead of using position sensors, rotor position and speed can be estimated with electrical signals and a control technique called Model Reference Adaptive System MRAS. This estimation method was first developed for the squirrel-cage induction machine in [56] and then enhanced in many other papers, e.g. [57-59]. It was first applied in DFIG in [60]. The MRAS observer requires two models of an induction machine; one whose parameters do not contain the estimated signal and another which uses this unknown signal. Comparing the states of those two models and introducing adequate feedback control, it is often possible to reconstruct the unknown signal in a closed-loop observer topology. MRAS observers of rotor position and speed mostly incorporate Phase-Locked Loop PLL, which synchronizes two vectors generated by the reference model and the adaptive one.

1.3.4 DFIGs grid-synchronization control methods

Most DFIG control methods do not address grid synchronization. This is an important issue which runs concurrently with protection [6],[7]. The established method for grid synchronization using field oriented control (FOC) [61] utilizes an outer voltage loop and an inner rotor current loop to achieve the synchronization of frequency, phase, and magnitude between the DFIG and the grid. Fig. 1.7. shows the diagram block of FOC method for synchronization process. The circuit breaker is closed when the stator and grid voltage and frequency are equal ($v_s = v_g$ and $f_s = f_g$). The phase lock loop system can calculate the stator and grid side voltage magnitude and phase that are used for controlling the rotor current direct-axis $i_{rd}*$. The quadrature-axis of rotor current $i_{rq}*$ is kept zero during synchronization process because no power flows between stator and grid sides.
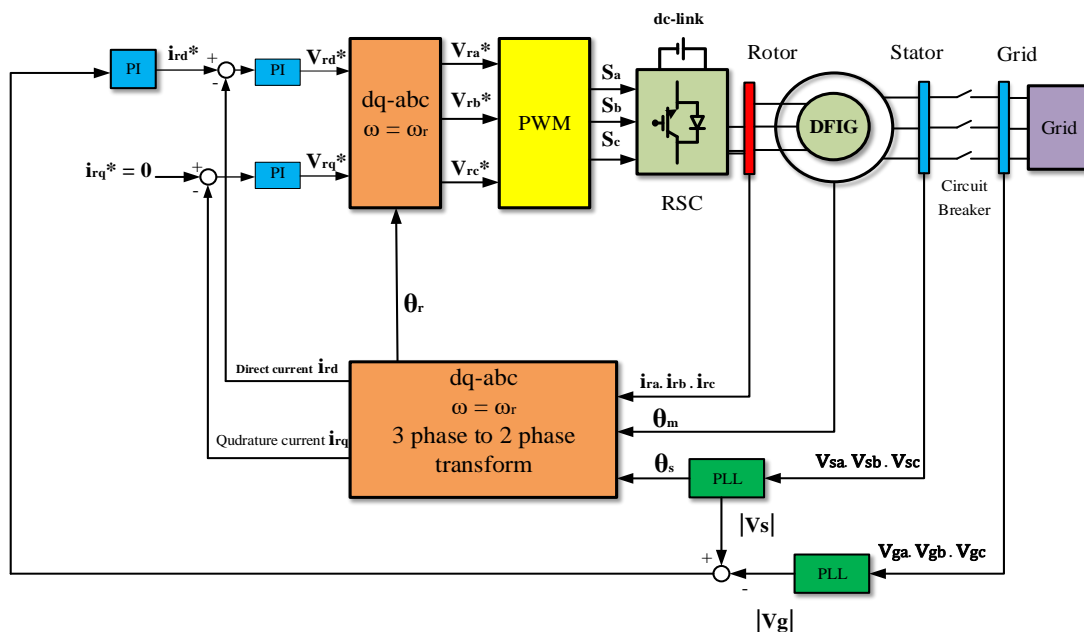
Fig. 1.7. Diagram block for FOC-based synchronization process.

These methods all inherit the drawbacks of FOC and require measurements of the grid and stator voltages, rotor currents and position, resulting in complex control algorithms. A direct voltage control scheme using integral variable structure control without a current control loop was presented in [61-64]. However, it still requires the measurement of the grid and stator voltages. In addition, because of its complexity, the transient response is compromised. Grid synchronization using DTC was proposed in 2002 [64] as depicted in Fig. 1.8. In comparison with the FOC, a better transient performance was achieved. This method used three PI regulators and required the measurement of the rotor position and currents, and the stator and grid voltages. In [65], a fast grid synchronization was achieved without the need for PI regulators and stator voltage measurement by introducing a virtual torque concept. Unfortunately, the stator voltage waveform was distorted because of large torque and flux ripples. This is a major obstacle to smooth grid connection. Still, the switching frequency is variable. Another important issue is the need for fast and flexible active and reactive power regulation after grid connection. This enables DG units to contribute to energy management and power quality improvement in a DG system. A grid synchronization strategy based on DPC was proposed in 2009, which could achieved smooth transition between synchronization and normal operation with active and reactive power regulation without changing control configurations [66]. This control strategy is almost identical to that proposed in [65] except that it uses the virtual power rather than the virtual torque and also predictive control was used for providing constant switching frequency.
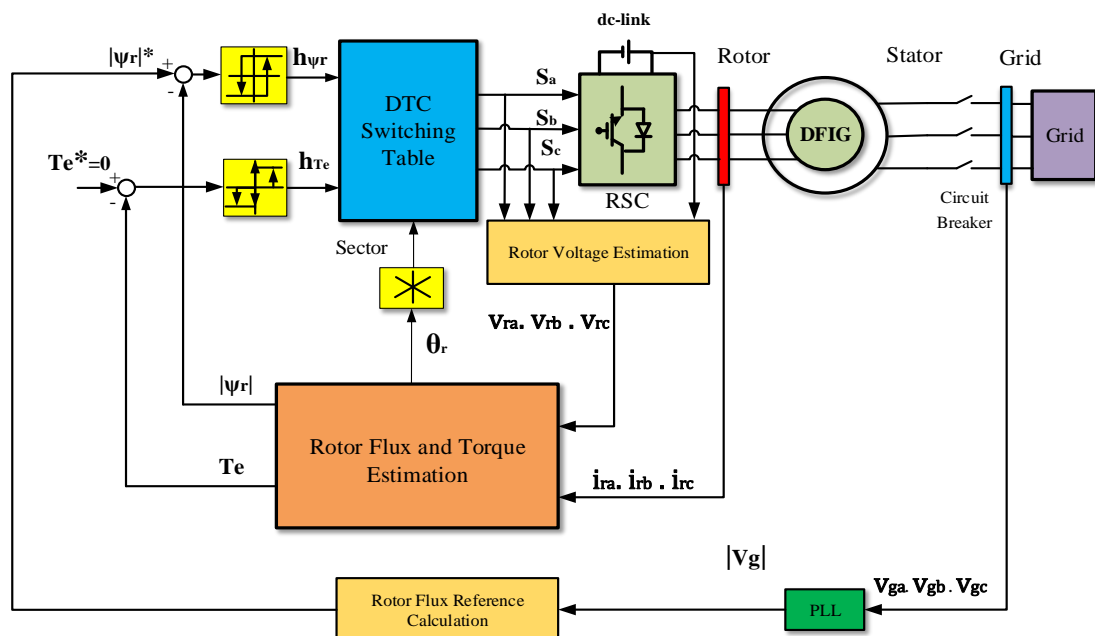
Fig. 1.8. Diagram block for DTC for DFIG grid synchronization.

1.4 Methodology of research

The basic concept of conventional control method for standalone DFIG is performed by simulation with MATLAB-SIMULINK. The control part of simulation in MATLAB receives and sends the data to the simpower system blocks for controlling the DFIG. The high number of sensors are considered as main drawbacks of conventional control. For overcoming these problems and with the understanding and knowledge of the conventional DRFVC and DTC, new torque and rotor flux controllers are proposed. Based on proposed controller for grid-connected mode, a controller is developed for stand-alone mode. The proposed controllers are then simulated to study on their effectiveness.

Once the simulation results are satisfied up from requirement of DFIG output power quality for all modes, the hardware prototype are built and implemented. The Hardware implementation is used to verify the feasibility of the proposed system. It consists of three main components, a digital signal processor (Dspace 1104), sensors and signal conditioning circuits and the power circuit. The DSP is responsible for running the entire control algorithm. The power circuit consists of sets of 3-phase Voltage Source Inverter (VSI) connected to rotor windings of a 3 kW wounded rotor induction machine. The wind turbine is emulated with 3 kW DC motor controlled by DC/DC converter. A sets of three-phase resistive loads are used the stand-alone mode, which can be parallel together to test the stand-alone voltage loop controller performance.

Chapter 2

Modeling and basic control of Standalone DFIG generation System

Chapter 2

Modeling and basic control of standalone DFIG generation system

2.1 Chapter Introduction

For a better understanding of the DFIG performance as well as studying all the possible transient behaviors of it, this chapter introduces the machine model. First, the model in the three-phase reference frame is introduced. Then, using coordinate transformations, the dynamic model in the dq rotating reference frame is presented. This model is useful for the study of all-important dynamic effects occurring during steady state and transient operations. Hence, it should be valid for any time variation of the voltages or currents generated by the inverter that supplies the generator.

This chapter is organised as follows. Section 2.2 gives the state-space representation of a three-phase system. Section 2.3 presents the mathematical model of the DFIG. The RSC converter models are described in Section 2.4.finaly Section in 2.5 the basic control design of standalone DFIG are detailed.

2.2 System configuration

The overall structure of a stand-alone wind turbine has been shown in Fig. 2.1. A back-to-back converter including two voltage-fed convertors with IGBT switches has been used in this structure, which are known as Load Side Converter (LSC) and Rotor Side Converter (RSC). This study is concerned only with the rotor side converter (RSC). It is assumed that the DC-link voltage is already provided for system. Hence, only DFIG and RSC models are given in this section.
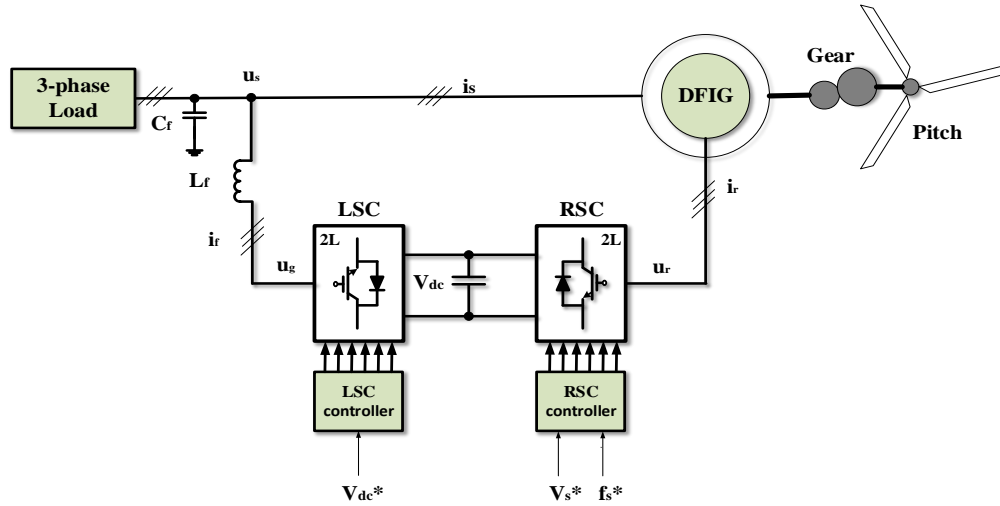
Fig. 2.1 Basic diagram of the standalone WPGSs based on DFIG.

2.3 Modeling of Doubly Fed Induction Generators

The three-phase symmetrical DFIG shown in Fig. 2.1. can be described as:
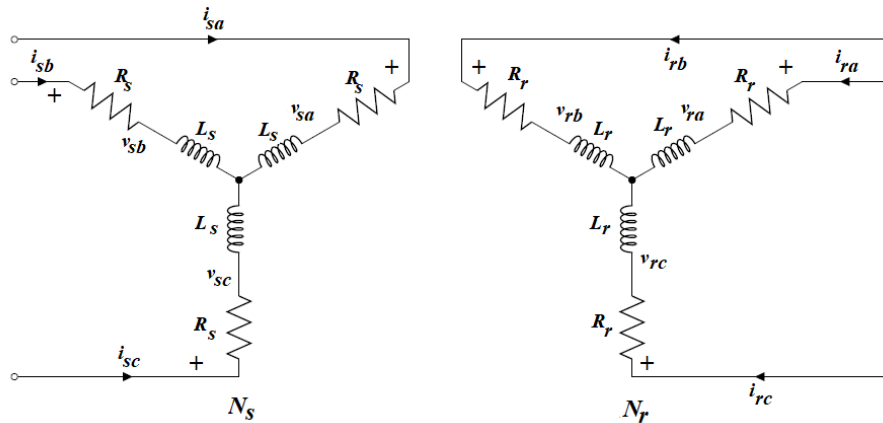
Fig. 2.2. Stator and rotor three-phase circuit of DFIG.

The voltage relations on rotor and stator sides are obtained by Kirchhoff's and Faraday's law:

$$\begin{bmatrix} v_{as} \\ v_{bs} \\ v_{cs} \end{bmatrix} = R_s + \begin{bmatrix} i_{as} \\ i_{bs} \\ i_{cs} \end{bmatrix} + \frac{d}{dt} \begin{bmatrix} \psi_{as} \\ \psi_{bs} \\ \psi_{cs} \end{bmatrix} \qquad (2.1)$$

$$\begin{bmatrix} v_{ar} \\ v_{br} \\ v_{cr} \end{bmatrix} = R_r + \begin{bmatrix} i_{ar} \\ i_{br} \\ i_{cr} \end{bmatrix} + \frac{d}{dt} \begin{bmatrix} \psi_{ar} \\ \psi_{br} \\ \psi_{cr} \end{bmatrix} \qquad (2.2)$$

The subscripts r and s denote rotor and stator quantities respectively. The subscripts a, b and c are used for phases a, b and c quantities, respectively. The symbols v and i are for voltages and currents and ϕ represents flux linkages. The stator and rotor winding resistances are R_s and R_r.

The flux linkages are coupled to the currents by the inductances:

$$\begin{bmatrix} \psi_{as} \\ \psi_{bs} \\ \psi_{cs} \end{bmatrix} = L_s \begin{bmatrix} i_{as} \\ i_{bs} \\ i_{cs} \end{bmatrix} + L_M \begin{bmatrix} i_{ar} \\ i_{br} \\ i_{cr} \end{bmatrix} \qquad (2.3)$$

$$\begin{bmatrix} \psi_{ar} \\ \psi_{br} \\ \psi_{cr} \end{bmatrix} = L_r \begin{bmatrix} i_{ar} \\ i_{br} \\ i_{cr} \end{bmatrix} + L_M^T \begin{bmatrix} i_{as} \\ i_{bs} \\ i_{cs} \end{bmatrix} \qquad (2.4)$$

The inductance matrices are defined by:

$$L_s = \begin{bmatrix} L_{ls} + L_m & -\frac{1}{2}L_m & -\frac{1}{2}L_m \\ -\frac{1}{2}L_m & L_{ls} + L_m & -\frac{1}{2}L_m \\ -\frac{1}{2}L_m & -\frac{1}{2}L_m & L_{ls} + L_m \end{bmatrix} \qquad (2.5)$$

$$L_r = \begin{bmatrix} L_{lr} + L_m & -\frac{1}{2}L_m & -\frac{1}{2}L_m \\ -\frac{1}{2}L_m & L_{lr} + L_m & -\frac{1}{2}L_m \\ -\frac{1}{2}L_m & -\frac{1}{2}L_m & L_{lr} + L_m \end{bmatrix} \qquad (2.6)$$

$$L_M = L_m \begin{bmatrix} cos(\theta_r) & cos(\theta_r + \frac{2\pi}{3}) & cos(\theta_r - \frac{2\pi}{3}) \\ cos(\theta_r - \frac{2\pi}{3}) & cos(\theta_r) & cos(\theta_r + \frac{2\pi}{3}) \\ cos(\theta_r + \frac{2\pi}{3}) & cos(\theta_r - \frac{2\pi}{3}) & cos(\theta_r) \end{bmatrix} \qquad (2.7)$$

The subscripts L_l and L_m relate to the leakage and magnetizing inductances respectively. The maximum amplitude of the mutual inductance between the stator and the rotor is L_m. The rotor electrical angular displacement regarding to the stator is defined from ω_r. The electrical rotor speed is calculated as.

$$\theta_r(t) = \int_0^t \omega_r dt + \theta_r(0) \qquad (2.8)$$

where $\theta_r(0)$ is the initial position of the rotor at $t = 0$. The mutual inductance matrix L_m is time-dependent. In order to eliminate the time dependency, the dq transformation will be used instead of abc. The DFIG modeling in (d-q) reference frame is reported in Appendix B-2

The electrical dynamic of the DFIG have been developed in the stator reference frame. The DFIG mechanical dynamic model is given by.

$$J\frac{d\omega_m}{dt} = T_m - T_e \qquad (2.9)$$

where J is the inertia of the machine, T_m is the mechanical torque and T_e is the electromagnetic torque.

2.4 State-space vector representation of three-phase systems

State-space vector representation makes an AC circuit simple to represent and easy to understand and analyze. As mentioned earlier, this study considers a three-phase wound-rotor IM, which is called doubly fed induction generator DFIG. The DFIG is supplied from a three-phase AC source. It is well known that the three phases (*a - b - c*) are located 120° apart in space, as shown in Fig. 2.3. They are linearly dependent on each other, which complicates the system model. To simplify the notation of three-phase electrical variables, such as voltage, current and flux, the variables can be modeled adequately using a two-axis reference frame. The two-axis representation of the three-phase system is called 'state-space vector representation'. This two-axis reference frame may be stationary in rotor (*α-β*) or synchronous (*d-q*), as shown in Fig. 2.3. For the state-space vector representation, the components of a particular variable along a - b - c coordinates are projected on *α-β* or *d-q* coordinates. The two coordinates in each reference frame are mutually perpendicular to each other, and linearly independent. This independence makes it possible to control both the flux and torque of an AC machine independently, similar to a separately excited DC machine.
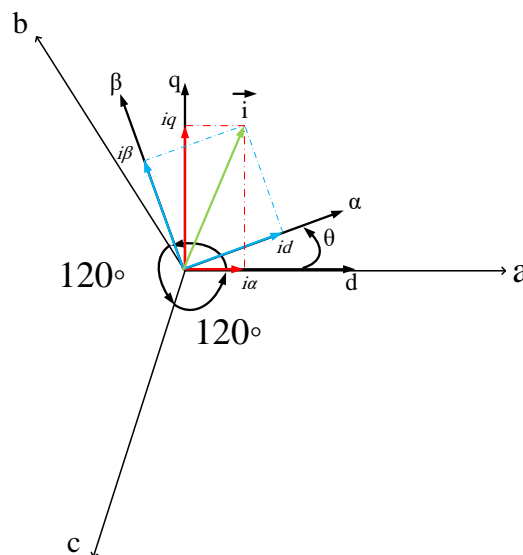
Fig. 2.3. State-space two-axis representation of three-phase (*a-b-c*) systems showing the relationship between the rotor (*α-β*) and synchronous (*d-q*) reference frames.

Using the current as an example, the transformation of the *a-b-c* frame to an *α-β* frame—which is known as Clarke transformation—is expressed in matrix form as

$$\begin{bmatrix} i_\alpha \\ i_\beta \end{bmatrix} = \frac{2}{3} \cdot \begin{bmatrix} 1 & -\frac{1}{2} & -\frac{1}{2} \\ 0 & \frac{\sqrt{3}}{2} & -\frac{\sqrt{3}}{2} \end{bmatrix} \cdot \begin{bmatrix} i_a \\ i_b \\ i_c \end{bmatrix}$$

Sometimes it is necessary to transform the α-β frame into a d-q frame, especially in vector control (i.e., FOC) design for motor drives. The transformation is called as Park

$$\begin{bmatrix} i_d \\ i_q \end{bmatrix} = \begin{bmatrix} \cos\theta_r & \sin\theta_r \\ -\sin\theta_r & \cos\theta_r \end{bmatrix} \cdot \begin{bmatrix} i_\alpha \\ i_\beta \end{bmatrix}$$

Where θ_r is the angle between the α-β and d-q reference frames, as shown in Fig. 2.3 Direct transformation from the a-b-c frame to the d-q frame (or vice versa) is also used for dynamic modelling of a three-phase system [107]. The current components of i_α and i_β are sinusoidal, as the current vector is rotates at a constant speed with respect to the rotor α-β frame. In contrast, the i_d and i_q components are normally constant or piece-wise constant, and are thus linearized. The aforementioned two transformations are equally applicable for voltage and flux, and the transformations are reversible means is also handy to be able to transform currents, voltages or flux linkages from the α-β (rotor) to the d-q (synchronous) reference frame and vice-versa. The transformation from the d-q reference frame to the rotor α-β reference frame is usually called as the inverse Park transformation and is given by

$$\begin{bmatrix} i_\alpha \\ i_\beta \end{bmatrix} = \begin{bmatrix} \cos\theta_r & -\sin\theta_r \\ \sin\theta_r & \cos\theta_r \end{bmatrix} \cdot \begin{bmatrix} i_d \\ i_q \end{bmatrix}$$

The state-space vector representation of the IM variables in both the *α-β* and *d-q* reference frames is

$$\text{Stator voltage:} \vec{v}_s = v_{s\alpha} + jv_{s\beta}, \vec{v}_s = v_{sd} + jv_{sq};$$

$$\text{Rotor voltage: } \vec{v}_r = v_{r\alpha} + jv_{r\beta}, \vec{v}_r = v_{rd} + jv_{rq};$$

$$\text{Stator current: } \vec{\imath}_s = i_{s\alpha} + ji_{s\beta}, \vec{\imath}_s = i_{sd} + ji_{sq};$$

$$\text{Rotor current: } \vec{\imath}_r = i_{r\alpha} + ji_{r\beta}, \vec{\imath}_r = i_{rd} + ji_{rq};$$

$$\text{Stator flux: } \vec{\psi}_s = \psi_{s\alpha} + j\psi_{s\beta}, \vec{\psi}_s = \psi_{sd} + j\psi_{sq};$$

$$\text{Rotor flux: } \vec{\psi}_r = \psi_{r\alpha} + j\psi_{r\beta}, \vec{\psi}_r = \psi_{rd} + j\psi_{rq}.$$

2.5 State-space vector model of the DFIG

There are three different preferred reference frames used in d and q axes calculations for induction machines simulation. Fig 2.3 shows the space vectors in the three reference frames, these frames can be classified according to the d and q axes rotation speed [12]:

• Stationary reference frame (known as the stator reference frame): The rotational speed is zero.

• Synchronous reference frame dq: the d and q axes rotate at the rotational speed ω_s of the stator flux or stator voltage.

• Rotor reference frame $\alpha\beta$: The α and β axes rotate at the rotor speed ω_m.

The state-space model of DFIG in the rotor α-β reference frame can be described by Eqs. (2.10)–(2.14):

Stator voltage equation: $\quad\quad\quad\quad\quad \vec{v}_s = R_s.\vec{\imath}_s + \frac{d}{dt}\vec{\psi}_s + j.\omega_m.\vec{\psi}_s$ $\quad\quad\quad$ (2.10)

Rotor voltage equation: $\quad\quad\quad\quad\quad\quad \vec{v}_r = R_r.\vec{\imath}_r + \frac{d}{dt}\vec{\psi_r}$ $\quad\quad\quad\quad\quad$ (2.11)

Stator flux equation: $\quad\quad\quad\quad\quad\quad\quad \vec{\psi}_s = L_s.\vec{\imath}_s + L_m.\vec{\imath}_r$ $\quad\quad\quad\quad\quad$ (2.12)

Stator flux equation: $\quad\quad\quad\quad\quad\quad\quad \vec{\psi}_r = L_r.\vec{\imath}_r + L_m.\vec{\imath}_s$ $\quad\quad\quad\quad\quad$ (2.13)

Electromagnetic torque equation: $T_e = \frac{3}{2}p\Im\mathrm{m}\,(\vec{\psi_r}.\vec{\imath_r})$ $\quad\quad\quad\quad\quad$ (2.14)

Also, the state-space model of a wound-rotor IM in the rotor d-q reference frame can be described by Eqs. (2.15)–(2.19):

Stator voltage equation: $\quad\quad\quad\quad \vec{v_s} = R_s.\vec{\imath_s} + \frac{d}{dt}\psi_s + j.\omega_s.\vec{\psi_s}$ $\quad\quad\quad$ (2.15)

Rotor voltage equation: $\quad\quad\quad\quad \vec{v_r} = R_r.\vec{\imath_r} + \frac{d}{dt}\vec{\psi_r} + j.\omega_r.\vec{\psi_r}$ $\quad\quad\quad$ (2.16)

Stator flux equation: $\quad\quad\quad\quad\quad \vec{\psi_s} = L_s.\vec{\imath_s} + L_m.\vec{\imath_r}$ $\quad\quad\quad\quad\quad$ (2.17)

Stator flux equation: $\quad\quad\quad\quad\quad \vec{\psi_r} = L_r.\vec{\imath_r} + L_m.\vec{\imath_s}$ $\quad\quad\quad\quad\quad$ (2.18)

where $\vec{v_s}$ is the stator voltage vector, $\vec{\imath_s}$ is the stator current vector, $\vec{\imath_r}$ is the rotor current vector, $\vec{\psi_s}$ is the stator flux vector, $\vec{\psi_r}$ is the rotor flux vector, R_s And R_r are the resistances per phase in stator and rotor, respectively. L_s, L_r are the inductances per phase in stator and rotor, respectively. L_m Is the mutual inductance, respectively, and ω_m is the electrical speed. L_{ls} and L_{lr} are respectively the leakage inductances of the stator and rotor windings. Te is the electromagnetic torque. The rotor angular frequency ω_m is related directly to the rotor angular speed Ω_m by the number of pole pairs p as

$$\omega_m = p.\Omega_m \quad \cdot (2.19)$$

Where, ω_s and Ω_m are the rotational speed of the synchronous reference frame, and the rotor reference frame respectively, which are related by the following relation: $\omega_r = \omega_s - \omega_m$, ω_r denotes the relative angular frequency between the synchronous reference frame and the rotating rotor reference frame.

2.6 Standalone DFIG equivalent circuit

The standalone DFIG dynamic equivalent circuit in the *dq* synchronous reference frame is shown in Fig. 2.4.
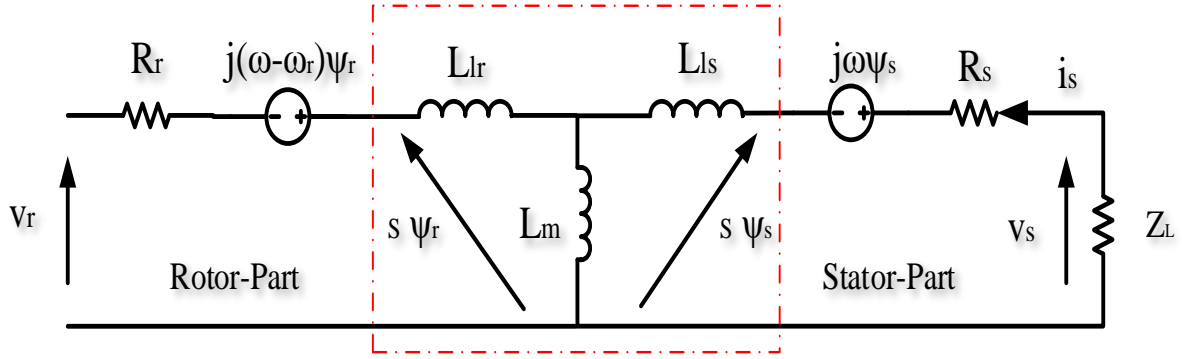
Fig. 2.4. Equivalent circuit of DFIG in arbitrary reference frame by rotation speed of ω.

Where,

$$L_s = L_{ls} + L_m$$
$$L_r = L_{lr} + L_m$$

Lls and *Llr* are the stator and rotor leakage inductances, respectively. ωr is the electrical rotor speed in rad/sec. ω is the rotation speed of the arbitrary reference frame in rad/sec. ω can take an arbitrary value which results in the conversion of the reference frame: stator stationary reference frame (ω = 0) , rotor stationary reference frame (ω = ωr), synchronous rotating reference frame (ω = ωs), where ωs is the synchronous speed in rad/sec. The model given in (2.15)–(2.19): holds for steady-state and transient conditions.

The stator and rotor fluxes relationship can be achieved by the manipulation of (2.17)-(2.18) as

$$\psi_s = \frac{L_s}{L_m} \cdot (\psi_r - \sigma \cdot L_r \cdot i_r) \quad (2.20)$$

$$\psi_s = \frac{L_m}{L_r} \cdot \psi_r + \sigma \cdot L_s \cdot i_s \quad (2.21)$$

2.7 RSC mathematical model

In this work, the RSC is a two-level (VSC) that has six IGBT power switches it intended for applying the FS-PCC method. The structure of the RSC and all rotor voltage vectors are depicted in Fig 2.4 The switching sequences S can be composed as the following equation:

$$S = \frac{2}{3} \cdot (S_a + a \cdot S_b + a^2 \cdot S_c) \quad (2.22)$$

Where $a = e^{-j2\pi/3}$, S_i=1 means S_i on, $\overline{S_i}$ means off, and $i = a, b, c$. all rotor voltage vector v are linked to the switching state S by

$$v = v_{dc}.S \qquad (2.23)$$

Where v_{dc} is the dc-link input voltage that supplies the RSC.
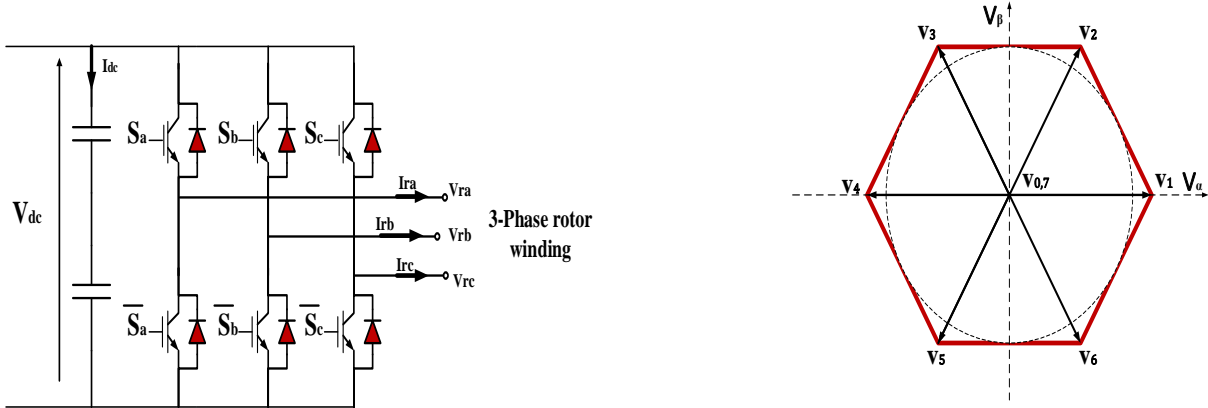
Fig. 2.5. Left: two-level voltage source inverter; right: voltage vectors.

Considering the possible eight voltage vᵢ (v₀–v₇) vectors switching states S (S₀–S₇), are obtained as shown in Table 1.

Table 2.1 Voltage vectors and switching states with index number.

States Switching			Vectors Voltage	Vectors
$S = [S_a$	S_b	$S_c]$	$v_i = [v_{i\alpha} \ v_{i\beta}]$	Number
$S_0 = [0$	0	$0]$	$v_0 = [0 , 0]$	0
$S_1 = [1$	0	$0]$	$v_1 = [2V_{dc}/3, 0]$	1
$S_2 = [1$	1	$0]$	$v_2 = [V_{dc}/3 , \sqrt{3}V_{dc}/3]$	2
$S_3 = [0$	1	$0]$	$v_3 = [-V_{dc}/3, \sqrt{3}V_{dc}/3]$	3
$S_4 = [0$	1	$1]$	$v_4 = [-2V_{dc}/3 , 0]$	4
$S_5 = [0$	0	$1]$	$v_5 = [-V_{dc}/3 , -\sqrt{3}V_{dc}/3]$	5
$S_6 = [1$	0	$1]$	$v_6 = [V_{dc}/3 , -\sqrt{3}V_{dc}/3]$	6
$S_7 = [1$	1	$1]$	$v_7 = [0 , 0]$	7

The switching states of the RSC are controlled by the switching pulses Sa, Sb, Sa as follows:

$$S_a = \begin{cases} 1 \ if \ S_a \ \text{on and} \ \overline{S_a} \ \text{off} \\ 0 \ if \ S_a \ \text{off and} \ \overline{S_a} \text{on} \end{cases} \quad (2.24)$$

$$S_b = \begin{cases} 1 \ if \ S_b \ \text{on and} \ \overline{S_b} \ off \\ 0 \ if \ S_b \ \text{off and} \ \overline{S_b} \text{on} \end{cases} \quad (2.25)$$

$$S_C = \begin{cases} 1 \ if \ S_c \ \text{on and} \ \overline{S_c} \ \text{off} \\ 0 \ if \ S_c \ \text{off and} \ \overline{S_c} \text{on} \end{cases} \quad (2.26)$$

2.8 Basic control strategy of the RSC for stand-Alone DFIG systems

The stand-alone wind energy systems issues are about, maintaining the voltage magnitude of the point of common coupling (stator voltage magnitude) and frequency constant since these systems are connected directly to the load. Moreover, the power quality in the stand-alone DFIG system is a significant issue. The purpose of the control strategy is to maintain the voltage magnitude and the frequency constant with high power quality regardless of the load connected to the stand-alone mode. In order to achieve the better performance of stand-alone DFIG system, a cascaded structure along with the SFOC theory is used for the control algorithm. The SVOC and the SFOC vector diagrams are depicted in Figure 2.5.

(a) stator voltage-oriented control   (b)   stator flux-oriented control
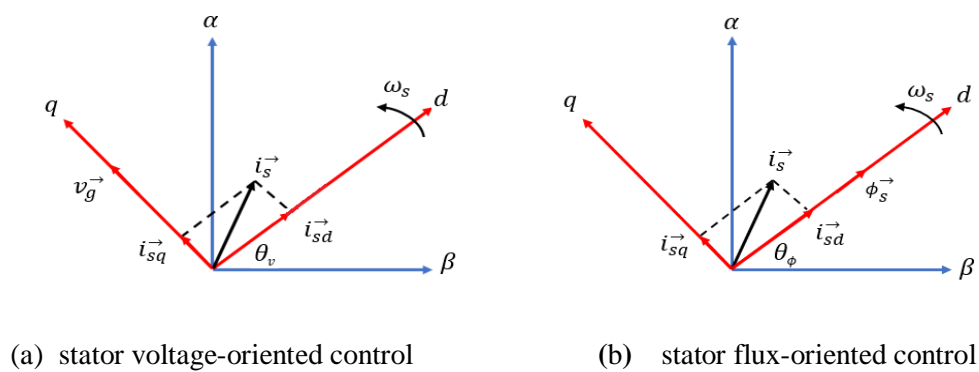
Fig 2.5 Vector diagram of the DFIG control system.

2.8.1 Stator field orientation control

The SFOC scheme independently controls the two-axis rotor currents (I_{dr}^* and I_{qr}^*) in a synchronously rotating reference frame dq aligned with the stator flux linkage vector position, as illustrated in the phasor diagram in Fig 2.6 The SFOC scheme is dependent on the correct estimation of the position of the stator flux linkage space vector. A common approach to estimating the flux linkage position is based on neglecting the stator resistive voltage drop and thus aligning the flux linkage space vector with the position that is lagging the stator voltage space vector by $90°$ [116]. With the SFOC approach, the flux linkage vector is conventionally aligned with the d-axis of the synchronously rotating reference frame. Furthermore, its angle θ_s with respect to the stator reference frame ($\alpha_s \ \beta_s$) can be simply obtained from the three-phase stator voltage measurements using the PLL [117].
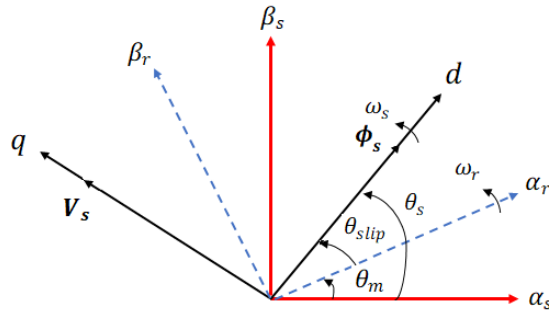
Fig. 2.6 Phasor diagram.

The rotor reference frame (α_r, β_r) position with respect to the stationary reference frame is calculated from the encoder output signals. In combination with θ_s, the rotor reference frame position is used for determining the real-time value of the rotor slip angle, θ_{slip}, in DSPACE. The real-time slip angle value is used for the transformation of all the relevant rotor variables to the synchronously rotating reference frame aligned with the flux linkage vector required for real-time SFOC algorithms. In the SFOC, the stator flux is aligned with the d-axis and kept constant.

$$\begin{cases} \psi_{ds} = \psi_s \\ \psi_{qs} = 0 \end{cases} \tag{2.27}$$

Considering the decoupling, the set of equation (B.2.1) of the stator and rotor voltages are simplified as:

$$\begin{cases} v_{ds} = R_s i_{ds} + \dfrac{d}{dt}\psi_{ds} \\ v_{qs} = R_s i_{qs} + \omega_s \psi_{ds} \end{cases} \tag{2.28}$$

$$\begin{cases} v_{dr} = R_r i_{dr} + \dfrac{d}{dt}\psi_{dr} - \omega_r \psi_{qr} \\ v_{qr} = R_r i_{qr} + \dfrac{d}{dt}\psi_{qr} + \omega_r \psi_{dr} \end{cases} \tag{2.29}$$

Neglecting the stator resistance and referring the DFIG to the chosen reference frame, the stator steady state voltage, flux and torque equations can be simplified as:

$$\begin{cases} v_{ds} \cong 0 \\ v_{qs} = \omega_s \psi_{ds} \end{cases} \tag{2.30}$$

The equations relating the stator currents to the rotor currents are deduced as:

$$\begin{cases} I_{ds} = \dfrac{\psi_{ds}}{L_s} - \dfrac{L_m}{L_s} I_{dr} \\ I_{ds} = \dfrac{\psi_{ds}}{L_s} - \dfrac{L_m}{L_s} I_{dr} \end{cases} \tag{2.31}$$

The flux equations are:

$$\begin{cases} \psi_{dr} = L_r \sigma I_{dr} + \frac{L_m}{L_s} \psi_{ds} \\ \psi_{qr} = L_r \sigma I_{qr} \end{cases} \tag{2.32}$$

where: $\sigma = 1 - \frac{L_m^2}{L_s L_r}$

Hence, the rotor voltage equations are defined as:

$$\begin{cases} v_{dr} = R_r i_{dr} + L_r \sigma \frac{di_{dr}}{dt} - \omega_r L_r \sigma i_{qr} + \frac{L_m}{L_s} \frac{d\psi_{ds}}{dt} \\ v_{qr} = R_r i_{qr} + L_r \sigma \frac{di_{qr}}{dt} + \omega_r L_r \sigma i_{dr} + \omega_r \frac{L_m}{L_s} \psi_{ds} \end{cases} \tag{2.33}$$

The equations relating the stator currents to the rotor currents are deduced as:

$$\begin{cases} \frac{di_{dr}}{dt} = \frac{1}{\sigma L_r} \left(v_{dr} - R_r i_{dr} + \omega_r L_r \sigma i_{qr} - \frac{L_m}{L_s} \frac{d\psi_{ds}}{dt} \right) \\ \frac{di_{qr}}{dt} = \frac{1}{\sigma L_r} \left(v_{qr} - R_r i_{qr} - \omega_r L_r \sigma i_{dr} - \omega_r \frac{L_m}{L_s} \psi_{ds} \right) \end{cases} \tag{2.34}$$

The torque equation is expressed as:

$$T_{em} = -p \frac{L_m}{L_s} \psi_{ds} i_{qr} \tag{2.35}$$

The active and reactive powers at the stator side of DFIG are:

$$\begin{cases} P_s = -v_{qs} \frac{L_m}{L_s} i_{qr} \\ Q_s = v_{qs} \frac{\psi_{ds}}{L_s} - v_{qs} \frac{L_m}{L_s} i_{dr} \end{cases} \tag{2.36}$$

Fig. 2.7. presents the classical SFOC control algorithm of the stand-alone DFIG system. From Figure 2.7, the three-phase stator voltage and current and the three-phase rotor current are measured. Instead, the reference synchronous angular frequency ω_s is set by the user depending on the operating frequency. Then, the stator angular angle of the flux θ_s is deduced from the integral of the set value of the synchronous angular frequency. Furthermore, an encoder is used for measuring the mechanical rotor angle converted to its electrical equivalent using the number of pair-poles. The three-phase parameters measured are then transformed into a synchronous dq-reference frame. It is worth noticing

that the three-phase rotor current is transformed into a synchronous dq-reference frame using the slip angular phase $\theta_r = \theta_s - \theta_m$.

The set value of the stator voltage magnitude $|V_s^*|$ is compared to the measured stator voltage magnitude $|V_s|$ obtained by $\sqrt{(v_{ds}^2 + v_{qs}^2)}$.

The error in the stator voltage magnitude is the input of the outer PI controller. The output of the outer PI controller is the d-axis rotor current reference. The d-axis rotor current reference is then compared to the d-axis rotor current using the inner PI controller. The d-axis rotor voltage reference is obtained from the subtraction of the output of the PI controller by the compensation terms, as shown in Fig 2.7. On the other hand, the q-axis current reference is chosen to force the d-axis flux linkage to aligne along the d-axis of the synchronous dq reference frame. The q-axis rotor current reference is then compared to its measured value to form the error signal which enter the inner PI controller. The output of the PI controller is then added to the compensation terms as depicted in Fig 2.7 to obtain the reference q-axis rotor voltage. Both the d-axis and q-axis rotor voltages references are then transformed into the abc/dq reference frame. These reference d-axis and q-axis rotor voltage quantities are inputted to the PWM function in order to obtained the actuating signals.

From Fig. 2.7, the decoupling terms are used in both current control loops in order to control the i_d and i_q independently. The decoupling terms, $\omega_r L_d i_d$ and $\omega_r L_q i_q$, are depicted from the two voltage equations of the DFIG (2.8)-(2.9). The two rotor voltage equations are coupled by the decoupling terms, $\omega_r (L_m/L_s \psi_s + \sigma L_r i_{dr})$ and $\omega_r \sigma L_r i_{qr}$ By subtracting/adding these terms in the current control loops, the two currents i_d and i_q can be controlled independently. This also simplifies the transfer function of the DFIG in the two current control loops. After some mathematical manipulations, the following transfer function of the DFIG for the d- and q-current loops are obtained:

$$G_d(s) = \frac{1}{\delta L_r s + R_r} = \frac{1}{R_r(\tau_r s + 1)} \qquad (2.37)$$

$$G_q(s) = \frac{1}{\delta L_r s + R_r} = \frac{1}{R_r(\tau_r s + 1)} \qquad (2.38)$$
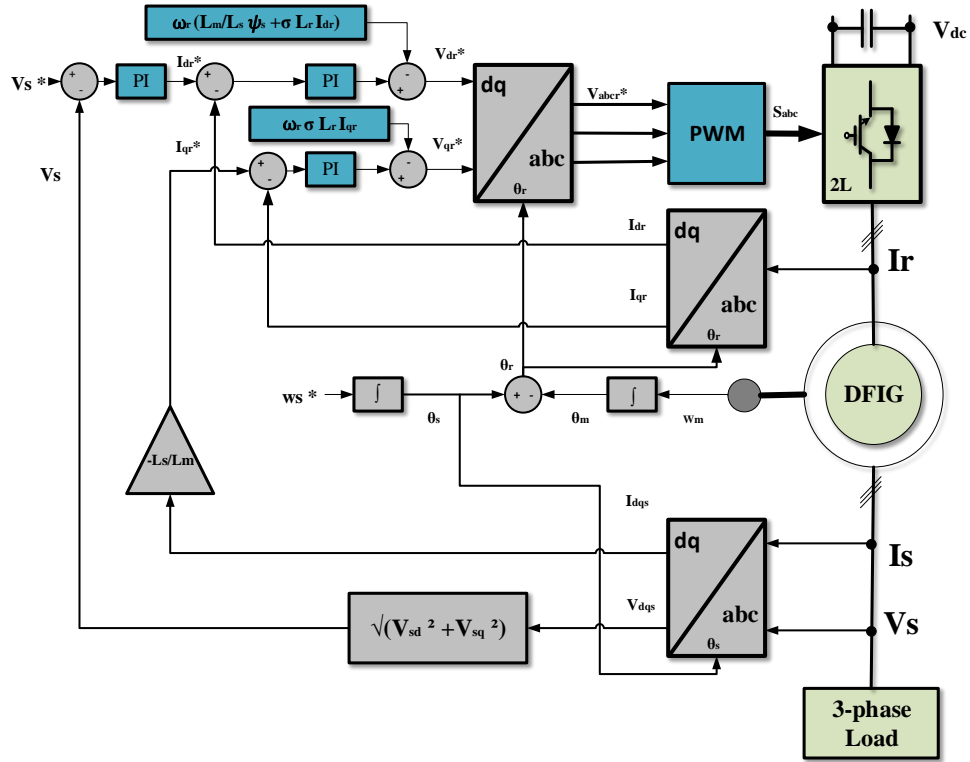
Fig. 2.7. Basic control strategy scheme of the RSC for stand-alone DFIG system.

Where $\tau_r = \frac{\delta L_r}{R_r}$ are the electrical time constants along the d- and q-axis, respectively, and s is the Laplace variable. The closed-loop systems of the current control along the d- and q-axis are shown in Fig. 2.9. The RSC is usually included in the design procedure of these closed-loop systems as a delay equal to [66]

$$T_d = \frac{T_s}{2}$$

where T_s is the sampling time.

In the s plane, the delay introduced by the RSC can be approximated by a first order lag system as [66]

$$v_{dq}(s) = e^{-sT_s} v_{dq}^*(s) \approx \frac{1}{(1+sT_d)} v_{dq}^*(s) \quad (2.39)$$

Also from Fig. 2.8, FOC is applied for the standalone DFIG to achieve the current-decoupling control. The stator flux vector is oriented along the d-axis, while the stator voltage vector needs to align along the q-axis to achieve voltage-decoupling control [28].

By forcing, the stator flux ψ_{sq} and stator voltage v_{sd} to be null the orientation is achieved. This leads to a dynamic first-order transfer function with a derivative-time equal to τ_s as below :

$$\psi_{sd} = |\psi_s| = \frac{L_m}{\tau_s.s+1}.i_{rd} \qquad (2.40)$$

Where stator time constant $\tau_s = \frac{L_s}{R_s}$, and by set $v_{sq} = \omega_s\psi_{sd}$, the closed-loop systems of the stator voltage control along the d-axis are shown in Fig. 2.9.,
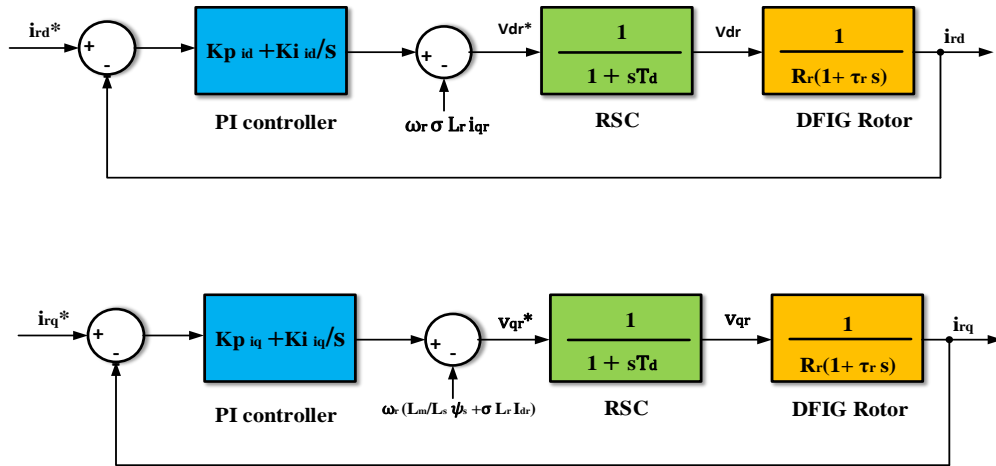
Fig. 2.8. Closed-loop system of the *d-q* axis current control [66].
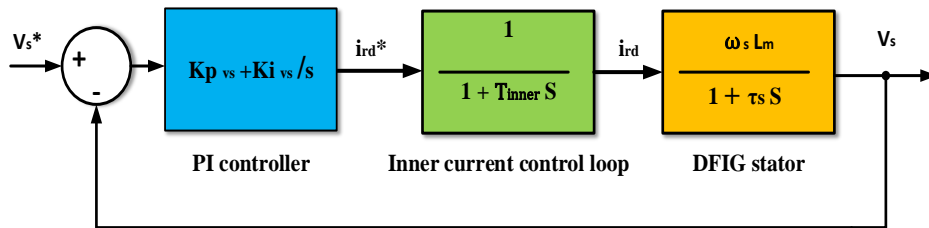
Fig. 2.9. Closed-loop system of the stator voltage magnitude control [66].

The design of the PI controllers parameters of the current and stator voltage can be usually carried out using the Amplitude optimum method or the pole placement method [67, 68]. The control strategies for the standalone DFIG generator based on SFOC can be divided into two main categories: direct field oriented control, and indirect field oriented control [65, 69–74]. In the following chapters, these categories of control strategies will be improved and cost reduced.

2.9 Chapter conclusion

In this chapter, the modelling and control strategies of the RSC in stand-alone based on VC-FOC are presented. The control function within the VC scheme has commonly been performed by using PI controllers. One challenge is how to tune the parameters of the PI control loops to provide optimal performance of the system. Many, studies have tuned/calculated the PI controller's

parameters, using conventional methods and it is difficult to find the optimal controller parameters based on these methods. Therefore, the next chapter will be focused on advanced control algorithms to obtain the optimal controller for RSC of standalone DFIG.

Chapter 3

Improved RSC control of standalone DFIG generation system: Approach-1

Chapter 3

Improved RSC control of standalone DFIG generation system: Approach-1

3.1 Chapter introduction

The field-oriented control (FOC) is an extremely traditional control technique that can be used for DFIG based systems. This method has been extensively utilized especially in industrial applications. The principle of this method is to transfer the rotor current into a dq rotational reference frame. The FOC technique is implemented through conventional inner PI controller beside the pulse width modulation (PWM) which can apply the switching sequences to the voltage source converter (VSC). The advantages and disadvantages of this algorithm have been already discussed in many works [71-80]. One of the advantages is that the FOC provides accurate current conservation, which is the major goal in control of electrical drives. However, since the PI controllers and the modulation stage is needed for hardware implementation, the complexity and the control system cost will increase. In the last years, Hysteresis Current Controllers (HCC) and Finite State Predictive Control (FS-PC) has been successfully used for several applications such as power electronics and electrical drives [72-76]. However, concerning the DFIG based WECS systems, only a HCC and FS-PCC and strategy has been described in [88, 94], where neither addressing the standalone operation mode nor the experimental implementation has been reported.

The major contribution of this chapter is to adopt the HCC and FS-PCC for the standalone DFIGs in order to overcome the above-mentioned disadvantages and improve the control of standalone DFIGs, this control approach seems not been covered yet by the previously published literature in the field of standalone DFIG applications. The idea of FS-PCC is to manipulate the discrete model of DFIG to predict the rotor current by each possible state. The switching state, that gives a minimal cost function value, will directly selected during the next sampling period. Consequently, neither PI current regulators nor pulse width modulators were needed, which is a vital advantage of the proposed HCC and FS-PCC when compared with previous control methods. The main challenge of this work is to improve stator voltage and frequency control at variable wind speeds and varying loads. Furthermore, simulation and experimental results are provided in this chapter. The attain results manifest that the suggested control strategy has perfect transient performance and steady-state

response during various load or speed variations. This chapter is structured as follows: in Section (II) HCC controller of the standalone DFIG system is presented. In Section III modeling of FS-PCC for standalone DFIG are presented. In Section IV, simulation and experimental results are extended for various operating conditions. Finally, a chapter conclusion is given in Section V.

3.2 Proposed HCC controller design for Standalone DFIG

The effective way to generate PWM control signals to the inverter is to use hysteresis current controllers (HCCs). This control type, also known as bang-bang control, is intended for the direct control of the AC phase currents, being very simple from a conceptual point of view and quite straightforward to implement[98].

3.2.1 Hysteresis Current Controllers

The switching strategy is done by using three hysteresis comparators, each being responsible to control separately the current in its corresponding phase, as shown in Fig 3.1
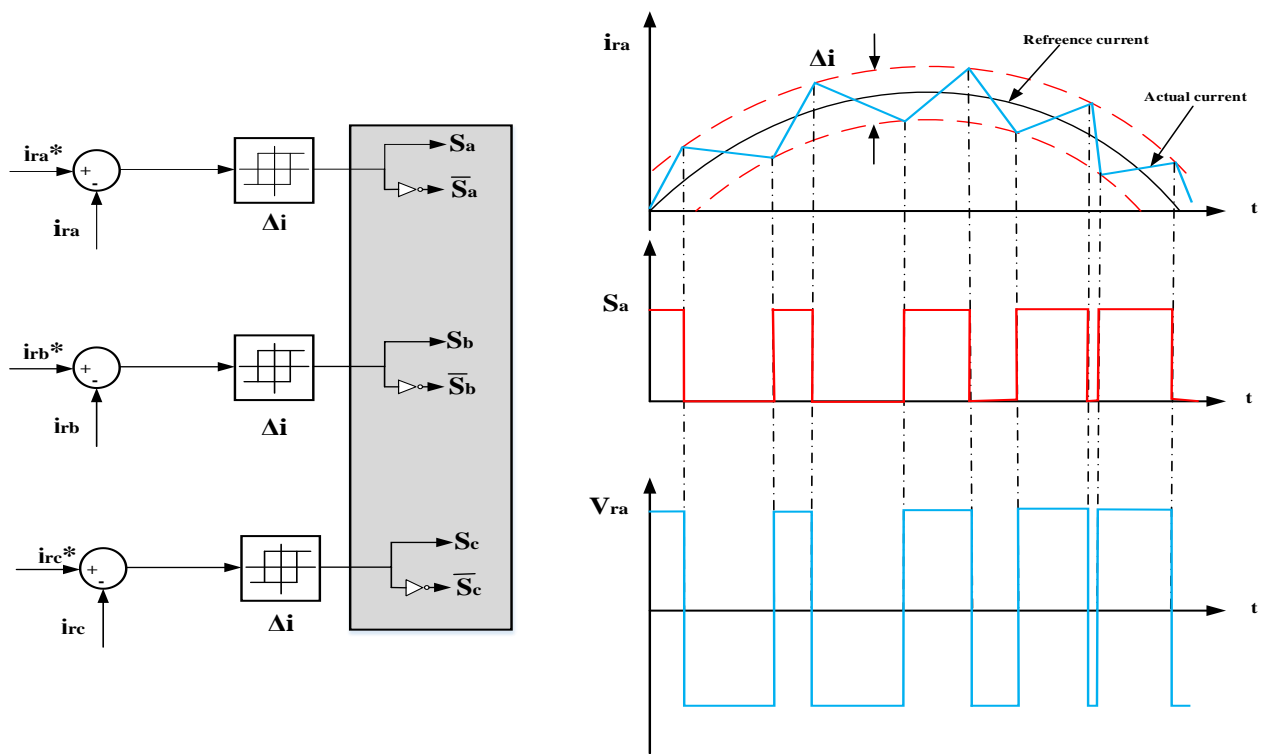
Fig. 3.1. Hysteresis current control operating principles.

Each controller determines the semiconductors switching states in each inverter arm in such a way that the corresponding phase current is kept within a defined hysteresis band Δi. the measured motor phase currents are subtracted to their reference signals and the resulting error is fed to the hysteresis comparators. If this error tends to pass the hysteresis band lower limit, the top power

switch of the corresponding phase is turned off, turning on the lower one. On the contrary, if the error tends to be greater than the higher limit, the top power switch is turned on and the bottom one is deactivated. In this way, the motor phase currents will be as much sinusoidal as smaller is the hysteresis band. However, this leads to the increasing of the semiconductors switching frequency and consequently, the inverter power losses.

The dynamic performance of this approach is considered to be excellent since maximum voltage values are applied to minimize the errors and it is only limited by the switching speed and load time constant. Furthermore, this technique is also very simple, presents an outstanding robustness, lack of tracking errors and it is very independent of the load parameters. As main disadvantages it can be pointed out its variable switching frequency, the fact that its discrete implementation does not guarantee that the error is strictly limited within the hysteresis band, the lack of interaction between the three phases which limits the generation of zero-voltage vectors and the increased switching losses at lower modulation or motor speed values.

3.2.2 Proposed HCC controller design for standalone DFIG

Fig. 3.2. presents the block diagram of this vector control strategy applied to a standalone DFIG, using current controllers to generate the RSC gate command signals. The terminal output voltage at the stator of DFIG is regulated by controlling direct axis rotor current (i_{rd}). The direct axis reference rotor current ($i_{rd}{}^*$) is obtained by processing the terminal voltage error between reference and estimated terminal voltage ($v_{an}{}^*$ and v_{an}) through PI (Proportional Integral) controller. As the stator of the DFIG is connected in Y- connected mode, so the magnitude $|v_s|$ of the stator voltage is calculated as:

$$| \boldsymbol{v_s}| = \sqrt{(\boldsymbol{v_{sd}}^2 + \boldsymbol{v_{sq}}^2)} \qquad\qquad (3.1)$$

Here DFIG generates as much power as needed by the load. so the system is not working on MPPT condition. so the speed is adjusted in such a way to generate required amount of power. The active power component of rotor current (i_{rq}) is calculated from the active power component of stator current (i_{sq}) as [9],

$$i_{rq}{}^* = -\frac{L_s}{L_m} i_{sq}{}^* \qquad\qquad (3.2)$$

The d and q axis reference rotor components ($i_{rd}{}^*$ and $i_{rq}{}^*$) are converted into three phase reference rotor currents $i_{rabc}{}^*$ using inverse park transformation with slip angle (θ_r) [98].

Where, $\qquad\qquad\qquad\qquad \theta_r = \theta_s - \theta_m \qquad\qquad\qquad (3.3)$

where θ_s is the angle calculated by integrating the fixed electrical speed ω_e (314 rad/sec). The θ_m is the electrical rotor angle calculated from the encoder pulses. These reference rotor currents (i_{ra} *, i_{rb} *, i_{rc} *) are compared with the sensed rotor currents (i_{ra}, i_{rb}, i_{rc}) and the current error is computed and the pulses are generated to the RSC accordingly using hysteresis current controller.

Fig. 3.2. Block diagram of the HCC for RSC.

3.3 Proposed finite-state predictive current control for standalone DFIG

The rotor currents can be predicted for all sectors of the rotor voltage, in the proposed FS-PCC algorithm, these predicted rotor currents will contrast with the reference value of rotor current and then are evaluated by a simple cost function. The minimum value of the cost function will reveal the optimal vector rotor voltage which will be applied for the RSC in the next sampling period. [90-94].

3.3.1 Rotor current prediction model

The prediction algorithm of the rotor current i_r is based on the discrete Euler-forward model of the complex rotor current of the DFIG as

$$\frac{di_r}{dt} \approx \frac{i_r(k+1) - i_r(K)}{T_s} \qquad (3.4)$$

T_s is the sampling time. Also, the rotor flux is estimated by:

$$\psi_r(k) = \psi_r(k-1) + T_s.\big(v_r(k) - R_r.i_r(k)\big) \quad (3.5)$$

Then the stator flux can be estimated by using the equation **(2.20)**

According to [2-3], the rotor current is predicted through the expression as follows:

$$i_r(k+1) = \left(1 + \frac{T_s}{\tau_\sigma}\right).i_r(k) + \frac{T_s}{\tau_\sigma + T_s}.\left\{\frac{1}{R_\sigma}\left[\left(\frac{k_s}{\tau_s} + k_s j\omega_m\right)\psi_s(k) + v_r(k) - k_s v_s(k)\right]\right\} \quad (3.6)$$

Where $k_s = \frac{L_m}{L_s}$; $\tau_s = \frac{L_s}{R_s}$; $\tau_\sigma = (L_r * \sigma)/R_\sigma$; $R_\sigma = R_r - R_s.k_s^2$.

In the actual systems that perform predictive control, a large amount of time calculation is required, and a large amount of retard time introduced during the excitation must be compensated. The time delay compensation of the FS-PCC algorithm must be accomplished by advancing the current prediction two-steps ahead [90]. For instance, supposing that the determined vector will be used at the time $(k + 1)$, then it is necessary to predict the current value at $(k + 2)$ time. By moving (15) one time-step forward, the equation of ir $(k + 2)$ can be written as :

$$i_r(k+2) = \left(1 + \frac{T_s}{\tau_\sigma}\right).i_r(k+1)$$
$$+ \frac{T_s}{\tau_\sigma + T_s}.\left\{\frac{1}{R_\sigma}\left[\left(\frac{k_s}{\tau_s} + k_s j\omega_m\right)\psi_s(k+1) + v_r(k+1) - k_s v_s(k+1)\right]\right\} \quad (3.7)$$

3.3.2 Minimization of the cost function

For the seven vectors of the rotor voltage which can be produced through the RSC, the rotor current will be predicted at the future sampling time. A cost function is made to evaluate all predicted rotor currents and it is used as a condition for selecting the best vector of the rotor voltage. The vector of the rotor voltage that minimizes the cost value will choose to use in the next period. The cost function is expressed by the absolute error between the predicted and reference rotor current, as the below equation:

$$g = \left|i_{r\alpha}^*(k) - i_{r\alpha}^p(k+2)\right| + \left|i_{r\beta}^*(k) - i_{r\beta}^p(k+2)\right| \quad (3.8)$$

Where $i_{r\alpha}^*(k)$ and $i_{r\beta}^*(k)$ are the reference of rotor currents in $\alpha\beta$ coordinate frame. Besides, $i_{r\alpha}^p(k+2)$ and $i_{r\beta}^p(k+2)$ are the predictive rotor currents.

3.3.3 Proposed FS-PCC controller design for Standalone DFIG

Fig. 3.3. shows the global control scheme of stator voltage and frequency control based FS-PCC, the output voltage-magnitude in the stator of DFIG is controlled by regulating the d-rotor current (i_{rd}). While the d-rotor current reference (i_{rd} *) can be generated after reducing the error between the desired and measured voltage-magnitude (v_{an} * and v_{an}) through a PI (Proportional Integral) controller [98]. This proposed FS-PCC is developed to be realized in a fixed $\alpha\beta$ rotor reference frame. the Park transformation matrix, the reference rotor currents in dq is transformed to $\alpha\beta$ coordinates by :

$$\begin{bmatrix} i^*_{r\alpha} \\ i^*_{r\beta} \end{bmatrix} = \begin{bmatrix} \cos(\theta) & -\sin(\theta) \\ \sin(\theta) & \cos(\theta) \end{bmatrix} \cdot \begin{bmatrix} i_{rd}{}^* \\ i_{rq}{}^* \end{bmatrix} \qquad (3.9)$$

Finally, to control the output stator frequency at the desired value fs=50 Hz, all the stator quantities must be synchronized with the dq rotating reference frame. Hene, the d and q axis of both stator voltages and stator currents are generated by transforming the three-phase stator quantities through the park transformation with angle (θ_s), which is obtained by integrating the reference stator frequency ω_s (314 rad/sec) [98].
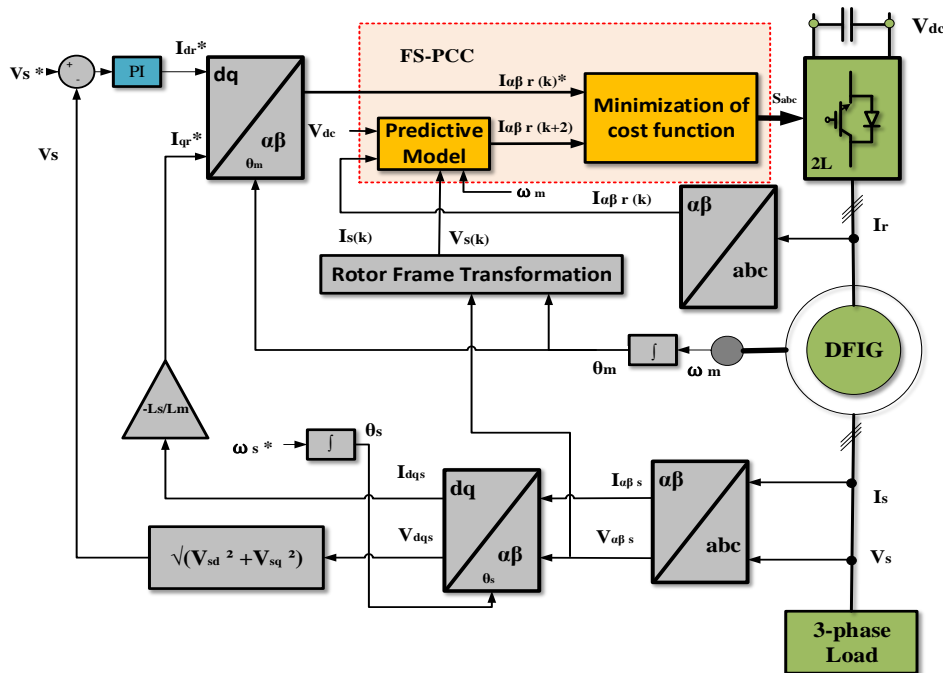
Fig. 3.3 Block diagram of FS-PCC for RSC.

3.4 Simulation model and experimental Setup

The simulation model has been built in Matlab/Simulink together with the SimPower Systems software. Moreover, the experimental results have been obtained using a test platform that developed in laboratory. The characteristics of the DFIG that used for simulation and experimental are reported in the Appendix (A). Fig. 3.4. portray the descriptive diagram and a picture of the experimental prototype setup, it is composed of a prime mover 3 kW DC motor, 3 kW DFIG, 4 kW/420Ω three-phase resistive load. Semikron module IGBT inverter. dSPACE 1104 control card, a host PC running with Matlab/Simulink software. The Hardware DS1004 card is exploited to implement the FS-PCC strategy, with a sampling time of 100 μs.
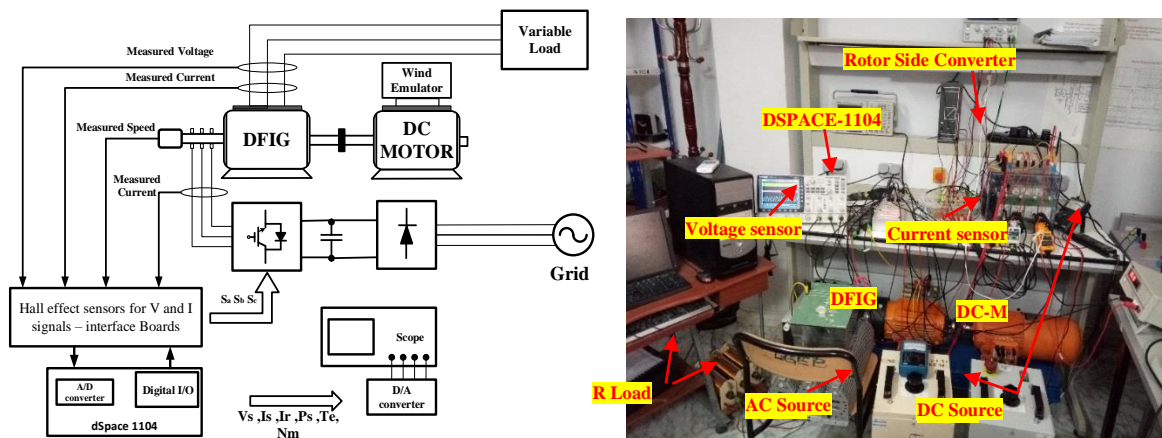
Fig. 3.4 A laboratory prototype of the experimental setup.

3.5 Obtained Results

to determine the performance of the proposed control methods, the behavior of the controlled system is evaluated during the following running conditions:

a) Steady Stator voltage-magnitude variation

b) Load change

c) Rotational speed variation

3.5.1 HCC

This section presents simulation and experimental examination test results to verify the behavior of the developed HCC.

a. Stator voltage-magnitude variation

In this test, the response of the standalone DFIG system to a step change in command stator-voltage magnitude (at fixed load and speed) is investigated. Fig. 3.4. (a), (b) presents the results of a step change of stator-voltage magnitude from 180 V to 250 V at 1.7 s and then change from 250 V to 180 at 3.7 s when the DFIG are driven with a constant speed of 1450 rpm and supply a fixed 2 Kw of

resistive load. Analyzing the response of the systems gives, the systems does not overshot the command voltage-magnitude. However, consider to the classical PI controller, optimization the PI gains can ensure notably faster response of the actual stator-voltage magnitude to step changes in the reference value, in terms of rise and settling times. This test illustrates the capability of the proposed control method for tracking the stator-voltage amplitude.

(a)   (b)

Time (s)   **Time (400ms/div)**
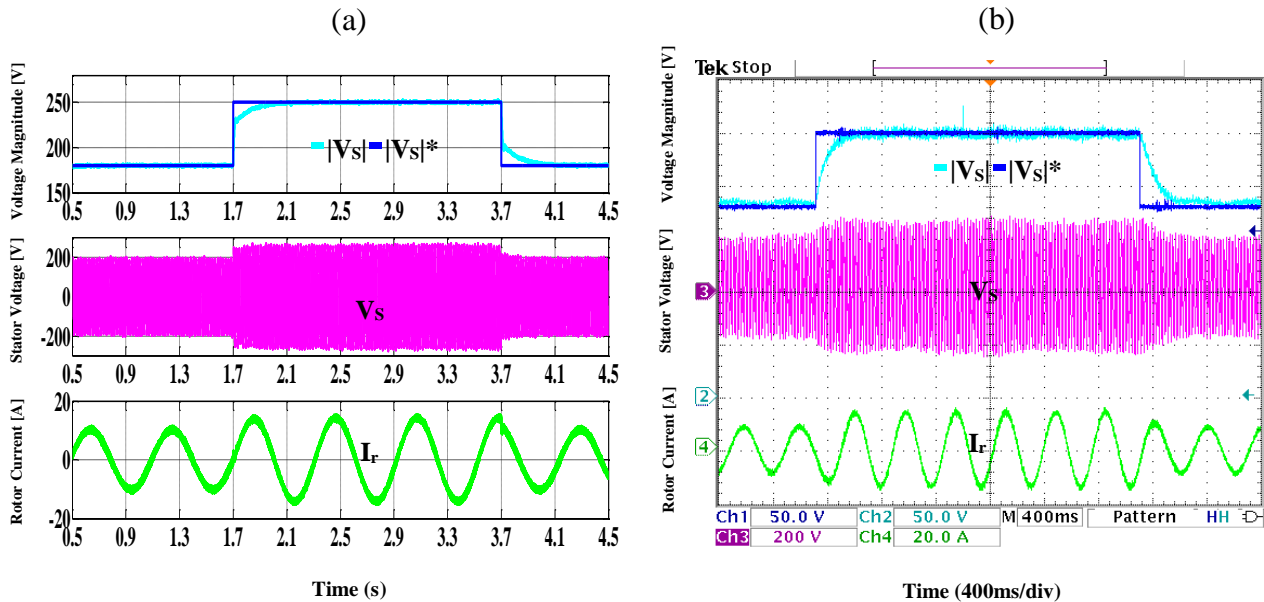
Fig. 3.5 HCC system response under step variation in the reference of stator voltage amplitude .a Simulation results .b Experimental.CH1: reference of stator voltage magnitude (50V/div), CH2: stator voltage magnitude (50V/div), CH3: stator phase voltage (200V/div), CH4: rotor phase current (20A/div).

b. Load change

In this test, the ability of proposed control method to reject load disturbances was investigated at 200V reference voltage magnitude, and 1450 rpm of rotor speed. The effect of applying an increase in load (from 20% to 75% rated 4 kw resistive load), then removing the last addition of load after 2 seconds was investigated. The system response of the proposed HCC with the PI controller are presented in Fig 3.5 (a), (b) and Fig 3.6 (a), (b)   It can be seen that the PI offers significant faster response with smaller overshoot / undershoot. The PI response over/undershoot is limited ±45 V. The rotor currents systems show an acceptable overshoot and ripples. Illustrates the ability of the proposed HCC to reject load disturbances is presented.
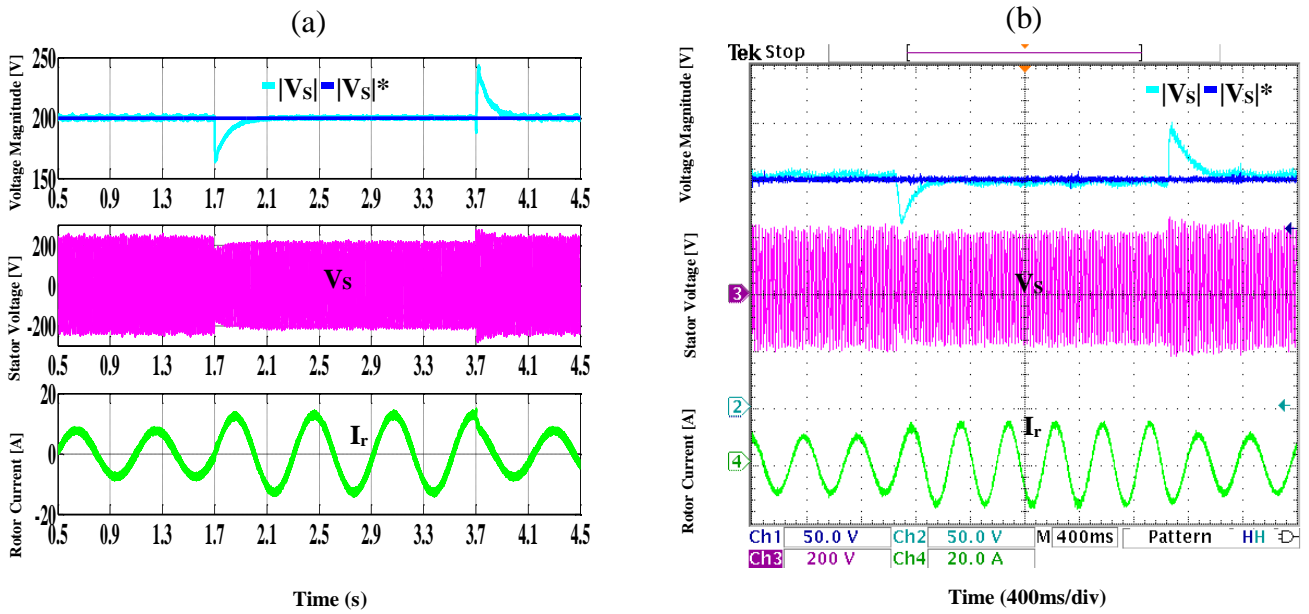
Fig. 3.6 HCC system response under load variety in the reference of stator voltage amplitude .a Simulation results .b Experimental.CH1: reference of stator voltage magnitude (50V/div), CH2: stator voltage magnitude (50V/div), CH3: stator phase voltage (200V/div), CH4: rotor phase current (20A/div).
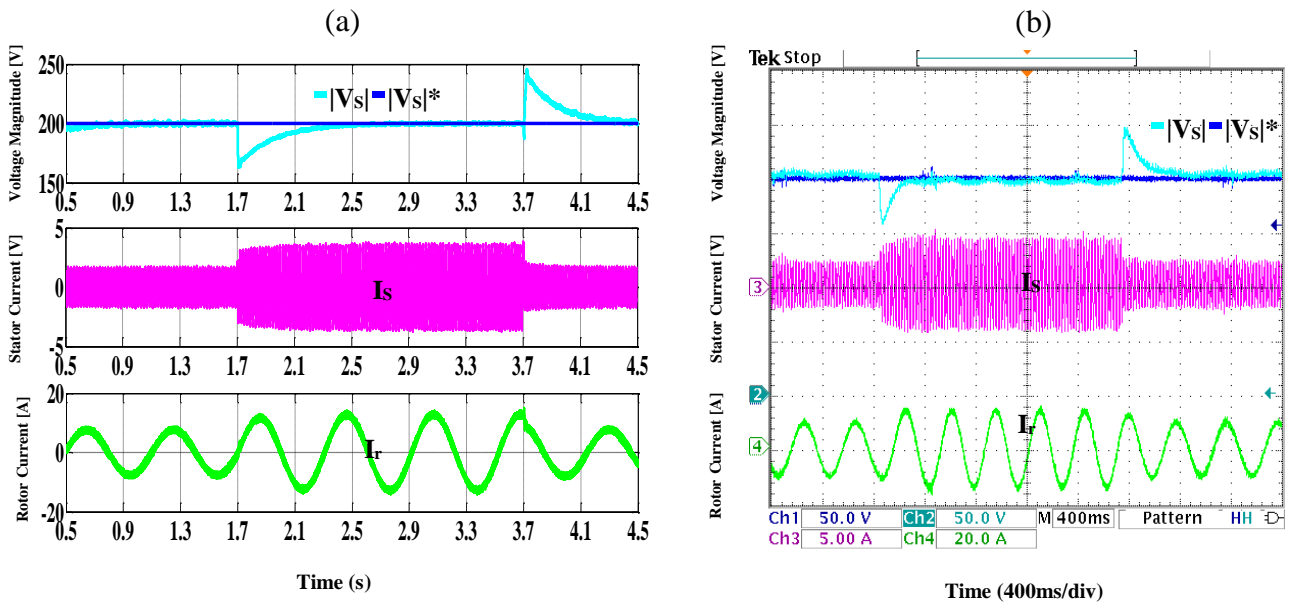
Fig. 3.7 HCC system response under load variety .a Simulation results .b Experimental. CH1: reference of stator voltage magnitude (50V/div), CH2: stator voltage magnitude (50V/div), CH3: stator phase current (5A/div), CH4: rotor phase current (20A/div).

c. Rotational speed variation

In this test, the case of a sudden change in rotor speed is concerned, simulated by a ±150 rpm change in rotor speed. The rotor speed are changed from 1450 rpm to 1300 rpm at fixed stator voltage magnitude and load. The response is plotted in Fig 3.8 (a), (b).It can be seen that the experimental

results are equivalent to the simulation results. The test results shows that the HCC transient perturbation is significantly smaller. The results confirm greater robustness of the HCC in case of sudden change in rotor speed.
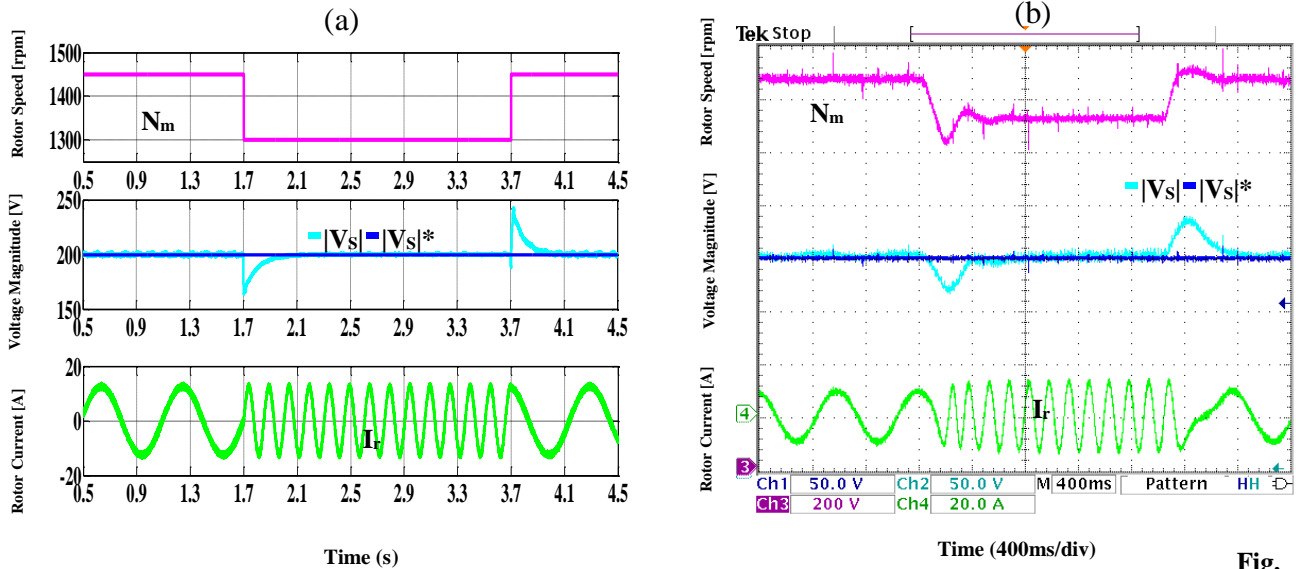
Fig.

3.8 HCC system response under rotor speed variety. CH1: rotor speed (200 rpm/div), CH2: reference of stator voltage magnitude (50V/div), CH3: stator voltage magnitude (50V/div), CH4: rotor phase current (20A/div).

3.5.2 FS-PCC

This section presents simulation and experimental examination test results to verify the behavior of the developed FS-PCC.

a. Stator voltage-magnitude variation

Firstly, the DFIG is driven with a constant speed of 1450 rpm and supplies a fixed 2 Kw of resistive load. To show the dynamic performance of the suggested technique, a variation in the reference of output voltage has been applied. the reference of the stator voltage amplitude has been varied from 200V to 280 V at 1.7 s from 280 to 200 at 3.7 s. The various simulation and the experimental test results are shown in Fig. 3.9-3.11. Fig 3.9 (a), (b) illustrates the reference and actual stator voltage amplitude stator phase voltage and rotor phase current. It is easily seen that the stator voltage amplitude has a perfect reference tracking capability for any change in reference value. Both simulation and the experimental show that the stator voltage and the rotor current have good sinusoid waveform due to the application of FS-PCC. The transient behaviors of the applied FS-PCC method for rotor current in the αβ axis are studied. Fig 3.10 (a), (b) presents the reference and measured rotor currents in the αβ axis in the presence of stator voltage steps, It can be noticed that the rotor currents are controlled successfully by the proposed FS-PCC method, which achieved a perfect transient

response during step change of the stator voltage. Also, Fig. 3.11 (a). (b) Show the variation of stator active power and electromagnetic torque of the generator with low ripples when the stator voltage amplitude is varied by increasing and decreasing its value.

Fig. 3.9 FS-PCC System response under step variation in the reference of stator voltage amplitude .a Simulation results .b
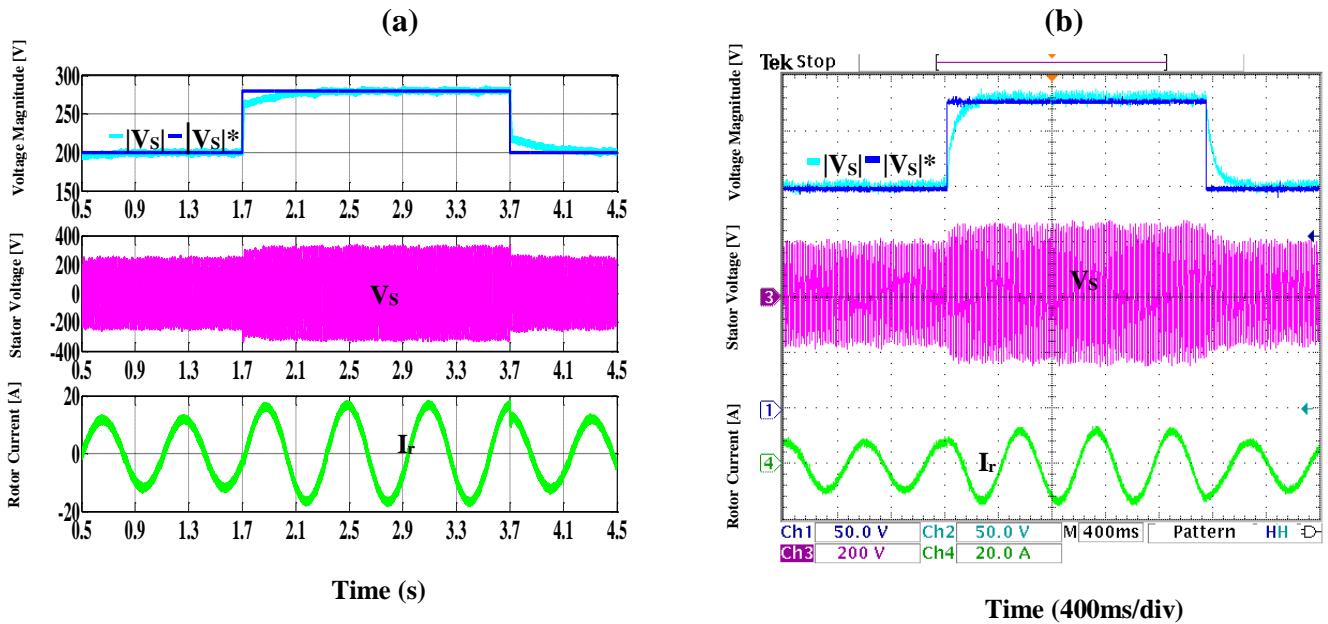
Experimental.CH1: reference of stator voltage magnitude (50V/div), CH2: stator voltage magnitude (50V/div), CH3: stator phase voltage (200V/div), CH4: rotor phase current (20A/div).
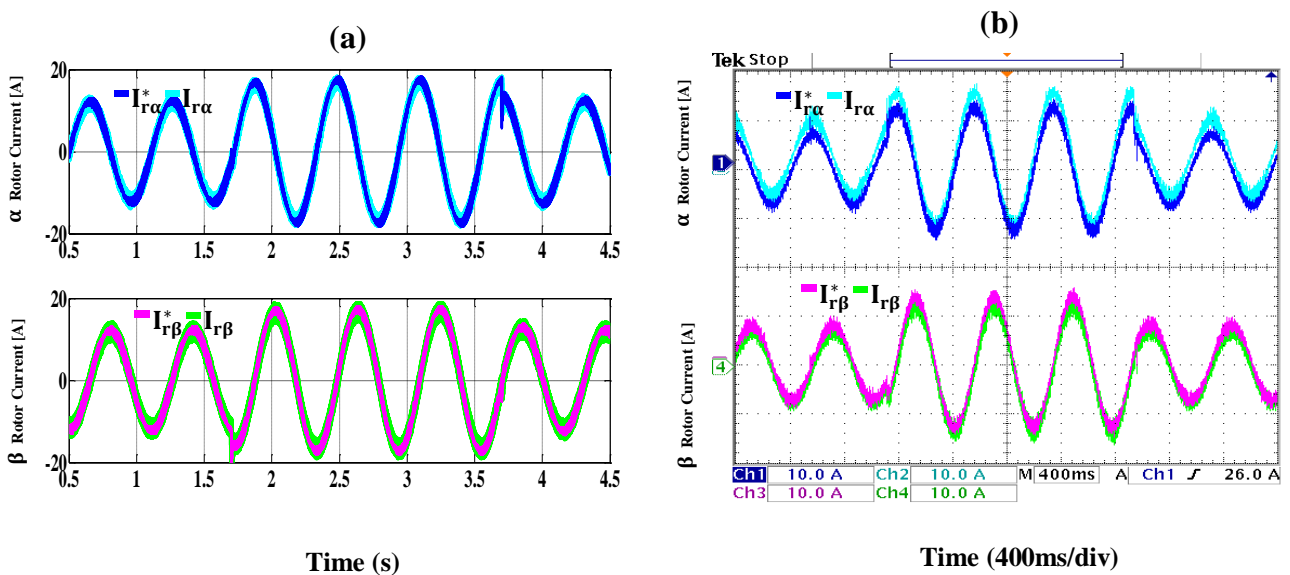

Fig. 3.10 FS-PCC rotor currents response in αβ under stator voltage change .a Simulation results .b Experimental.CH1: reference and measure rotor current in α axis (10A/div), CH2: reference and measure rotor current in β axis (10A/div).
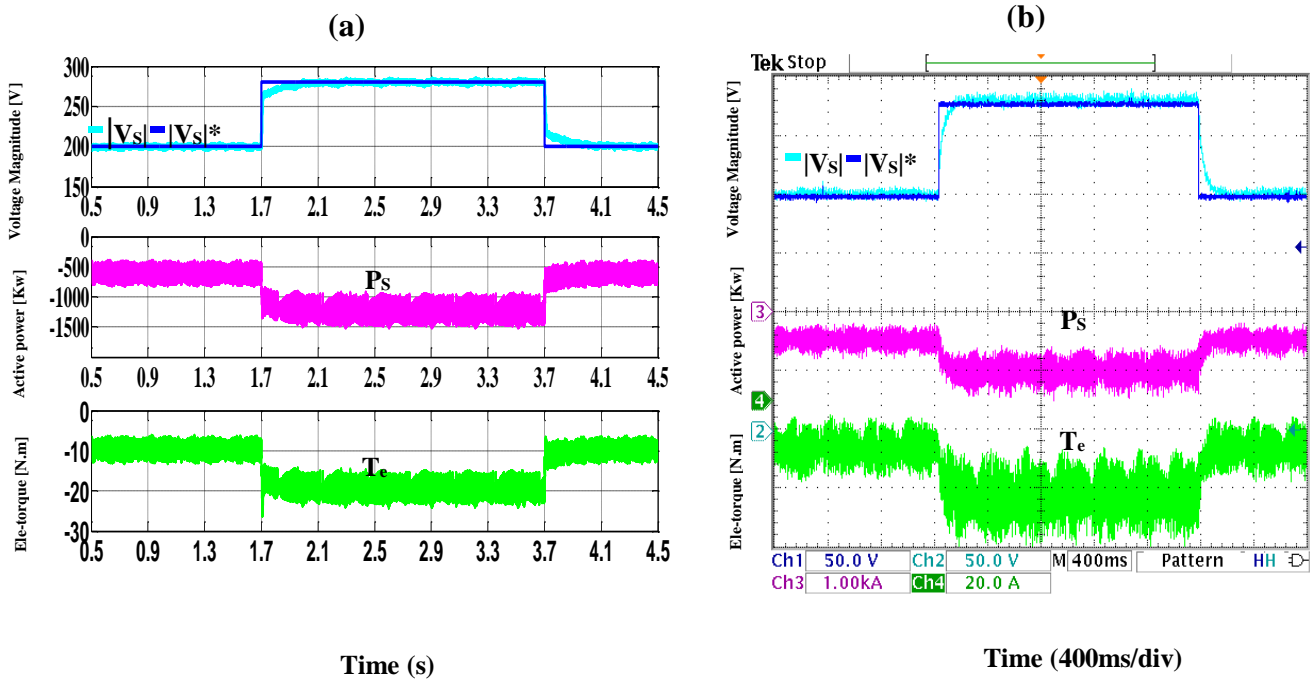
Fig. 3.11 FS-PCC system response under step variation in the reference of stator voltage amplitude .a Simulation results .b Experimental.CH1: reference of stator voltage magnitude (50V/div), CH2: stator voltage magnitude (50V/div), CH3: stator active power (1KW/div), CH4: electromagnetic torque (20N.m/div).

b. Load change

To investigate the impact of the load change, which is connected to the stator of DFIG, the load is increased from 2 kW to 4 kW at 1.7 s and is decreased from 4 kW to 2 kW at 3.7 s when the DFIG operates with a constant rotor speed of 1450 r/min. The various simulation results and experimental tests are obtained with the proposed FS-PCC strategy under the variation in load value are shown in Fig 3.12-3.14. Fig 3.12 (a) and (b), illustrates the reference and measured stator voltage amplitude, stator current, and rotor current, It is obvious that stator voltage amplitude has been affected by load application, by showing an undershoot, then the amplitude has been recovered quickly because of regulation loop. Also, the increase and decrease of the stator and rotor current is due to the increase and decrease in load value. Fig 3.13 (a) and (b), show that the stator voltage remains fixed at the desired value of 250 V despite the load variations. Fig 3.14 (a) and (b) show that the variation of stator active power and electromagnetic generator torque is evident due to the load variation. The negative value indicates that the delivered quantity is towards the load.
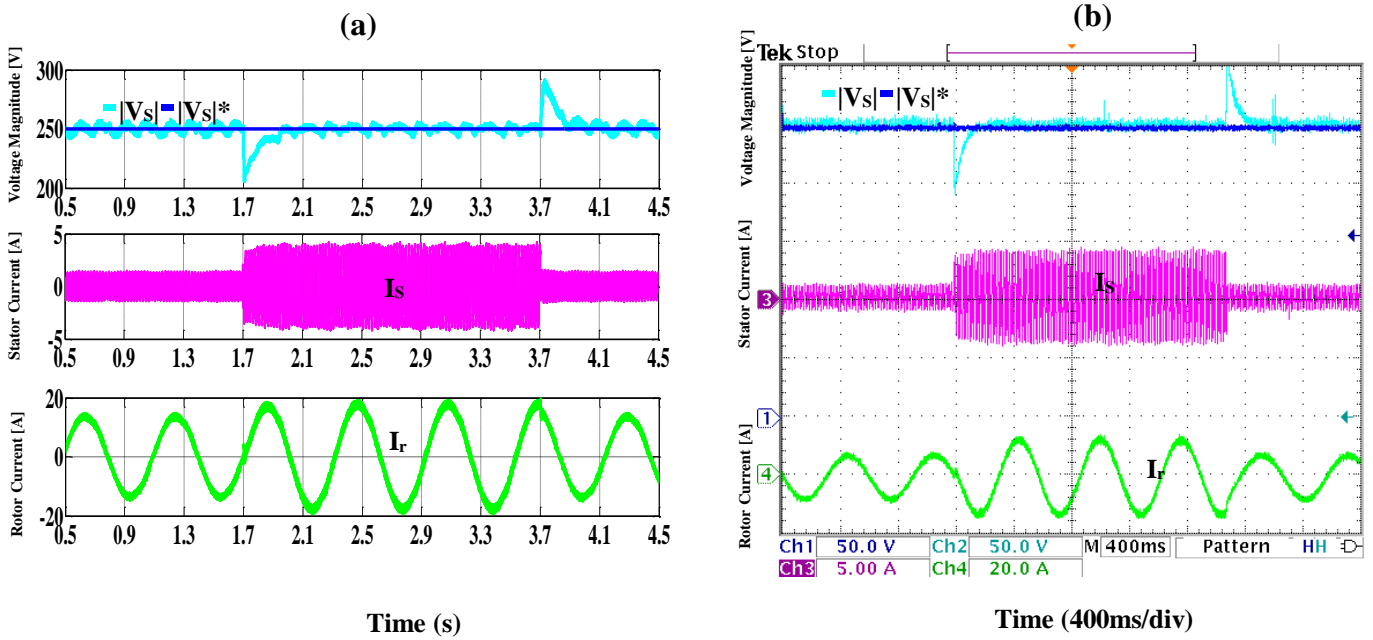
Fig 3.13 FS-PCC System response under load variety .a Simulation results .b Experimental. CH1: reference of stator voltage magnitude (50V/div), CH2: stator voltage magnitude (50V/div), CH3: stator phase current (5A/div), CH4: rotor phase current (20A/div).


Fig 3.14 FS-PCC system response under load variety .a Simulation results .b Experimental. CH1: reference of stator voltage magnitude (50V/div), CH2: stator voltage amplitude (50V/div), CH3: stator phase voltage (200V/div), CH4: rotor phase current (20A/div).

Fig 3.14 FS-PCC System response under load variety .a Simulation results .b Experimental.CH1: reference of stator voltage magnitude (50V/div), CH2: stator voltage amplitude (50V/div), CH3: stator active power (1KW/div), CH4: electromagnetic torque (20N.m/div).

6.3 Rotational speed variation

To reveal the stability of the suggested FS-PCC strategy, the responses of the system are analyzed during emulating a different wind gust scenario has been considered. The speed of the DFIG is suddenly decreased from 1450 to 1300 rpm at 1.7 s, and increased from 1300 to 1450 rpm at 3.7s. This test has been done with a fixed load of 2 kW and stator voltage 250 V. The obtained results during this rotor speed change are shown in Fig 3.15-3.16. Fig 3.15 (a) and (b), illustrates the rotational speed, the reference and actual stator voltage amplitudes, the rotor current. It can be seen that the magnitude is not affected at all and tracks the reference perfectly for the entire period of test. Fig 3.16 (a) and (b), illustrates the rotational speed, the slip angle, stator voltage, and rotor current, it is also seen that the variation of the frequency of rotor current is evident due to the rotor mechanical speed variation. Thus, from zoom (1) and (2) it is observed that the stator voltage frequency remains constant at 50 Hz despite the variation in rotor speed due to the sum of the mechanical and electrical rotor current frequency.

(a)   **(b)**
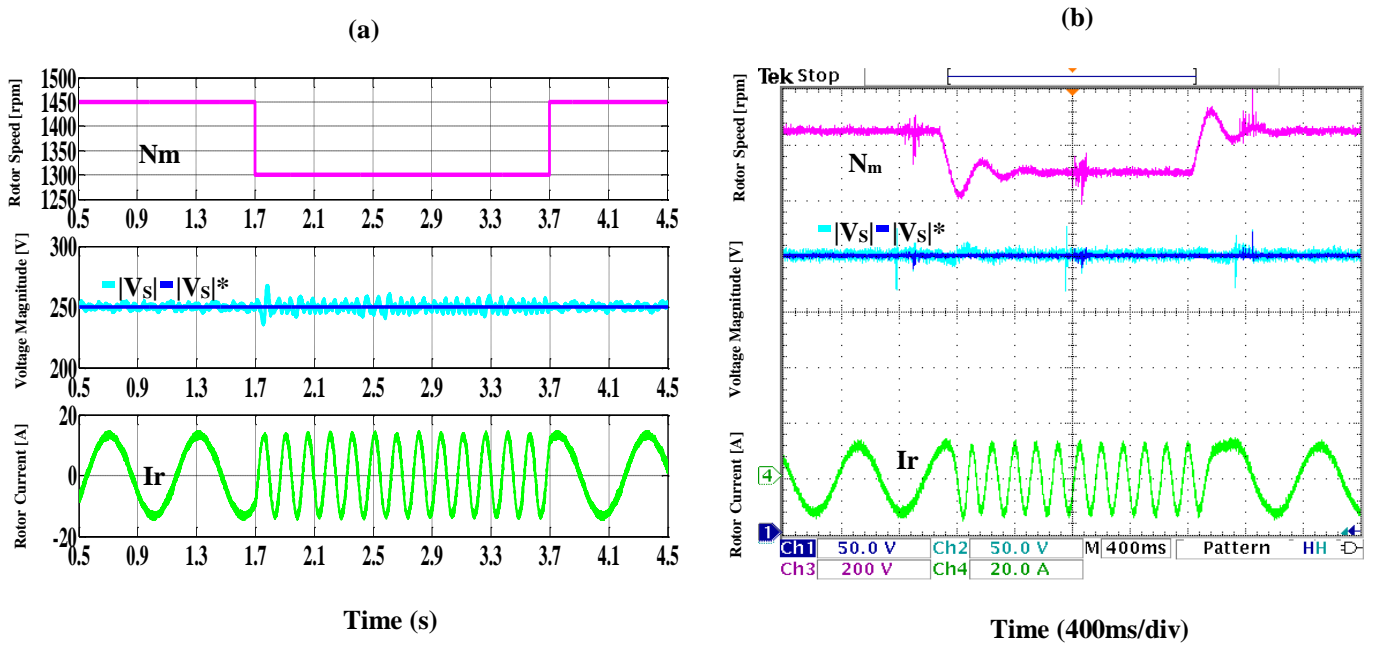
Fig 3.15 FS-PCC system response under rotor speed variety .a Simulation results .b Experimental. CH1: rotor speed (200 rpm/div), CH2: reference of stator voltage amplitude (50V/div), CH3: stator voltage magnitude (50V/div), CH4: rotor phase current (20A/div).

(a)   **(b)**
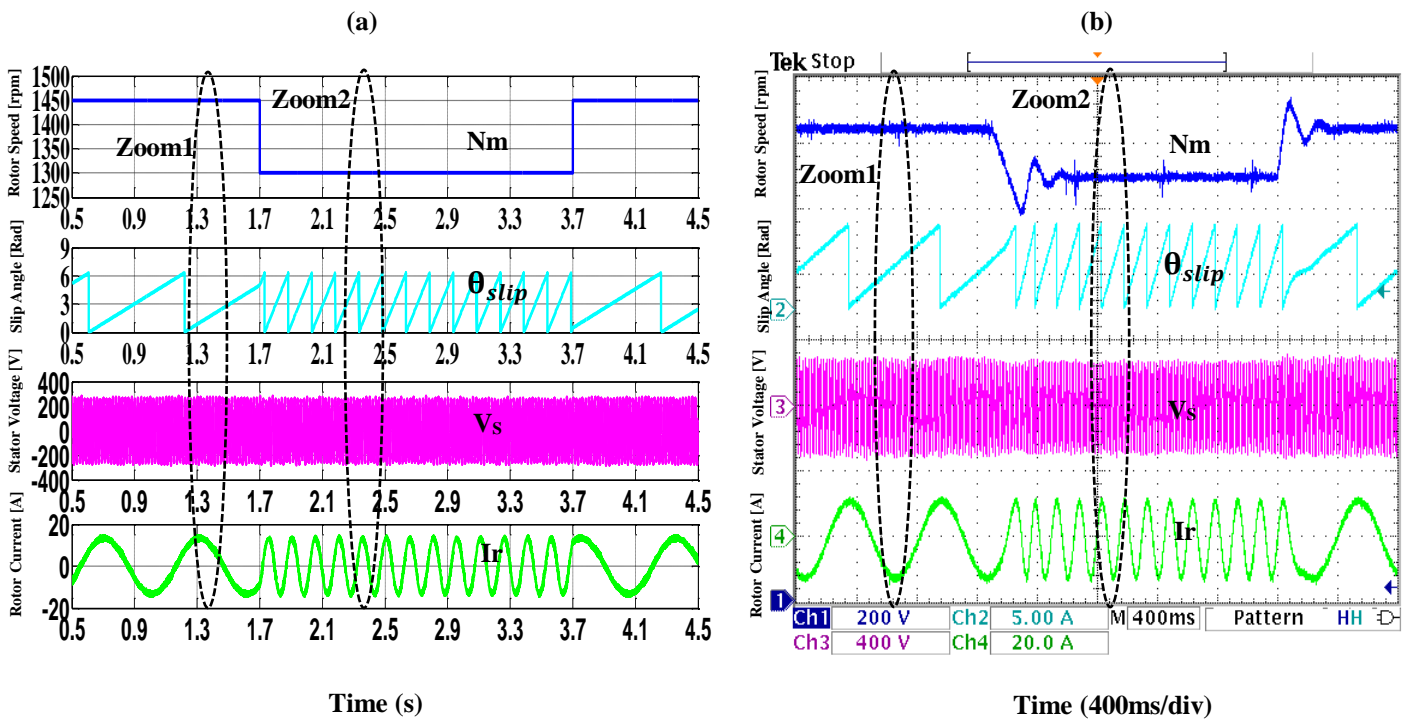
Fig 3.16 FS-PCC system response under rotor speed variety. a Simulation results .b Experimental. CH1: rotor speed (200 rpm/div), CH2: Slip Angle (5 rad/div), CH3: stator phase voltage (400V/div), CH4: rotor phase current (20A/div).

Zoom1

Time (s)

Time (20ms/div)

Zoom2

Time (s)

Time (40ms/div)
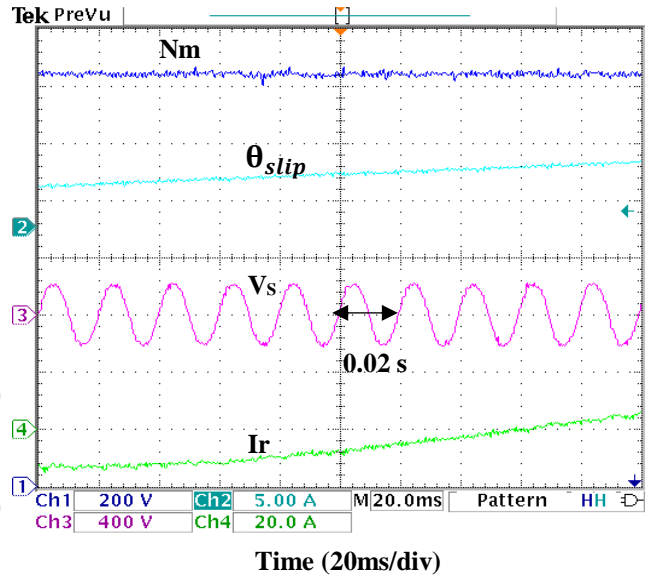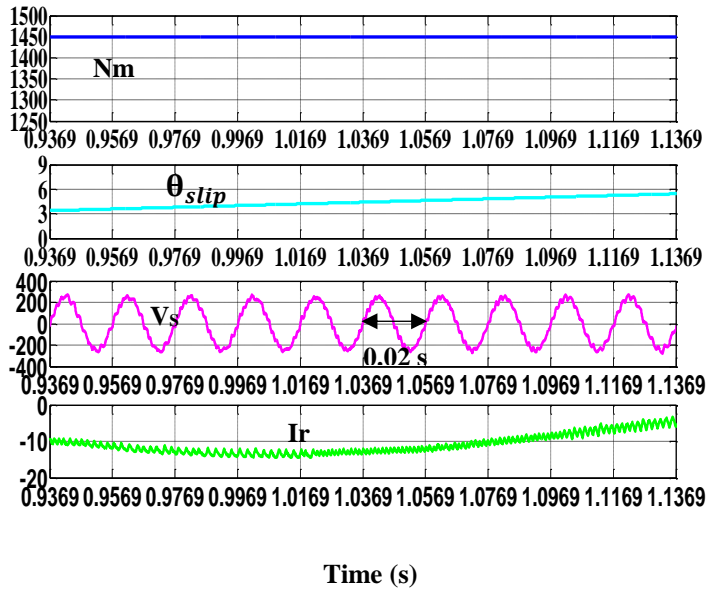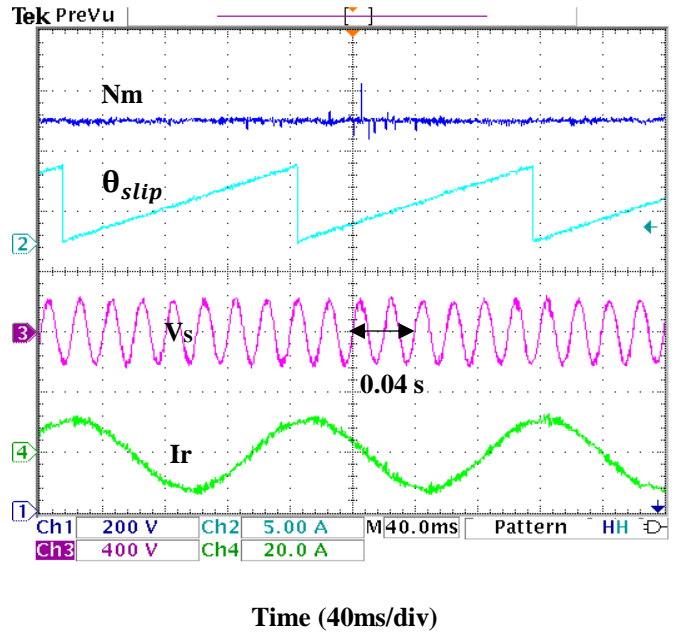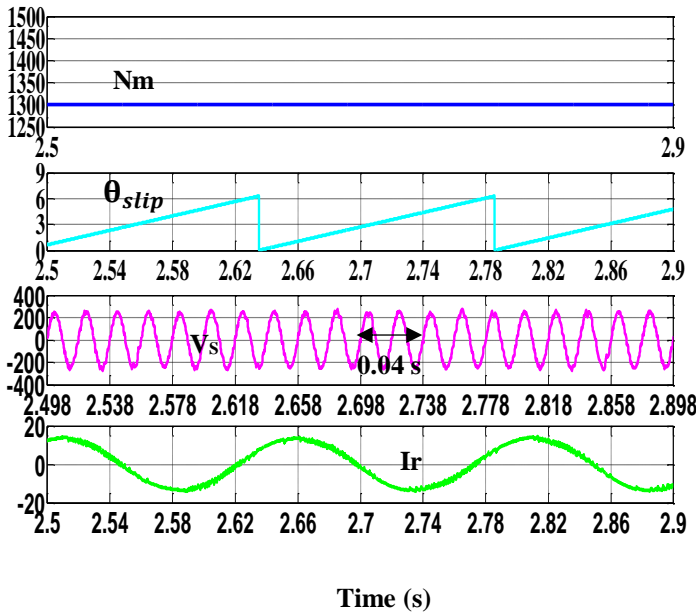
3.6 Chapter conclusion

In this chapter, a simple and effective HCC and FS-PCC algorithms for the stator voltage and frequency control for a standalone DFIG has been developed. The proposed controllers does not require an inner PI controller or a complex modulation stage, which greatly simplifies the design process. Moreover, it is easy to implement in the experimental bench, thereby keeping the proposed control algorithm straightforward for the handling of constraints. Simulation results and experimental tests in a laboratory with a 3 kW DFIG scale setup confirm the proposed control algorithms and show the feasibility and effectiveness of the proposed HCC and FS-PCC concerning different operating conditions.

Chapter 4

Improved RSC control of standalone DFIG: Approach-2

4.1 Chapter introduction

Most of the strategies that have been used to control the DFIG are based on FOC; this control scheme requires complex computational tasks and very accurate values for the machine parameters. In addition, the stator currents and rotor speed sensors are necessary to be implement; these requirements may lead to an in accuracy when operating under sensor faults. Direct control techniques Direct Torque control and direct rotor flux vector control (DTC and DRFVC) can overcome these drawbacks with their reduction of computations and the simplified control algorithm, which is sensorless and does not require a large number of coordinate transformations. The DTC or DRFVC plan does not oblige axes change as all the conventional controlling methods because are completed in stationary reference frame. Therefore, this scheme does not experience the ill effects of parameter changes to the way that different control methods do. Likewise there is no feedback control loop of current because of which the control activities don't experience the inherent defers in the present regulators, no PWM'S, no regulators of PI, and no stator currents or speed sensors. Therefore, it is a sensor less regulatory method, which works the DFIG free from obliging a shaft hopped on mechanical detector. Here on-line stator voltage magnitude and frequency regulators are utilized for loop closing. Here the rotor flux and torque are controlled specifically IN DTC by utilizing hysteresis controllers. More details are discussed later.

In this chapter, the DRFVC and DTC are proposed for standalone DFIG that is presented in detail. Further, several simulations and experimental are shown in order to demonstrate the performances and feasibility of these algorithms.

4.2 Improved RSC control based direct rotor flux vector control and space vector modulation (DRFVC-SVM)

4.2.1 Description of proposed DRFVC-SVM control scheme

The general structure of DRFVC-SVM approach is given by the block diagram of Fig. 4.1.The basic idea of this strategy is the decoupling between the amplitude and the argument of the rotor flux vector. Indeed, the reference amplitude of rotor flux vector will be imposed through the stator-voltage magnitude control loop, in the other side the reference argument will be calculated according to frequency regulation control loop. The DRFVC is mainly based on an inner predictive rotor flux controller that selects the rotor voltage reference that insure providing of the desire rotor flux vector. Finally, the rotor voltage reference will be modulated by an SVM modulation technique, which ensures a constant commutation frequency.

The DRFVC-SVM control algorithm can be summarized into the following steps:

- Stator-voltage magnitude and frequency estimation

- Reference rotor-flux vector magnitude evaluation through stator-voltage magnitude control loop.

- Reference rotor-flux vector angle evaluation through frequency control loop.

- Rotor-flux estimation and elaboration using the inner predictive control loop.

- Rotor-voltage reference selection in αβ rotor-reference frame.

- Pulses generation after rotor-voltage reference modulation using SVM technique.

In the following sections, each step corresponding this algorithm is explained.
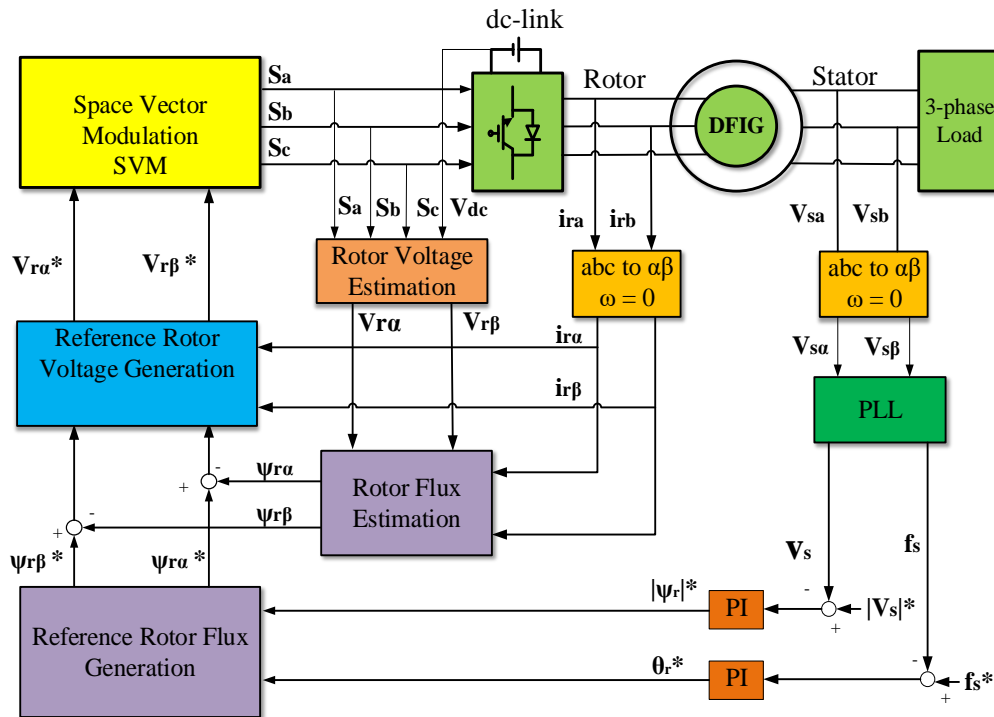
Fig. 4.1. Block diagram of the proposed DRFVC.

4.2.2 Stator-Voltage magnitude control loop

In the proposed DRFVC method, the stator-voltage amplitude is regulated by adjusting the rotor-flux magnitude, as shown in the upper control loop of Fig. 4.1. The purpose of this subsection is to illustrate the relationship between the stator-voltage amplitude and the rotor-flux magnitude.

Initially, the stator voltage $\vec{\psi}_r$ is calculated versus the stator flux $\vec{\psi}_s$. The equivalent circuit of Fig. 2.4 is transferred to the stator-flux reference frame, by choosing $\omega = \omega_s$, thus under steady state, the stator flux becomes constant (dc value), meaning that

$$\frac{d}{dt}\vec{\psi}_s = 0 \qquad (4.1)$$

On the other hand, considering the load Z_L, and Supposing the standalone DFIG is connected to unitary power factor microgrid (PF=1), based on that the DFIG will feed only the reel part of load impedance $Z_L=R_L+jL_L\omega_s$. So the stator current $\vec{i}_s$ can be obtained versus the stator voltage $\vec{v}_s$ as:

$$\vec{i}_s = -\frac{\vec{v}_s}{R_l} \qquad (4.2)$$

By substituting (4.2) and (4.21) in (2.10), $\vec{v}_s$ can be obtained versus the rotor flux $\vec{\psi}_r$ as:

$$\vec{v}_s = \frac{L_m}{L_r} \cdot \frac{j\omega_s R_l}{(R_l+R_s)+j\omega_s \delta L_s} \vec{\psi}_r \qquad (4.3)$$

Therefore,

$$|\vec{v}_s| = \frac{L_m}{L_r} \cdot \frac{\omega_s R_l}{\sqrt{(R_l+R_s)^2+(\omega_s \delta L_s)^2}} |\vec{\psi}_r| \qquad (4.4)$$

Equation (4.4) shows that stator-voltage amplitude $|\vec{v}_s|$ has direct relationship with rotor-flux magnitude $|\vec{\psi}_r|$, therefore, a PI controller can be employed to regulate $|\vec{v}_s|$ by controlling $|\vec{\psi}_r|$.

4.2.3 Stator-Voltage frequency control loop

In the proposed method, the stator-voltage frequency ωs is regulated by the rotor-flux angle. This frequency is the sum of the mechanical rotor speed ωm and the slip frequency ωr

$$\omega_s = \omega_m + \omega_r \qquad (4.5)$$

According to (4.1), to keep ωs constant, ωm changes must be compensated by controlling ωr. Since ωs has direct relationship with ωr, a PI controller can be used to regulate the stator-voltage frequency, where its output is the reference of slip frequency ωr*.

As shown in Fig. 4.1, by integrating ωr*, the reference of rotor-flux angle θr is obtained

$$\theta_r^* = \int \omega_r^* \, dt \qquad (4.6)$$

4.2.4 Referenced Rotor Flux Vectors calculation

The rotor flux amplitude $|\psi_r|^*$ and slip angular reference θ_r^*, which are the output of the PI controller of the stator voltage magnitude and its frequency respectively, will use to calculate the components of the rotor flux reference. In the rotor reference frame (α, β), the coordinates of the reference rotor flux $\psi_{\alpha r}^*$ and $\psi_{\beta r}^*$ are calculated from the polar coordinates according to the following expressions:

$$\psi_{r\alpha}^* = |\vec{\psi_r}|^* \cos(\theta_r^*) \qquad (4.7)$$

$$\psi_{r\beta}^* = |\vec{\psi_r}|^* \sin(\theta_r^*) \qquad (4.8)$$

4.2.5 Referenced rotor voltage vectors calculation

The coordinates of references of rotor voltage vectors $v_{\alpha r}^*$ and $v_{\beta r}^*$ in (α, β) rotor reference frame are determined by the following equations:

$$v_{r\alpha}^* = \frac{\psi_{\alpha r}^* - \psi_\alpha}{T_s} - R_r i_{r\alpha} \qquad (4.9)$$

$$v_{r\beta}^* = \frac{\psi_{r\beta}^* - \psi_{r\beta}}{T_s} - R_r i_{r\beta} \qquad (4.10)$$

Finally, they are introduced to the SVM block, which use them to control the inverter switches (S_a, S_b, S_c).

4.2.6 Space vector modulation algorithm

The SVM technique refers to a special switching scheme of the six power transistors of a three-phase pulse width modulation (PWM) inverter. In fact, the SVM technique uses eight sorts of different switch modes of the inverter to control the rotor flux to advance the reference flux circle. Eight types of switch modes correspond to eight space voltage vectors that contain six active voltage vectors and two zero voltage vectors as shown in Fig 4.2 (a).

(a)   (b)
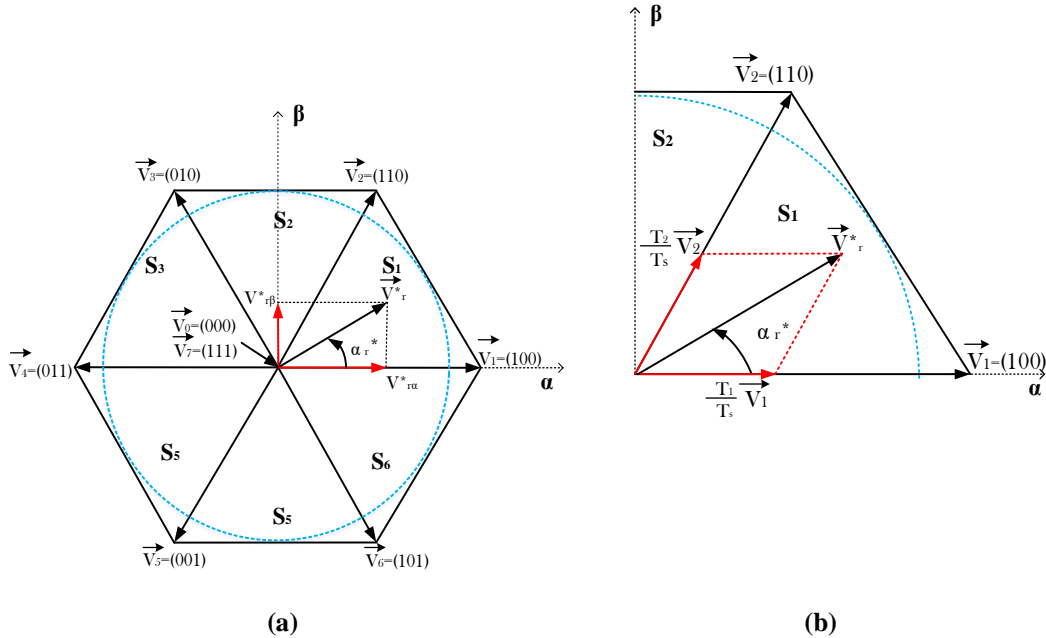
Fig. 4.2. (a) Basic switching vectors and sectors. (b) Projection of the reference voltage vector on two adjacent vectors.

The reference voltage vector $\vec{v}_r$, defined by the reference voltage components (v_α^*, v_β^*) calculated by the vector control, can be synthetized through an average relationship between two neighboring active vectors. Zero vectors are used to fill-up the gap to a constant sampling interval.

Taking as an example a reference vector in Sector 1, as shown in Fig 4.2 (b). This vector can be represented by the summation of two non-zero vectors $\vec{v}_1$ and $\vec{v}_2$ for appropriate time periods, which will give direction, with the addition of zero vectors to scale the vector. The modulation algorithm is made up of three steps over the switching period Ts as shown Fig 4.3. The first step applies the non-voltage vector $\vec{v}_1$ for a period T_1. The second step applies a non-zero vector $\vec{v}_2$ for a period T_2. until the voltage has the same phase as $\vec{v}_r^{\,*}$. The resulting vector until now will be same with the reference vector $\vec{v}_r^{\,*}$. The last step applies a zero vector for time $T_0 = (T_s - T_1 - T_2)$ until time T_s is reached.
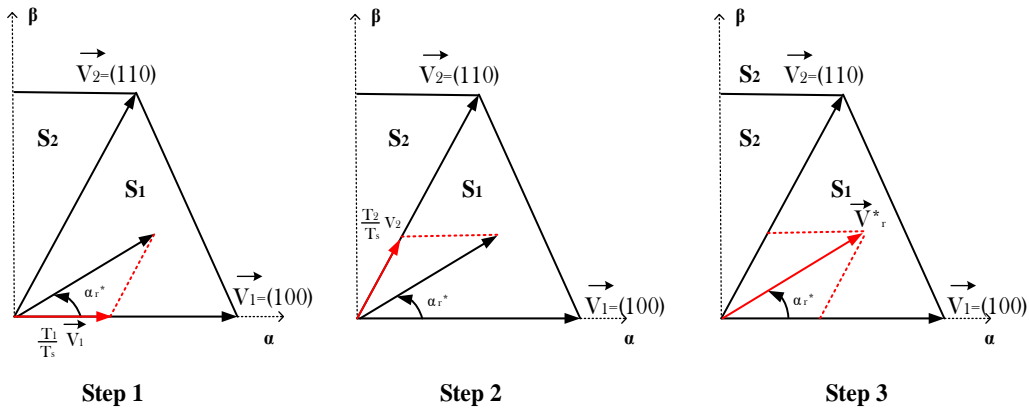
Fig. 4.3 Modulation algorithm steps.

This three step modulation algorithm can be represented by the mathematical expression:

$$\int_0^{T_s} \vec{V}_{ref} = \int_0^{T_1} \vec{V}_1 \, dt + \int_{T_1}^{T_1+T_2} \vec{V}_2 \, dt + \int_{T_1+T_2}^{T_s} \vec{V}_{0,7} \, dt \quad (4.11)$$

It can be expressed as

$$\vec{V}_{ref} = \frac{T_1}{T_s}\vec{V}_1 + \frac{T_2}{T_s}\vec{V}_2 + \frac{T_0}{T_s}\vec{V}_{0,7} \qquad (4.12)$$

Since the reference vector $\vec{v}_r^{\,*}$ is assumed to exist in sector I ($0 \leq \alpha_r^* \leq 60\circ$), as shown as the Fig 4.2, (3.2) can be represented by

$$\left|\vec{v}_r^{\,*}\right|\cos\alpha_r^* = \frac{T_1}{T_s}\left|\vec{V}_1\right| + \frac{T_2}{T_s}\left|\vec{V}_2\right|\cos\frac{\pi}{3} \qquad (4.13)$$

$$\left|\vec{v}_r^{\,*}\right|\sin\alpha_r^* = \frac{T_2}{T_s}\left|\vec{V}_2\right|\sin\frac{\pi}{3} \qquad (4.14)$$

Thus

$$\left|\vec{v}_r^{\,*}\right|\cos\alpha_r^* = \frac{T_1}{T_s}\left(\frac{2}{3}V_{dc}\right) + \frac{T_2}{T_s}\left|\vec{V}_2\right|\cos\frac{\pi}{3} \qquad (4.15)$$

$$\left|\vec{v}_r^{\,*}\right|\sin\alpha_r^* = \frac{T_2}{T_s}\left(\frac{2}{3}V_{dc}\right)\sin\frac{\pi}{3} \qquad (4.16)$$

Where V_{dc} is the input DC voltage (the DC rail voltage), $\left|\vec{v}_r^{\,*}\right|$ is the magnitude of the reference vector $\vec{v}_r^{\,*}$, and α_r^* is the phase of the reference vector. The time periods T$_1$, T$_2$ and T$_0$ can be calculated using (3.3) so that

$$T_1 = \frac{\sqrt{3}\left|\vec{v}_r^{\,*}\right|}{V_{dc}} T_s \sin(\frac{\pi}{3} - \alpha_r^*) \quad (4.17)$$

$$T_2 = \frac{\sqrt{3}\left|\vec{v}_r^{\,*}\right|}{V_{dc}} T_s \sin(\alpha_r^*) \quad (4.18)$$

$$T_0 = T_s - T_1 - T_2 \quad (4.19)$$

The previous equations are also valid for the remaining sectors by knowing in which sector the reference vector is located and by making α_r^* corresponding to the angle between the immediately previous basic vector and the reference vector. From above analysis, it is seen that both modulus and angle of rotor flux-linkage vector can be directly controlled by proper space voltage vector with SVM. Several switching patterns can be generated according to the choice of the zero vectors and the sequence in which the vectors are applied within the switching cycle. the most commonly used are based on a symmetrical distribution of the basic switching vectors since they generate less harmonic distortion. A switching pattern can be considered where every PWM period starts and ends with zero vectors and the amount of $\vec{v}_0$ inserted is the same as that of $\vec{v}_7$. In this case, there will be two zero vectors per T_s so that the zero interval is divided into two equal halves of length $T_0/2$. These half intervals are placed at the beginning and end of every sampling interval. If the half at the beginning is realized as $\vec{v}_0$, that at the end is realised as $\vec{v}_7$, and vice versa. According to this, the SVM voltage vectors sequence and timing plans can be defined, as shown in Table. 4.1.

Table. 4.1 SVM voltage vectors sequence and timing plan.

Sector	Voltage vector sequence	Voltage Vector Timing
1	$\vec{v}_0 \to \vec{v}_1 \to \vec{v}_2 \to \vec{v}_7 \to \vec{v}_2 \to \vec{v}_1 \to \vec{v}_0$	$T_0/2 \to T_1 \to T_2 \to T_0 \to T_2 \to T_1 \to T_0/2$
2	$\vec{v}_0 \to \vec{v}_3 \to \vec{v}_2 \to \vec{v}_7 \to \vec{v}_2 \to \vec{v}_3 \to \vec{v}_0$	$T_0/2 \to T_2 \to T_1 \to T_0 \to T_1 \to T_2 \to T_0/2$
3	$\vec{v}_0 \to \vec{v}_3 \to \vec{v}_4 \to \vec{v}_7 \to \vec{v}_4 \to \vec{v}_3 \to \vec{v}_0$	$T_0/2 \to T_1 \to T_2 \to T_0 \to T_2 \to T_1 \to T_0/2$
4	$\vec{v}_0 \to \vec{v}_5 \to \vec{v}_4 \to \vec{v}_7 \to \vec{v}_4 \to \vec{v}_5 \to \vec{v}_0$	$T_0/2 \to T_2 \to T_1 \to T_0 \to T_1 \to T_2 \to T_0/2$
5	$\vec{v}_0 \to \vec{v}_5 \to \vec{v}_6 \to \vec{v}_0 \to \vec{v}_6 \to \vec{v}_5 \to \vec{v}_0$	$T_0/2 \to T_1 \to T_2 \to T_0 \to T_2 \to T_1 \to T_0/2$
6	$\vec{v}_0 \to \vec{v}_1 \to \vec{v}_6 \to \vec{v}_0 \to \vec{v}_6 \to \vec{v}_1 \to \vec{v}_0$	$T_0/2 \to T_2 \to T_1 \to T_0 \to T_1 \to T_2 \to T_0/2$

The construction of this symmetrical pulse pattern is accomplished for two consecutive T_s intervals, being the PWM carrier switching frequency defined as $f_c = f_s/2$. Finally, it is worth noting that during the sampling interval, the desired reference vector is approximated in the average sense. However, instantaneously, the actual vectors produced by the inverter are different from the reference vector which means that current harmonics are always present.

4.2 Improved RSC control based Direct Torque Control

4.2.1 Description of proposed DTC control scheme

The proposed controller design is depicted in Fig 4.4, whereby the stator-voltage amplitude and frequency are regulated by two separated closed-loops. The upper loop is responsible for adjusting the reference of rotor-flux magnitude by controlling the voltage amplitude, where stator-voltage amplitude larger a larger rotor-flux generates. While the reference of electromagnetic torque is tuned in the lower loop by controlling the frequency. Each of these loops contains a PI controller and a hysteresis-controller. The output signals of the hysteresis-controllers (h_{ψ_r} and h_{Te}) determine if the rotor-flux magnitude $\vec{\psi}_r$ and torque Te should be decreased or increased. Based on these signals and rotor-flux position, the appropriate voltage-vector is selected from the switching-table and is applied to rotor, by inverter.
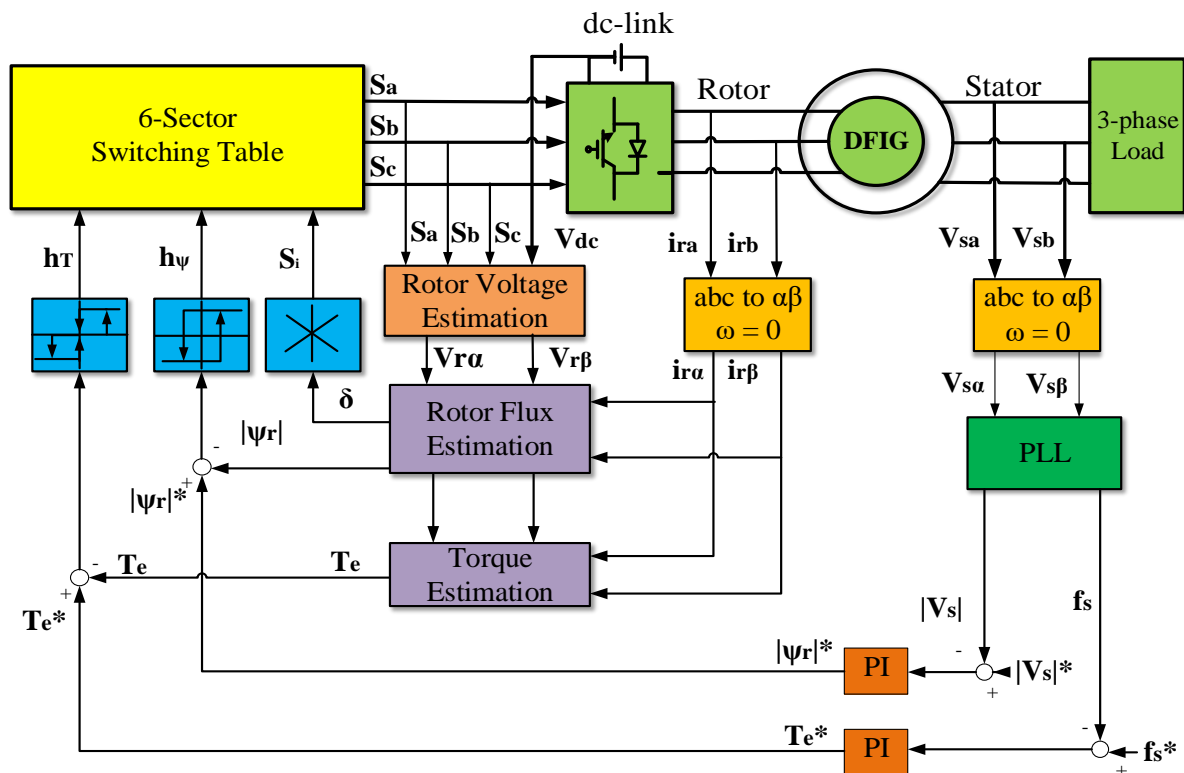
Fig. 4.4. Block diagram of the proposed DTC.

The proposed control method consists of two kind of parts: regulator parts and estimator parts. The regulator parts are detailed in the following subsections as being the main parts of the proposed controller, while the estimator parts are explained in section-IV.

The DTC control algorithm can be summarized into the following steps:

- Stator-voltage magnitude and frequency estimation

- Torque and rotor flux estimation

- Desired torque and rotor-flux vector magnitude evaluation.

- Comparison between reference and estimated values.

- Torque and rotor flux errors (e_{ψ_r} and e_{Te}) elaboration through torque and rotor flux hysteresis controllers.

- Rotor-flux vector position and sector identification.

- Rotor-voltage vector selection from switching table.

In the following sections, each step corresponding this algorithm is explained.

4.2.2 Electromagnetic Torque and Rotor Flux Reference evaluation based Stator-Voltage magnitude and frequency droop control method

In case of, a standalone DFIG connected to AC-microgrid system, the control scheme targets are regulation of AC voltage magnitude and frequency, along with meeting the load requirement. In this section, an inner DTC control scheme are integrated where rotor flux and load torque requirement is adjusted by, voltage magnitude and frequency droop-control method in order produce a constant stator-voltage magnitude and frequency and meet the deferent load power value during the entire operating period. This is done with small increments and decrements of $\left|\vec{\psi_r}\right|^*$ and $T_e{}^*$ as a function of the measured stator-voltage magnitude and frequency respectively, by using a PI controller, as follows:

In order to evaluate the desire rotor flux magnitude, The stator-voltage magnitude droop control low can be expressed as:

$$\left|\vec{\psi_r}\right|^* = k_p(|\vec{v}_s|^* - |\vec{v}_s|) + k_i \int (|\vec{v}_s|^* - |\vec{v}_s|)\, dt \quad (4.20)$$

Where $|\vec{v}_s|^*$ and $|\vec{v}_s|$ are the reference and the measured stator-voltage magnitude, respectively. Similarly, in order to evaluate the desire electromagnetic torque from the generator, we proposed that stator-frequency droop control law can be defined as

$$T_e{}^* = k_p'(f_s{}^* - f_s) + k_i' \int (f_s{}^* - f_s)\, dt \quad (4.21)$$

where $f_s{}^*$ and f_s are the the reference and measured stator frequency of the DFIG, respectively,

4.2.3 Direct Torque Control

DTC is a popular direct control strategy is widely used, for the three phase drive system due to the improved dynamics and less requirement for computation [18]-[21]. the torque and the rotor flux are controlled using the hysteresis controllers and a switching table for choosing the voltage vectors [2, 31–33, 56–58]. DTC is an effective alternative technique for the vector control mainly according to the control variables that are used in both algorithms. In DTC-DFIG , the electromagnetic torque and the rotor flux of the machine are used as primary control variables, but in the FOC the q and d components of the rotor current and the speed measurement are necessary when the stator flux orientation is used [12]. Moreover, In FOC based control accurate parameter estimation is required, while in DTC based control only resistance of rotor need to be measured accurately.

The advantages and features of DTC over FOC can be summarized according to [20–22] as:

• Fast torque response.

• Minimized dependency on machine parameters.

• Reducing the complexity of vector control algorithm, less coordinate transformations, the modulation technique and current PI controllers are not needed.

• The speed measurement are not required.

The idea of the direct torque control for standalone DFIG can be extended from motoring mode to generation mode with same control structure. The only difference in generation mode is that the torque reference is negative and the stator flux vector lags to rotor flux vector as shown in Fig 4.5. The DTC technique is based on the direct regulation of the electromagnetic torque and the rotor flux. Thus, Conventional DTC for DFIG is discussed in this section;

Motoring mode   **Generating mode**
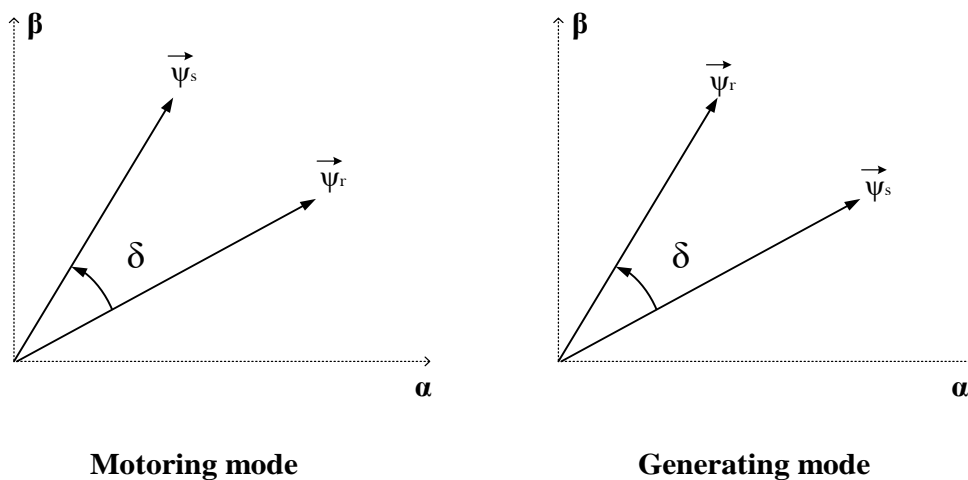
Fig. 4.5. Stator and rotor flux vector at motoring and generating states.

4.2.3.1 Control of rotor flux

The relationship between the rotor voltage, current and rotor flux vectors of a DFIG machine in the $\alpha\beta$ rotor-reference frame is given by

$$\vec{v}_r = R_r \vec{\imath}_r + \frac{d\vec{\psi}_r}{dt} \quad (4.22)$$

Basing on the above equation in rotor frame, the rotor flux equation can be expressed as follows:

$$\vec{\psi}_r = \int \vec{v}_r - R_r \vec{\imath}_r \, dt \quad (4.23)$$

Considering that the control of the switches of the inverter is done by control sampling period T_e and that at each of these periods the states S_a, S_b, and S_c are kept constant, the use of the numerical method makes it possible to obtain an expression of rotor flux at k + 1 in the following form

$$\vec{\psi}_r(k+1) = \vec{\psi}_r(k) + (\vec{v}_r(k) - R_r \vec{\imath}_r(k))T_s \quad (4.24)$$

Here, assuming the voltage drop across the rotor resistance (R_r) is small to be ignored, Then (4.24) can be written as:

$$\vec{\psi}_r(k+1) = \vec{\psi}_r(k) + \vec{v}_r(k)T_s \quad (4.25)$$

Where: $\vec{\psi}_r(k)$: is the rotor flux vector at the current sampling period.

   $\vec{\psi}_r(k+1)$: is the rotor flux vector at the next sampling period.

   $\vec{v}_r(k)T_s$: is the variation of the rotor flux vector.

(4.25) implies The rotor flux vector's extremity moves in direction given by the rotor voltage vector and making a circular trajectory. Means, the rotor flux can be controlled by the application of the most suitable rotor voltage during a sample time T_s.

4.2.3.2 Control of electromagnetic torque

Supposing the standalone DFIG is connected to unitary power factor microgrid (PF=1), based on that the DFIG will feed only the reel part of load impedance $Z_L = R_L + jL_L\omega_s$. In this case, the stator and rotor flux vectors, are linked by the following relation:

$$\vec{\psi}_s = \frac{L_m}{L_r} \cdot \frac{1}{1 + j\omega_s \delta\tau_L} \vec{\psi}_r \quad (4.26)$$

Where: $\tau_L = \frac{L_s}{R_s + R_L}$

The angle between these two vectors is given by:

$$\delta = Arctan\, g(\omega_s \delta\tau_L) \quad (4.27)$$

Finally, between the modules of the two flux vectors, we have the following relation:

$$\left|\vec{\psi}_s\right| = \frac{L_m}{L_r} \cdot \frac{1}{1 + j\omega_s \delta\tau_L} \left|\vec{\psi}_s\right| \quad (4.28)$$

The general relationship between the electromagnetic torque and the load angle is governed by:

$$T_{em} = \frac{3}{2} p \frac{L_m}{\delta L_s L_r} \left|\vec{\psi}_s\right| \cdot \left|\vec{\psi}_s\right| \cdot \sin(\delta) \quad (4.29)$$

Where:

p is the number of poles pairs.

$\vec{\psi}_s$, $\vec{\psi}_r$ are stator and rotor flux vectors.

δ angle between the stator and rotor flux vectors.

From expression (14), it is clear that the electromagnetic torque is controlled by the stator and rotor flux amplitudes. However, those quantities are maintaining constant when the stator voltage magnitude is constant. For that, the torque is conventionally controlled by adjusting the load angle δ, if the stator flux vector is ensured invariant during one sampling period by set the sampling time value as (Ts<< $\delta\omega_s\tau_L$).

Fig. 4.6. Illustrates, the rotation motion of the rotor flux vector controlled by rotor voltage vectors, in Thus, can rapidly change δ and achieve a fast dynamic response of the electromagnitique torque.
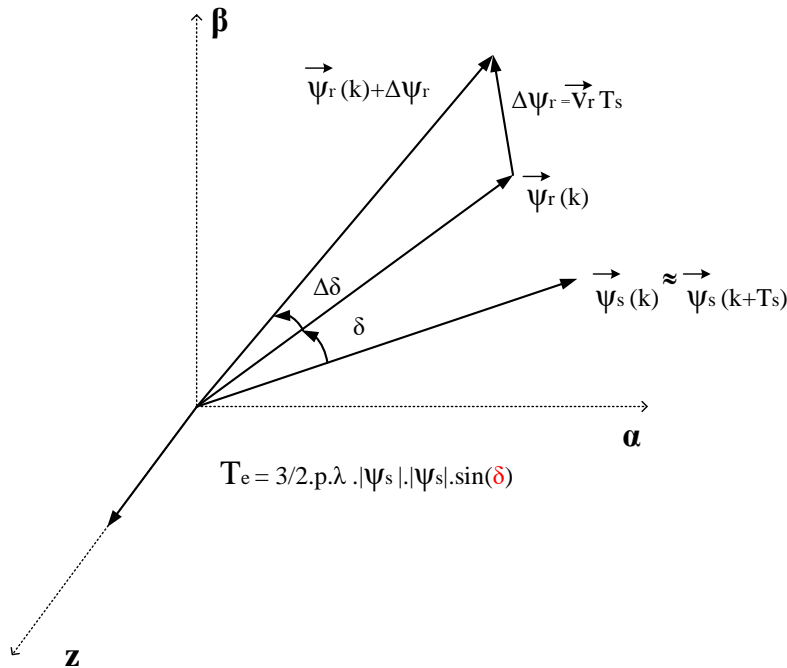
Fig. 4.6. Principles of DTC in αβ reference frame.

4.2.3.3 Torque and flux comparator

To regulate the rotor-flux magnitude and torque, The estimated and reference values are compared, then the resulting error is delivered to two hysteresis controllers, as shown before in Fig. 4.4.: one

for the electromagnetic torque and the other for the rotor flux. A three-level hysteresis comparator is used for the torque, and a two-level hysteresis comparator is used for the flux, as shown in Fig. 4.7.
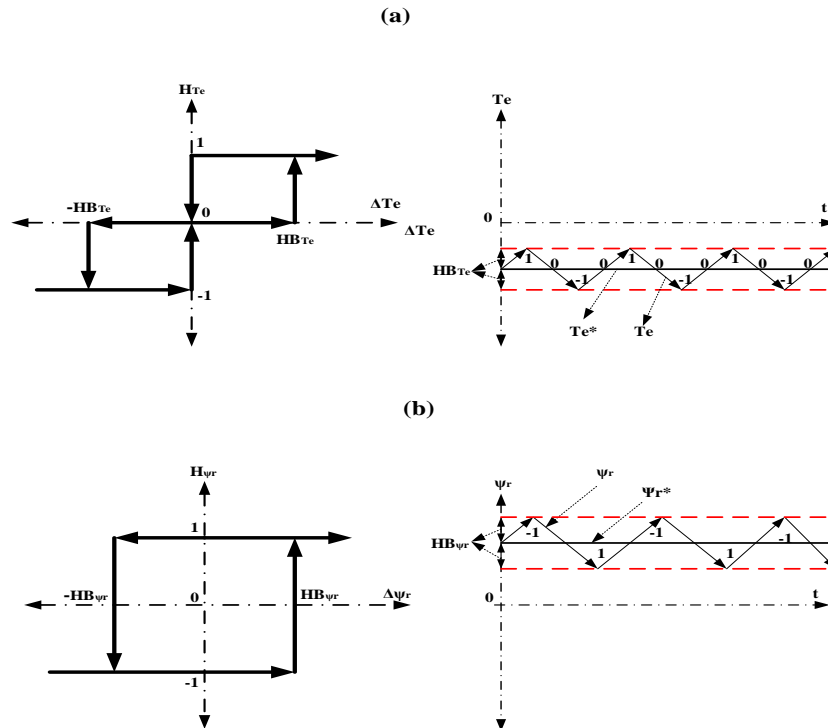
Fig. 4.6. (a) Three-level hysteresis comparator for the torque control,**(b)** Two-level hysteresis comparator for flux control.

As can be noted, the output of the torque controller is represented by a variable h_{Te} , which indicates directly if the amplitude of the torque must be increased ($h_{Te} = 1$) in sub-synchronous speed, or ($h_{Te} = -1$) when must be increased in sub-synchronous speed. ($h_{Te} = 0$) when the torque must be decreased for both sub-synchronous or super-synchronous. Depending on the input torque error (ΔTe). The conditions of the torque comparator are given as (with T_{em} * is the torque reference value) :

$$h_{T_e} = \begin{cases} 1 & if : \Delta Te = T_e^* - Te \geq HB_{Te} \\ 0 & if : -HB_{Te} < \Delta Te = T_e^* - Te > HB_{Te} \\ -1 & if : \Delta Te = T_e^* - Te \leq -HB_{Te} \end{cases} \quad (4.30)$$

Here, h_{T_e} and HB_{Te} are the torque status signal and the hysteresis band of the torque. A similar scheme is used with the rotor flux; the error obtained serves as an input of the two-level hysteresis comparator. If the error is positive $h_{\psi_r} =1$; the flux magnitude should be increased, and when the error is negative $h_{\psi_r} = -1$, the magnitude of flux should be decreased. The conditions of the flux comparator are given as follows (with ψ_r* is the rotor flux reference and actual value respectively):

$$h_{\psi_r} = \begin{cases} 1 & if : \Delta\psi_r = \psi_r^* - \psi_r \geq HB_{\psi_r} \\ -1 & if : \Delta\psi_r = \psi_r^* - \psi_r < -HB_{\psi_r} \end{cases} \quad (4.31)$$

Thus, h_{ψ_r} and HB_{ψ_r} are the rotor flux status signal and the hysteresis band of the rotor flux and $\Delta\psi_r$ is the rotor flux error between the reference and actual value.

4.2.3.4 Switching Strategy and rotor voltage selection

Spatial orientation of rotor winding is assumed as shown in Fig. 4.7. For a six-pulse RSC according to its switching positions (S1 to S6), there are six nonzero active voltage space vectors (V1 to V6) and two zero voltage vectors (V0 and V7) as shown in Fig. 4.7. One switch per leg of the VSI conduct at any time, i.e., if S1 is ON, then S4 is OFF and vice versa.1 represents ON condition of top switch while 0 represents the ON state of the lower switch of the same leg. In order to make an appropriate selection of switching vectors, phasor plane is divided into six, 60° sectors (1,2, . . . ,6) as shown in Fig. 4.7. Based on the location (sector) of rotor flux, output of torque and flux comparator Vr(k) is applied, where Vr(k represent the vector to be applied in kth sector.

Orientation of stator and rotor flux-linkage vector changes from subsynchronous speed to supersynchronous speed. In this section, analysis of effect of switching vectors on torque and flux for both subsynchronous and supersynchronous speed is considered and switching strategy is explained.
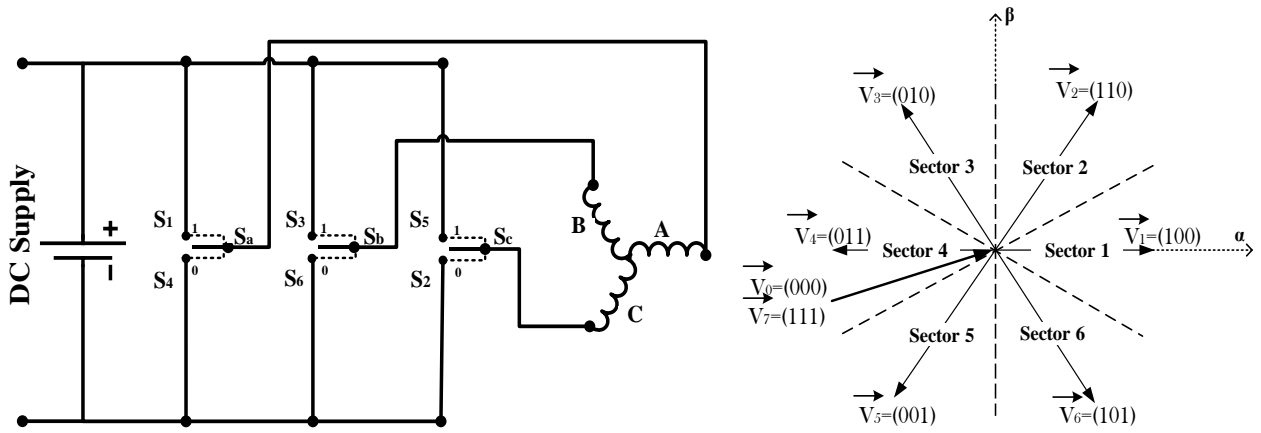
Fig. 4.7. RSC switching positions and voltage switching vectors.

a. Rotor voltage selection for super-synchronous speed of operation

In super-synchronous speed of operation, rotor and stator flux vector are rotating clockwise direction, the spatial orientation of rotor flux and stator flux is shown in Fig. 4.5. Assuming rotor flux is positioned in sector-1, if V6 is applied then, torque magnitude will increase due to increase in angle between $\vec{\psi}_s$ and $\vec{\psi}_r$. If zero vector V0 or V7 is applied, it keeps the rotor flux vector while the stator flux vector continues its rotation in clockwise direction, which reduces the torque angle

and hence reduces the magnitude of torque. By generalizing this for any sector, if flux vector is in k^{th} sector, then application of zero vector decreases torque magnitude and application of Vk-1 will increase the torque magnitude, k-1 represent the previous sector number.

Similarly, two rotor voltage vectors may be selected to increase or decrease the amplitude of the rotor flux linkage respectively, assuming rotor flux is positioned in sector-1, and if V6 is applied, the rotor flux amplitude will increase. Application of V5 will decrease the rotor flux amplitude. It can be generalized that, if rotor flux is in kth sector, then Vk-1 will increase the flux magnitude and Vk-2 will decrease the rotor flux magnitude.

b. Rotor voltage selection sub-synchronous speed of operation

In sub-synchronous speed of operation, Both rotor and stator flux linkage vector rotates in counter-clockwise direction and the spatial orientation of stator flux and rotor flux in rotor reference frame, is given in Fig. 4.5. Similar analysis to sub-synchronous speed is carried out and explained in this section. Assuming rotor flux is positioned in sector-1, if V2 is applied then, torque magnitude will increase due to increase in angle between $\vec{\psi}_s$ and $\vec{\psi}_r$. If zero vector is applied then, it keeps the rotor flux vector while the stator flux vector continues its rotation in counter-clockwise direction, which decreases the torque angle, and hence decreases the magnitude of torque. It can be generalized for any sector, if rotor flux vector is in kth sector, then application of zero vector decrease the torque magnitude and application of Vk+1 will increase the torque magnitude. Effect of active vectors on rotor flux magnitude is analyzed in this section similar to that of sub synchronous speed of operation. Likewise, the rotor voltage V2 and V3 are selected to increase and decrease the magnitude of the rotor flux respectively when $\vec{\psi}_r$ is in sector-1 and is rotating counter-clockwise. It can be generalized that, if rotor flux is in kth sector, then Vk+1 will increase the rotor flux magnitude and Vk+2 will decrease the rotor flux magnitude. Based on the above analysis of the effect of rotor voltage vectors on rotor flux magnitude and torque, six-sector switching table is formulated to control torque and rotor flux in both sub-synchronous and super-synchronous speed operation, as shown in Table. 4.2.

Table. 4.2. DTC switching table.

h_{ψ_r}	h_{Te}	Sector 1	Sector 2	Sector 3	Sector 4	Sector 5	Sector 6
	1	V_6	V_1	V_2	V_3	V_4	V_5
1	0	V_7	V_0	V_7	V_0	V_7	V_0
	-1	V_2	V_3	V_4	V_5	V_6	V_1
	1	V_5	V_6	V_1	V_2	V_3	V_4
-1	0	V_0	V_7	V_0	V_7	V_0	V_7
	-1	V_3	V_4	V_5	V_6	V_1	V_2

4.6 Obtained simulation and experimental results

To evaluate the performance of the two proposed control strategies, a simulation study is performed first using a simulation model of the DFIG system under analysis, afterwards the experimental tests are carried out in order to provide a comparative analysis of simulation and experimental results. The experimental setup presented in the previous chapter is also used here to test the standalone DFIG with the DRFVC and DTC strategy. It is complemented without stator current and a rotor speed sensor so that the standalone DFIG is optimally controlled. The standalone DFIG stator-voltage magnitude and frequency control, which is formerly discussed was implemented using the Matlab/Simulink software. As sensor feedback signals, the control system requires the three rotor phase currents and the actual three stator phase voltages, and the DC bus voltage in order to correctly generating the six gate command signals for each inverter IGBT. Furthermore, The Control Desk software is used for the real-time management, and graphical visualization of the process data.

To show the performance of the proposed control methods, the behavior of the controlled system is evaluated during the following running conditions:

a) Steady Stator voltage-magnitude variation

b) Load change

c) Rotational speed variation

The steady-state performance of the standalone DFIG with the two proposed control strategies is here shown. Several tests, conducted at different operating conditions are presented and discussed. The simulation and experimental results are plotted side by side in order to better evaluate the agreement between them

4.6.1 DRFVC

In this section, the DRFVC test result for standalone DFIG is given. The value of the proportional and integral gains of the PI controllers of stator voltage magnitude and frequency control used in the simulation study are the same as the ones used in experimental tests, the two PI controllers parameters of proposed DRFVC strategies are given in Appendix C in Table C.1. Also, The sampling period is set at Ts =10 μs for simulation and Ts =300 μs for experimental. For all the next tests the reference of the stator-voltage frequency is fixed at 50 Hz as the desire value for load equipment which is mainly connected to the stator.

a. Stator voltage-magnitude step variation

The effectiveness of the proposed DRFVC strategy for the standalone DFIG, in terms of dynamic response under stator-voltage magnitude step variation is investigated, Fig. 4.8. and Fig. 4.9. show the stator voltage transition from 150 V to 250 V at t=1s and vice versa at t=3s, with a constant load and rotor speed applied to the generator.

Simulation Results
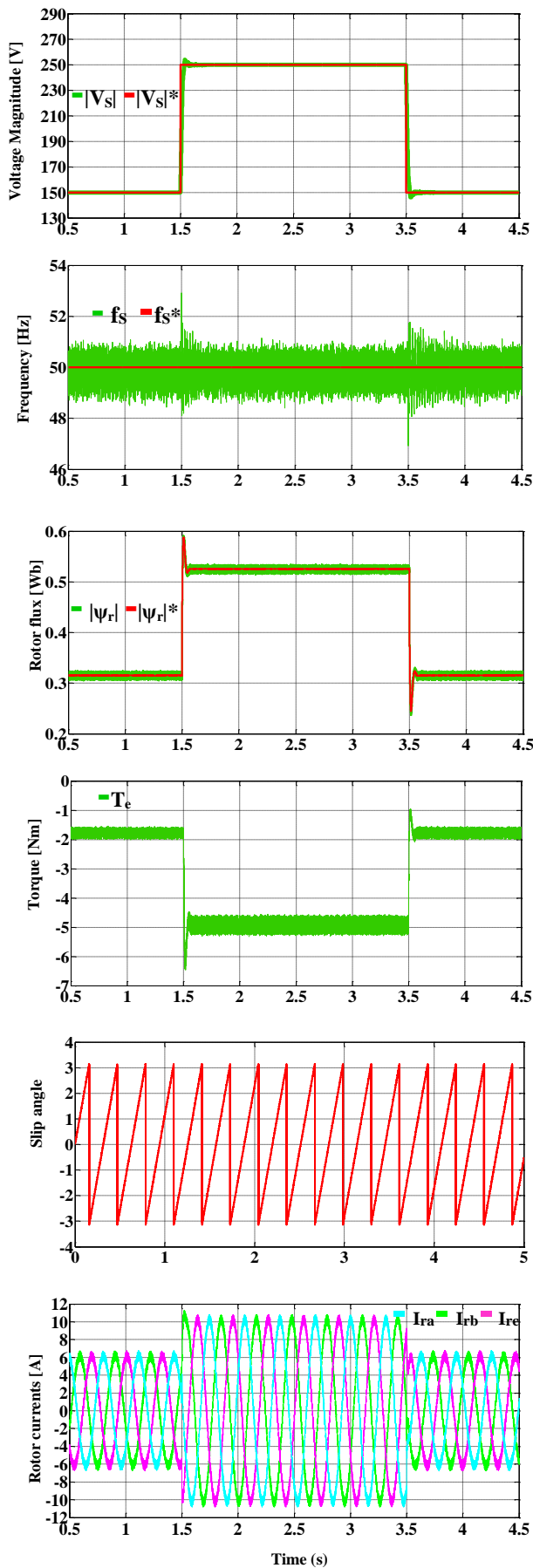
Experimental Results
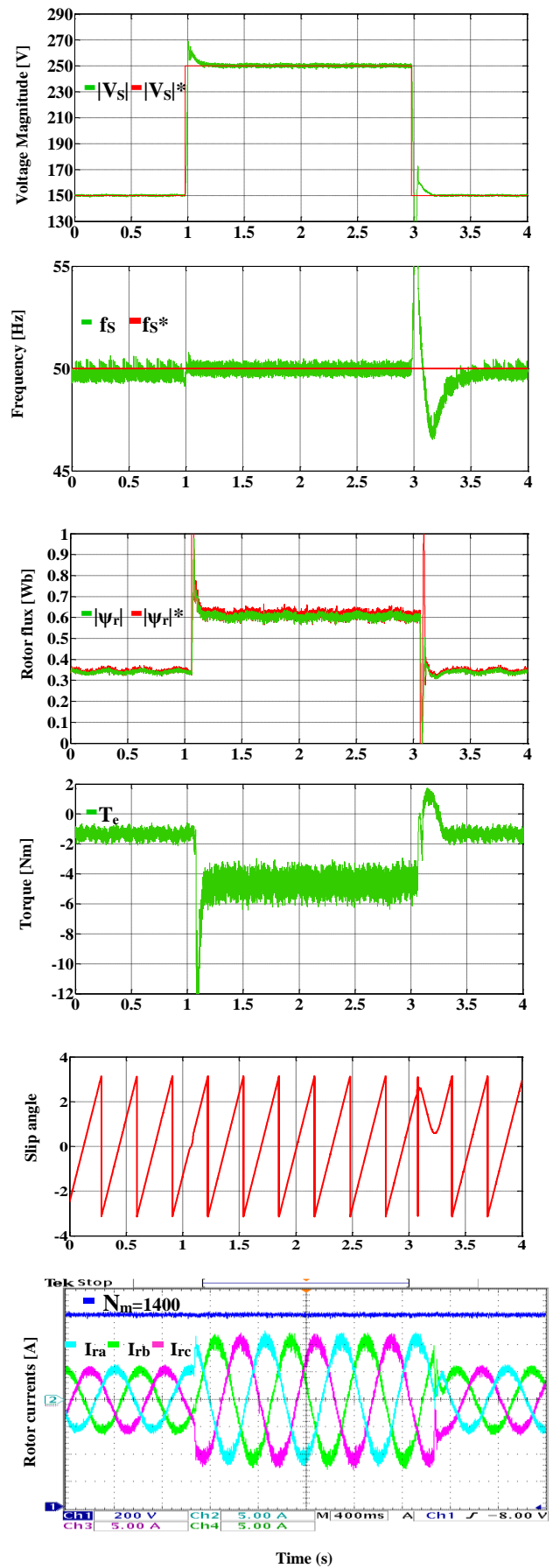
Fig. 4.8. Voltage-reference change test with the standalone-DFIG operating at fixed-load. From top to bottom: Stator voltage magnitude, stator frequency, rotor flux, electromagnetic torque, slip angle, and rotor current waveform. (Left) Simulation results. (Right) Experimental test.

It can be seen, both stator voltage and frequency tracks their reference value accurately without any significant overshoot. Moreover, the stator-voltage rise time for the proposed control strategies is approximately 0.2s, which yield fast dynamic response. It is worthy to know that the response time of stator-voltage and frequency can be improved arbitrarily by adjusting both of PI controller gains. It is also possible to observe that rotor flux and stator voltage have similar profiles, which is expected since they related linearly when the stator frequency kept constant at the desire value.

During the step-up variation period, the torque developed by the generator is the rated one, after reaching the desired stator voltage and frequency; it develops a torque of 6 N.m to satisfy the required load torque. In the experimental tests, during the operation at stator-voltage magnitude equal to 200V, the estimated torque exhibits an oscillation of 2 N.m, which is introduced by the DC/DC buck converter that controls the DC motor (prime mover). In addition, the rotor current also shows an expected behavior since it changes according to the operating condition of the DFIG system. This happens because the rotor-flux magnitude is calculated and updated in real-time through the PI controller and it relies on the variation of stator-voltage magnitude, as well as the rotor current magnitude.

Fig. 3.9. shows a zoomed version of the three phase stator-voltages waveforms obtained in this test. It can be seen, that the three phase are observed to have balanced-sinusoidal waveforms and have a fast response at the set of voltage magnitude and frequency reference value. This test illustrates the effectiveness of the proposed method for control of the stator-voltage amplitude and frequency accurately and independently.

b. Load variation

To further evaluate the performance of the proposed DRFVC strategies, a load variation test was conducted. In this test, the DFIG is changed to torque control mode by set a constant value of stator-voltage and setting manually the value of load, while the controlled prime mover (DC motor) acts to fix the rotor speed at 1400 rpm. A step change of the load, from 15% to 40 % (of 4 kW rated value) at 1 s is imposed to the DFIG while it is running at 1400 rpm and produce 200V of stator voltage. Then the load is reduced by -25% (of 4 kW rated value) at 3 s. The results obtained for the load change test are shown in Fig. 4.10. and Fig. 4.11. Fig. 4.10. From top to bottom, the curves are the reference and estimated stator-voltage magnitude, frequency, rotor flux, estimated torque, slip angle, and the measured rotor currents. As can be noticed, the estimated voltage magnitude and frequency tracks

very well their references value with a small overshoot and undershoot, thus demonstrating the high performance of the developed controller for DFIG system. Furthermore, the rotor flux follow it reference value it can be notice that the rotor flux is roughly constant during this test due the fixed value of stator voltage and frequency in this test, which means that the control strategies regulate very well the stator voltage and frequency. Moreover, the profiles of the estimated torque and the load value are identical which has an expected behavior. It can be seen, the torque ripple content decreases with the increase of the load torque. In addition, during this test, it is possible to observe a change of the rotor current, which is due to the change in value of torque.
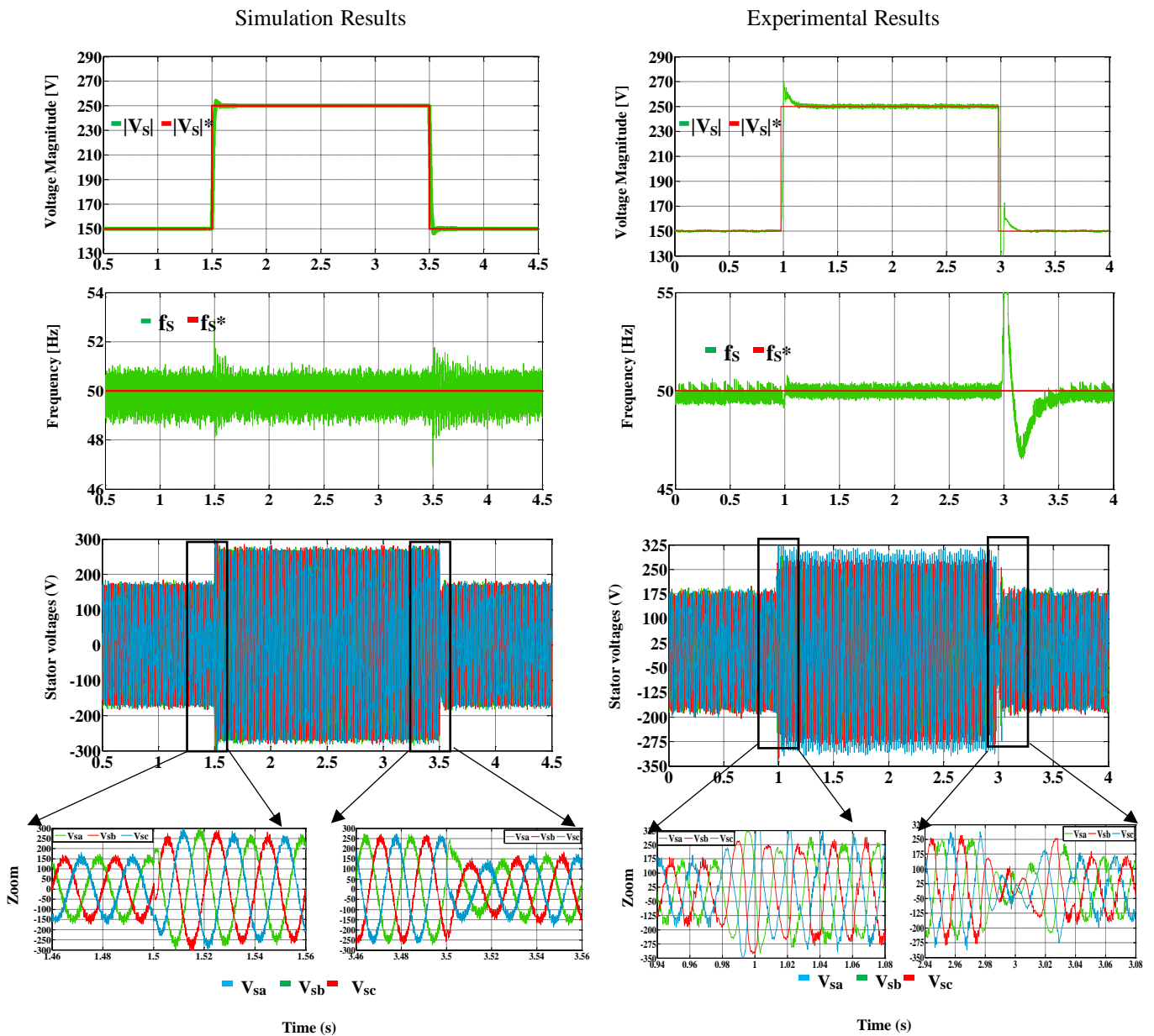
Fig. 4.9. Three phase stator voltage-waveforms during voltage magnitude step change. From top to bottom: Stator voltage magnitude, stator frequency, and Stator voltage waveform. (Left) Simulation results. (Right) Experimental test.
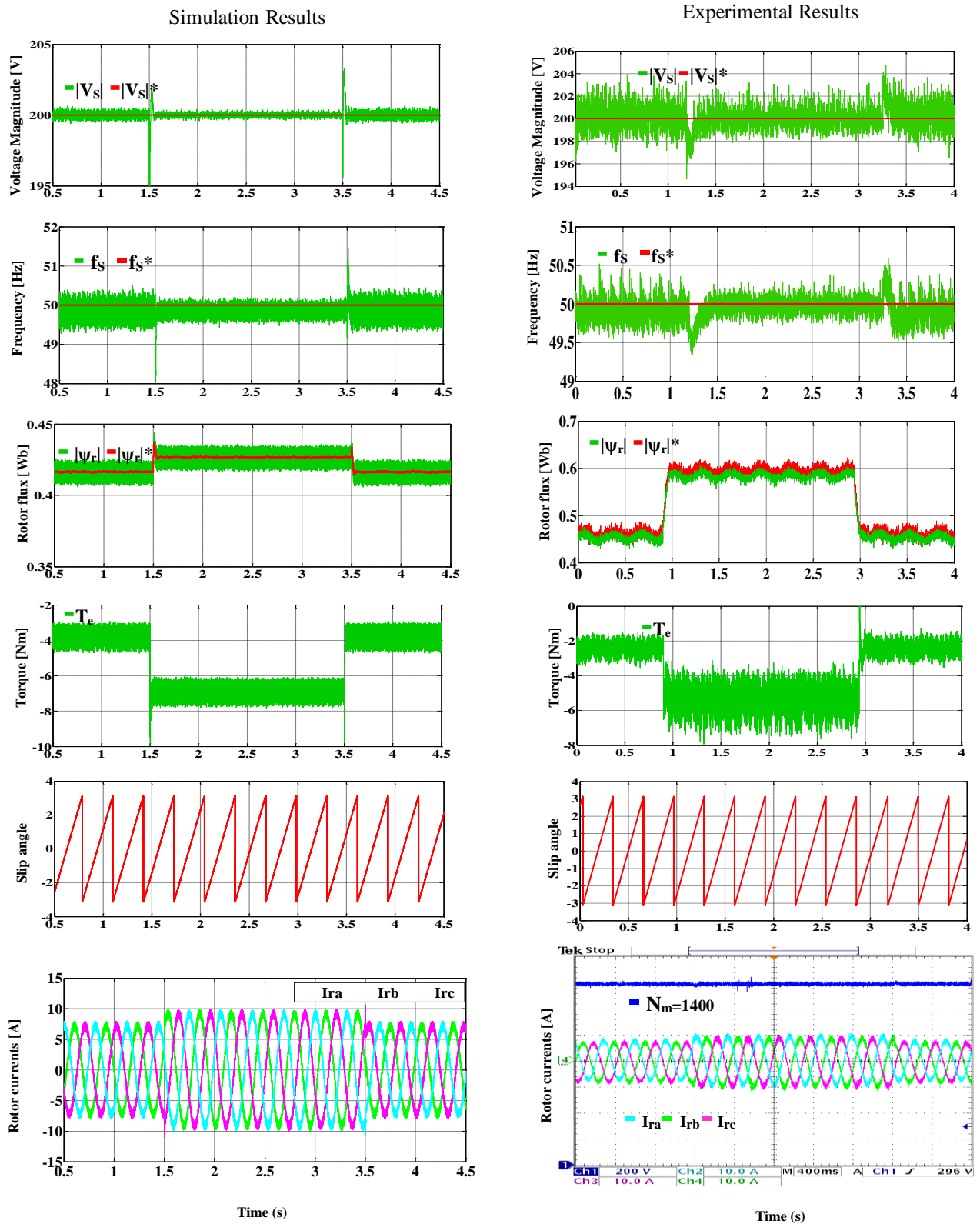
Fig. 4.10. Load change test with the standalone-DFIG operating at fixed Voltage-reference. From top to bottom: Stator voltage magnitude, stator frequency, rotor flux, electromagnetic torque, slip angle, and rotor current waveform. (Left) Simulation results. (Right) Experimental test.

The results shown in Fig. 4.10 are also supported by the results shown in Fig. 4.11., which are a zoomed version of the stator current obtained in this test. According to these results, the variation of stator current amplitude is due to the variation of the load, the stator current are observed to be sinusoidal, which can be considered has a very good quality.

This test results proves that the DRFVC strategies are able to track the desired reference voltage and frequency with an acceptable overshoot and undershoot within a wide load variation scale.
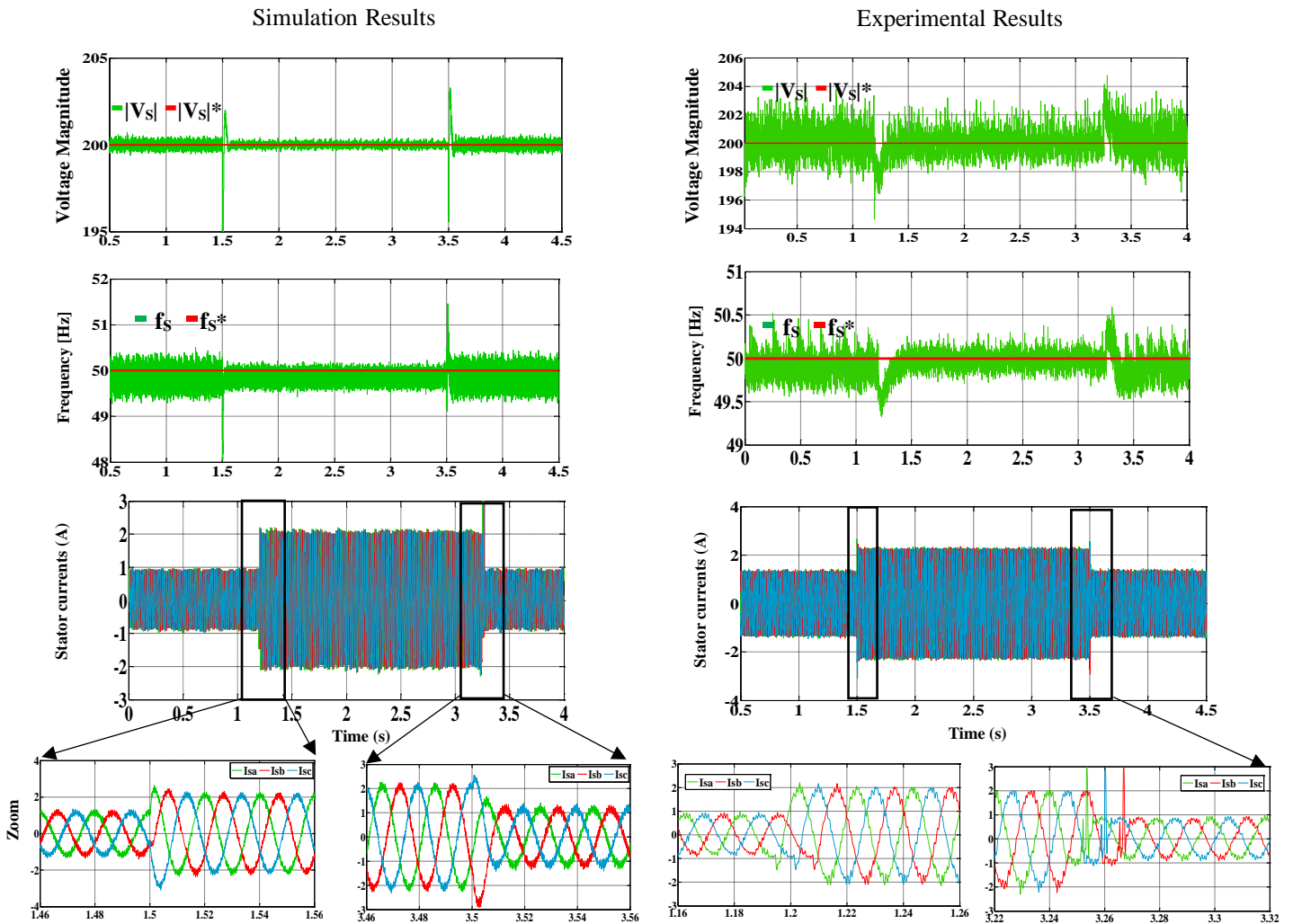
Fig. 4.11. Three phase stator currents-waveforms during load change. From top to bottom: Stator voltage magnitude, stator frequency, stator voltage waveform. (Left) Simulation results. (Right) Experimental test.

c. Rotor speed variation around synchronous speed

To observe the performance of the DFIG controlled by proposed controller based DRFVC in the whole speed range a slip-speed ω_r reversal test is tested. This test was conducted with the DFIG initially running at 1400 rpm subsynchronous speed with fixed stator voltage and load, then imposing a ramp reference speed ended to supersynchronous speed equal to 1600 rpm at t = 3 s.

The obtained results are shown in Fig. 4.12. It can be seen that the DFIG generator works well in the whole speed range. During the transient period (0.5 → 3 s), the stator voltage and frequency are kept

at their desire value (200V-50 Hz). At t = 2s when passing through the synchronous speed, the direction of rotor flux rotation is reversed which conduct to the change of the polarity of the rotor currents resulting in a phase shaft of 180◦. Moreover, it is possible to observe that the sector number, which represents the rotor-flux position at each time ascends in sub-synchronous speed operation, whereas, it is changed to descending in super-synchronous speed operation. This means that the direction of rotor-flux vector is reversed when the rotor-speed exceeds the synchronous-speed.
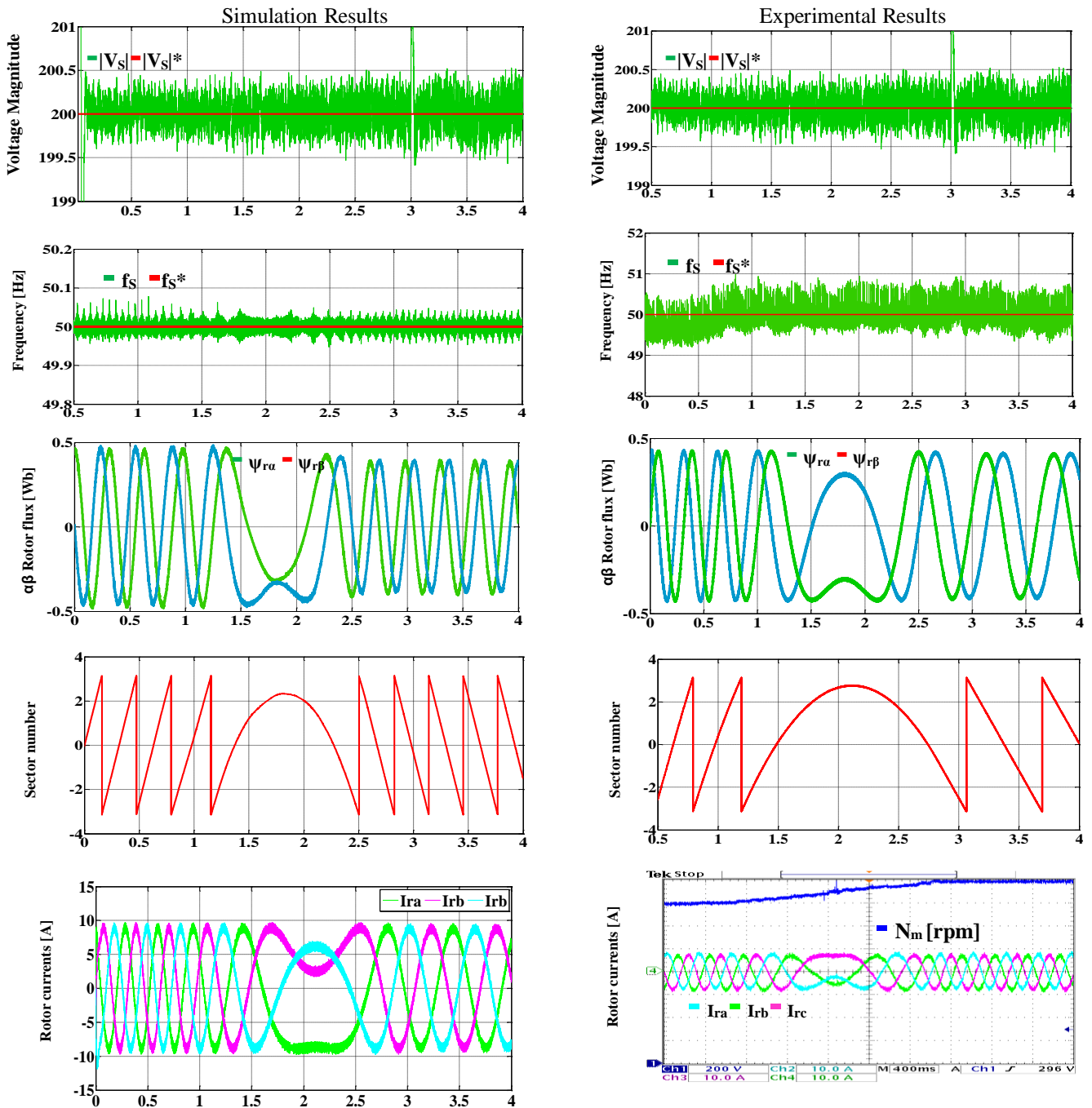
Fig. 4.12. Rotor speed change test with the standalone-DFIG operating at fixed Voltage-reference. From top to bottom: Stator voltage magnitude, stator frequency, rotor flux, electromagnetic torque, slip angle, and rotor current waveform. (Left) Simulation results. (Right) Experimental test.

Furthermore, the obtained results in Fig. 4.13. indicate that the stator voltage waveforms has the same controlled value of magnitude and frequency (200V-50Hz) at deferent of rotor speed as 1480 and 1550 rpm. In the same time, they are balance and clean from the harmonics frequency, which is an expected result since the control of stator voltage magnitude and frequency, is the mean target of proposed control approach. Hence, these test results demonstrating the ability of proposed controller to assert the DFIG operate with constant stator voltage and frequency around synchronous-speed, and ensuring the stability of the generator in the full speed range.

Finally, looking to these results, a very good agreement between the simulation and experimental results is observable. At all operating conditions, the generator rotor flux closely follow their desired reference with an acceptable ripple.
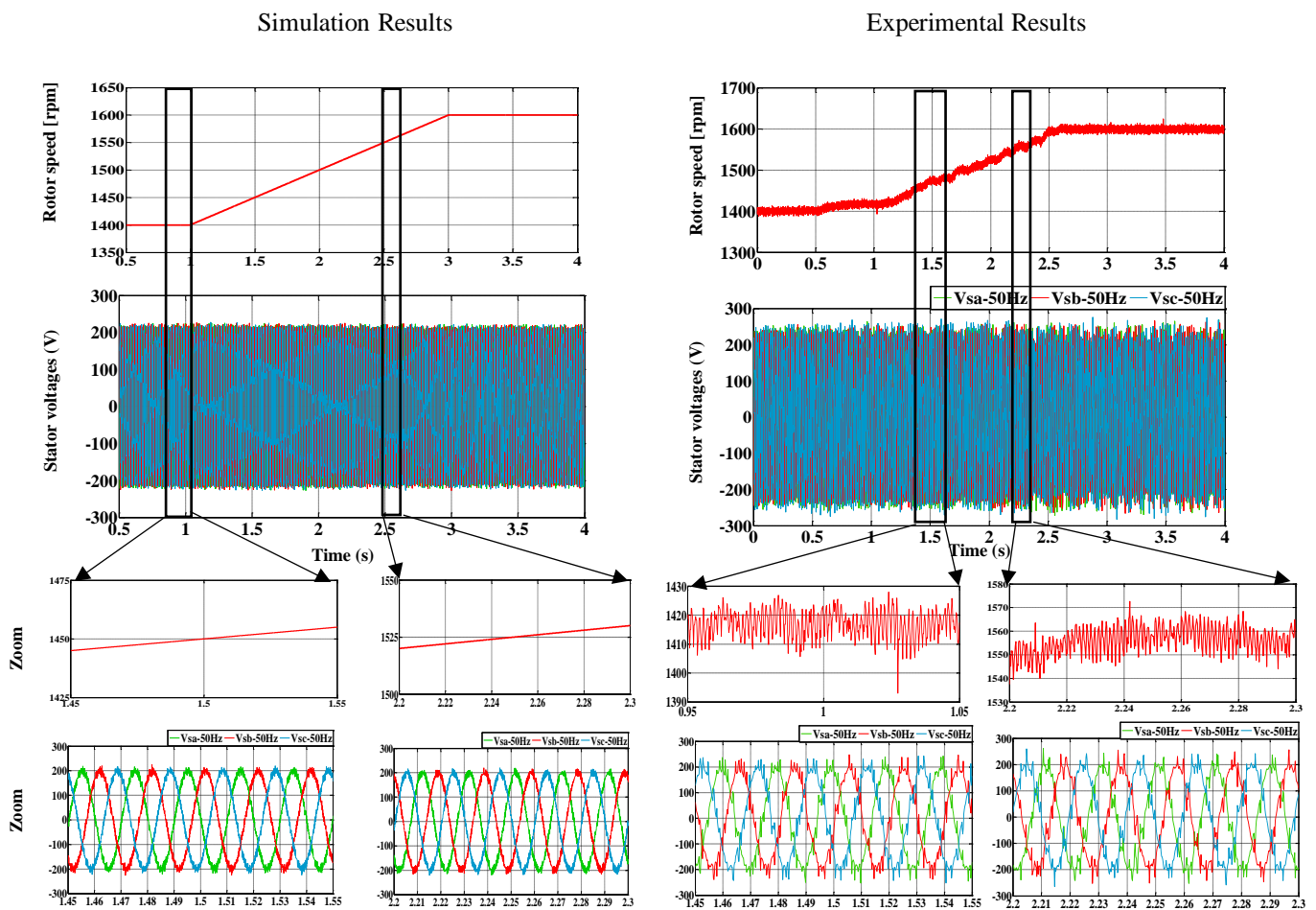

Fig. 4.13. Three phase stator voltage-waveforms during rotor speed change. From top to bottom: Stator voltage magnitude, stator frequency, rotor flux, stator current waveform. (Left) Simulation results. (Right) Experimental test.

4.6.2 DTC

In this section, the DRFVC test result for standalone DFIG is given. It is good to note that the value of the proportional and integral gains of the PI controllers of stator voltage magnitude and

frequency control used in the simulation study are the same as the ones used in experimental tests, the two PI controllers parameters of proposed DTC strategies are given in Appendix C in Table C.2. Same for the torque and flux hysteresis controllers were configured with a hysteresis band equivalent to 2% of their corresponding rated values. Also, The sampling period of the proposed controller based DTC strategy is set at Ts =10 µs for simulation and Ts =300 µs for experimental, For all the next tests the reference of the stator-voltage frequency is fixed at 50 Hz as the desire value for load equipment which is mainly connected to the stator.

a. Stator voltage-magnitude step variation:

The stator-voltage magnitude step response of the DTC strategy while the load is constant and the rotor speed is fixed at 1400 rpm is investigated and presented in Fig. 4.14. Initially, the generator is started with 150 v and a load torque of 3 N.m, after that a step stator-voltage reference of 100 V is imposed at t = 1 s. and then is returned back by -100V at $t = 3\ s$.

As can be seen, the stator voltage and frequency tracks their references value accurately with small overshoot. Moreover, the stator-voltage rise time for the DTC strategy is approximately 0.5 s. however, the rise-time and overshoot of the stator-voltage and frequency can be determined arbitrarily by adjusting both of PI controller gains. In this control strategy, the rotor flux and torque references is determined based on the stator voltage magnitude and frequency control Loop. As can be seen in Fig. 4.14., the estimated rotor flux and torque developed by the DFIG follow their reference value, which are increase when the stator voltage increase and vice versa. In the experimental results, during operating at 250 V voltage magnitude, the estimated torque exhibits an oscillation of 2 N.m, which is introduced by the DC chopper that controls the prime mover (DC motor) due to the overloading operation. Moreover, it is possible to observe that during this test the rotor current amplitude increase and decrease respects to the stator-voltage magnitude variation. Fig. 4.15 shows a zoomed version of the three phase stator-voltages waveforms obtained in this test. It can be seen from this figures that the three phase has a balanced sinusoidal waveforms and takes a fast response, at the set reference value of voltage magnitude and frequency.

This test illustrates the effectiveness of the proposed method for control of the stator-voltage amplitude and frequency accurately and independently.

b. Load variation:

Fig. 4.16. illustrates the dynamic response of the generator system to the load step change, which is loaded and unloaded by 20% of (4 kW rated Power) in instants t=1s and t=3s respectively, with the DFIG operating at a constant stator voltage of 200V and rotor speed of 1400 rpm. In this test, the DFIG is operated in the torque control mode, by setting manually the load value in stator, while the
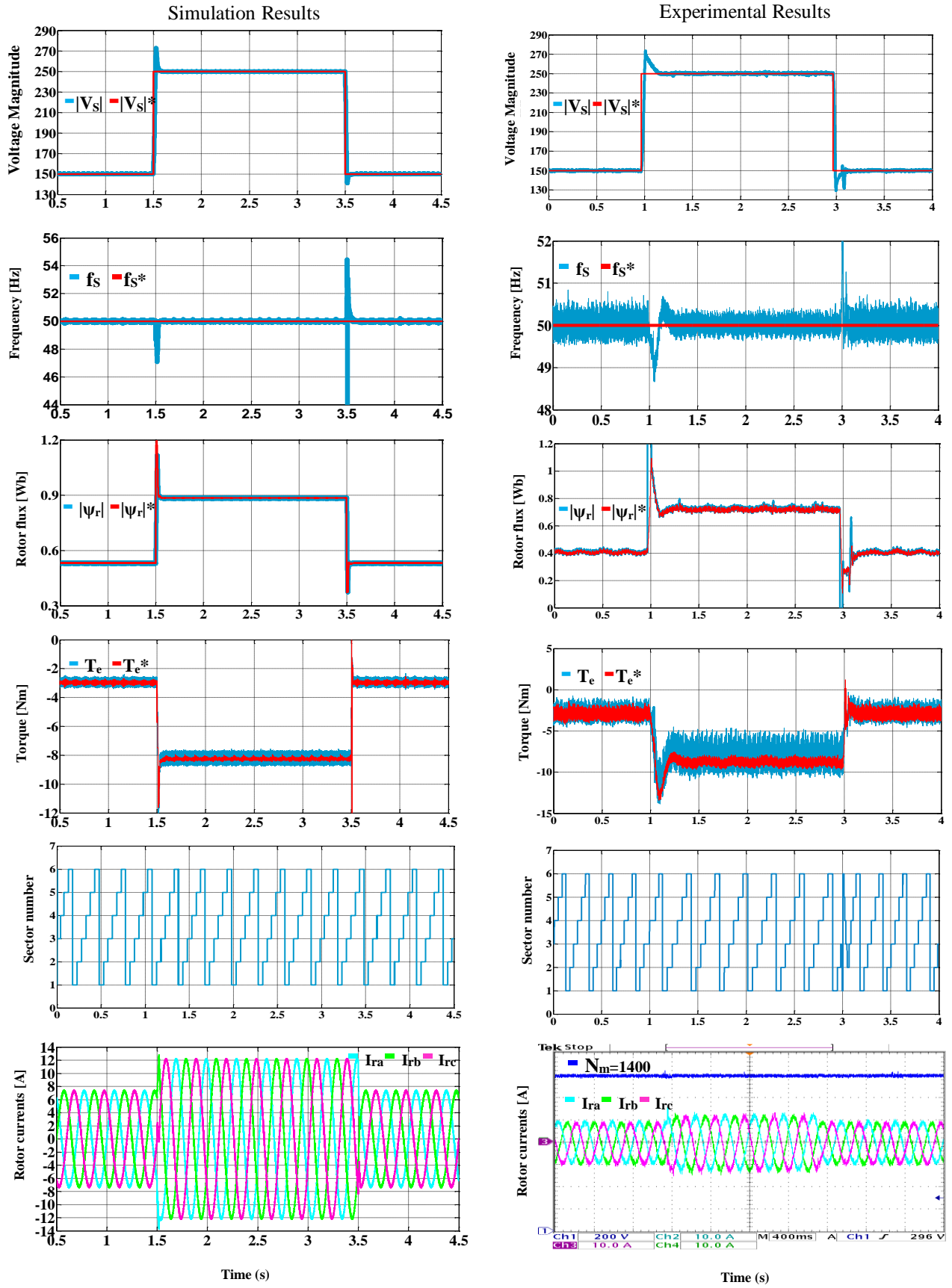
Fig. 4.14. Voltage-reference change test with the standalone-DFIG operating at fixed-load. From top to bottom: Stator voltage magnitude, stator frequency, rotor flux, electromagnetic torque, sector number, and rotor current waveform. (Left) Simulation results. (Right) Experimental test.

prime mover DC drive is operated in constant speed control mode in order to maintain the stator voltage roughly constant during the test. The results show that the estimated stator voltage and frequency tracks very well their reference value with an ignorable overshot, which handle by the controller action during short time. Moreover, the variation profiles of the estimated torque and load are identical due to the action of proposed controller to prevent the frequency drop. Furthermore, the obtained results indicate that there is a decoupled control of the rotor flux and electromagnetic torque developed by the DFIG.
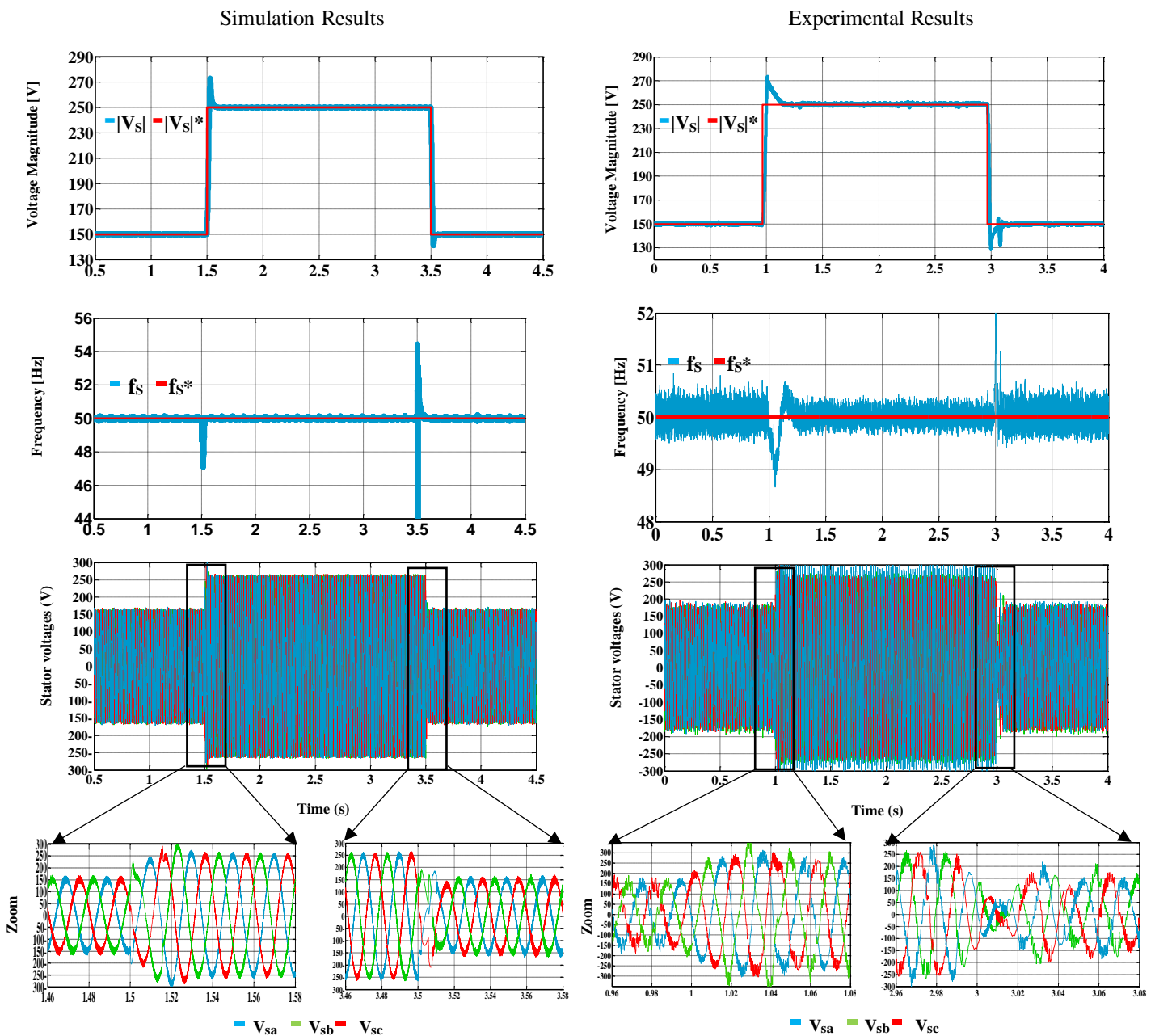
Fig. 4.15. Three phase stator voltage-waveforms during voltage magnitude step change. From top to bottom: Stator voltage magnitude, stator frequency, stator voltage waveform. (Left) Simulation results. (Right) Experimental test.
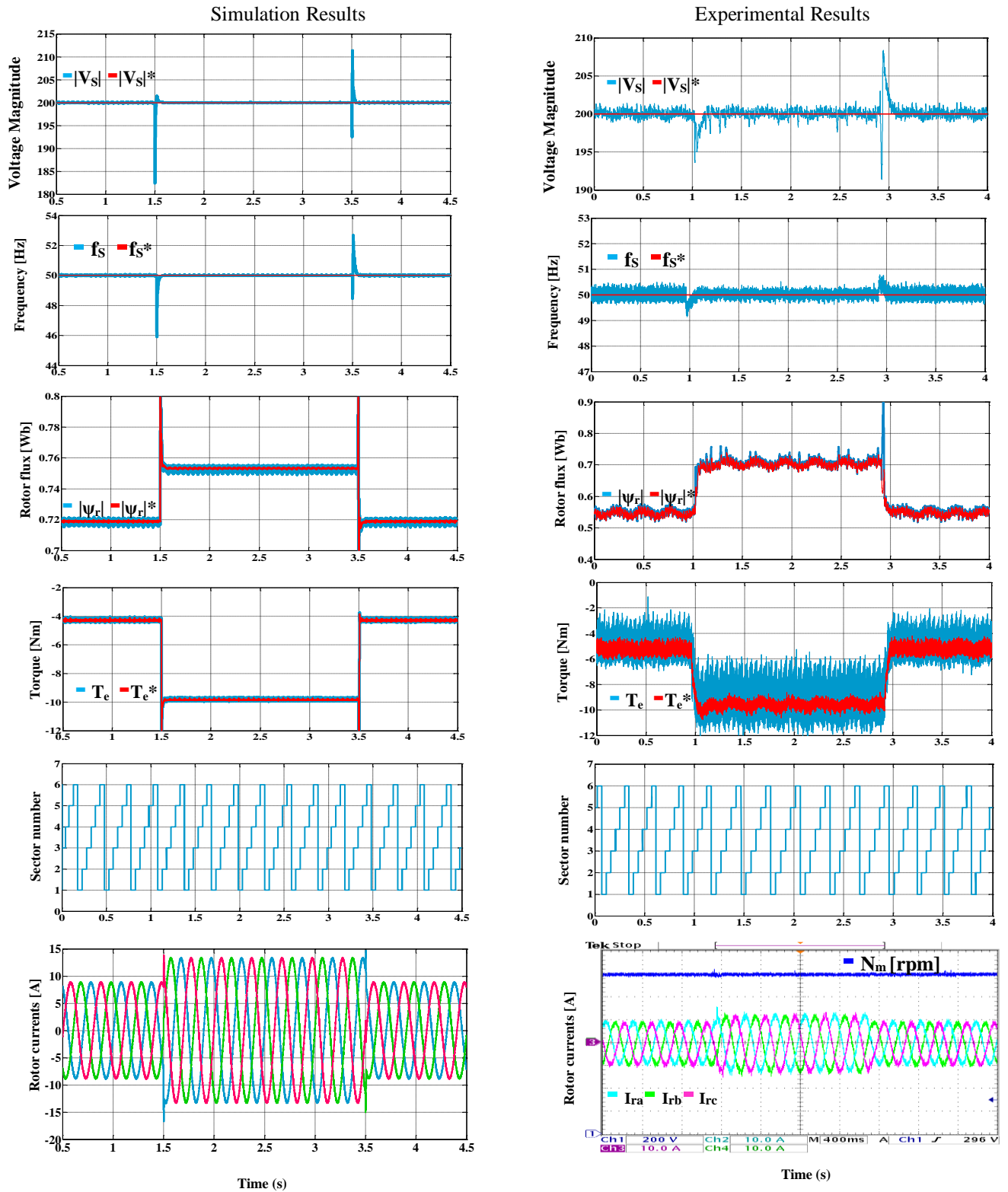
Fig. 4.16. Load change test with the standalone-DFIG operating at fixed Voltage-reference. From top to bottom: Stator voltage magnitude, stator frequency, rotor flux, electromagnetic torque, sector number, and rotor current waveform. (Left) Simulation results. (Right) Experimental test.

It is also visible that the electromagnetic torque is regulate by load angle, which is an expected result since the rotor flux level is approximately fixed and set to the generator stator-voltage rated value. In the experimental results, the torque ripple content decreases with the increase of the load torque. In addition, during this test, the rotor phase currents are increase due to the increase of load, and decrease when the load decrease, hence same discussions as before apply. Fig. 4.17. shows a zoomed version of the stator phase currents response obtained in this test. It can be seen from this figures that they varies according to the load level applied to the generator. Furthermore, they has balance sinusoidal waveforms and less harmonic frequency due to the load nature and proposed control performance.
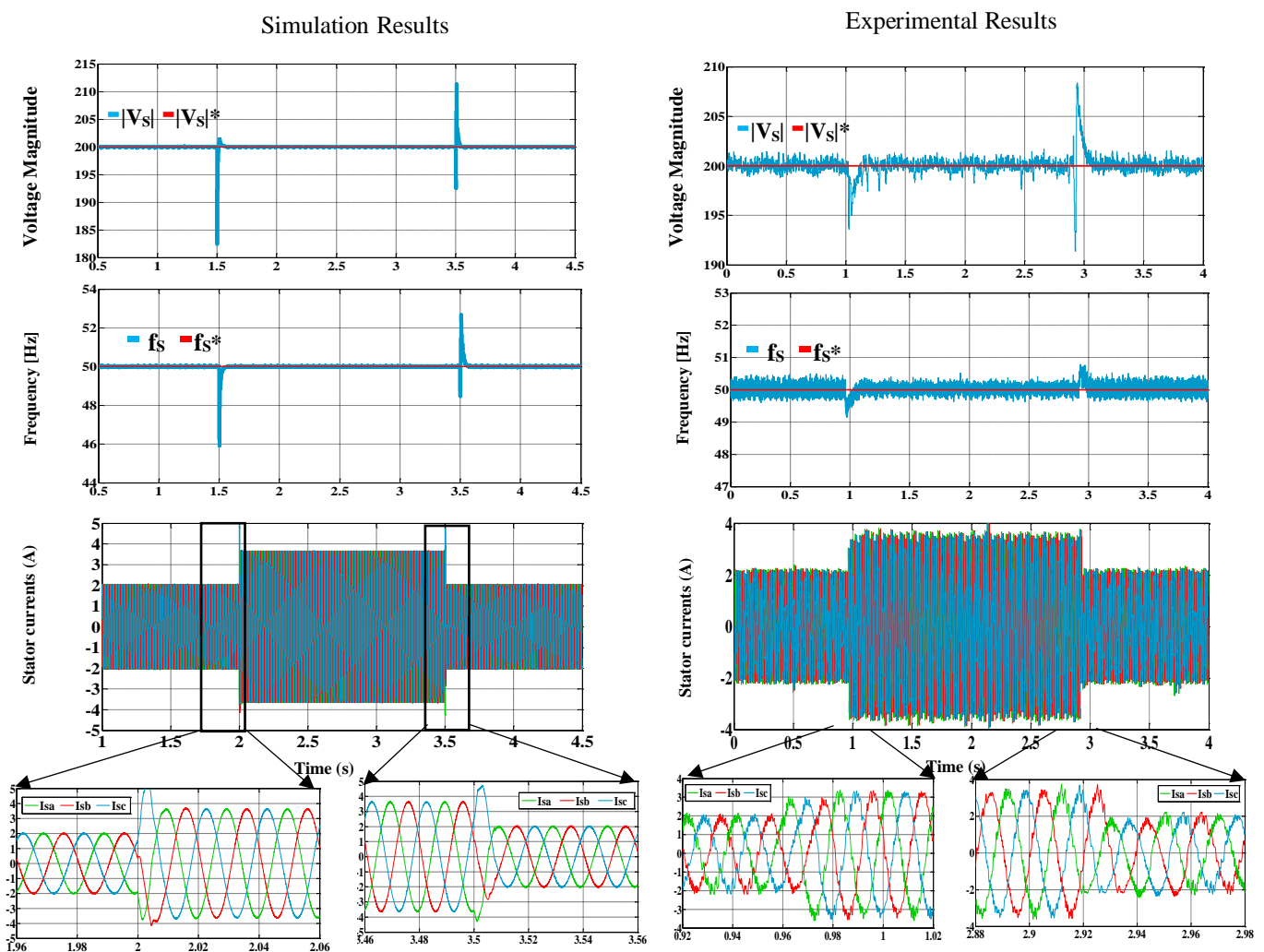
Fig. 4.17. Three phase stator currents-waveforms during load change. From top to bottom: Stator voltage magnitude, stator frequency, stator voltage waveform. (Left) Simulation results. (Right) Experimental test.

From this test, it is evident to conclude that the applied proposed approach is able to allow the DFIG produce a constant rated of stator voltage and frequency in steady state operation within a wide load variation scale.

c. Rotor speed variation around synchronous speed:

To observe the performance of the DFIG controlled by proposed controller based DTC in the whole speed range a slip-speed ω_r reversal test is tested. This test was conducted with the DFIG initially running at 1400 rpm subsynchronous speed with fixed stator voltage and load,
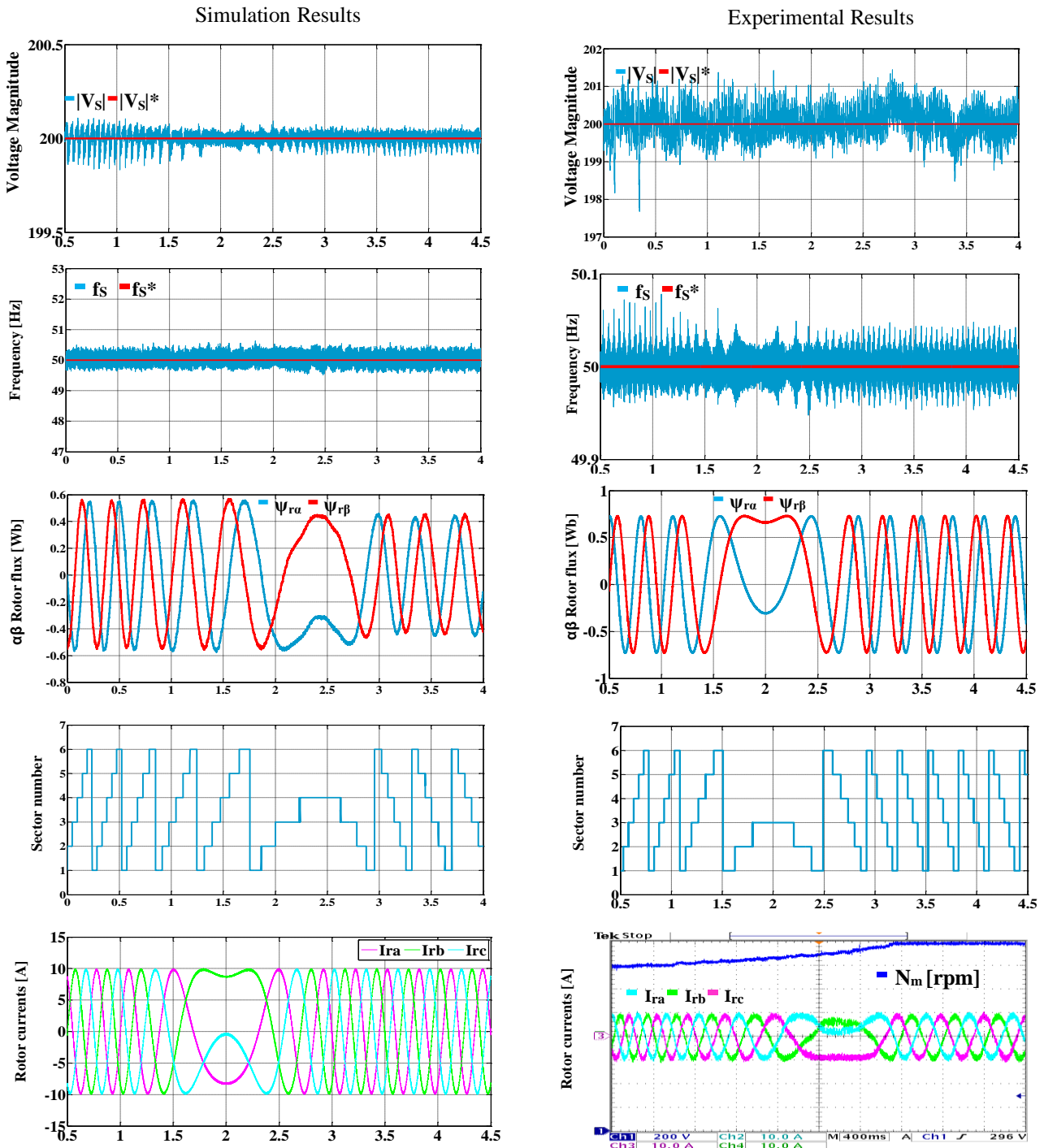
Fig. 4.18. Rotor speed change test with the standalone-DFIG operating at fixed Voltage-reference. From top to bottom: Stator voltage magnitude, stator frequency, rotor flux, electromagnetic torque, slip angle, and rotor current waveform. (Left) Simulation results. (Right) Experimental test.

then imposing a ramp reference speed ended to supersynchronous speed equal to 1600 rpm at t = 3 s. The obtained results are shown in Fig. 4.18. It can be seen that the DFIG generator works well in the whole speed range. During the transient period (0.5 → 3 s), the stator voltage and frequency are kept at their desire value (200V-50 Hz).
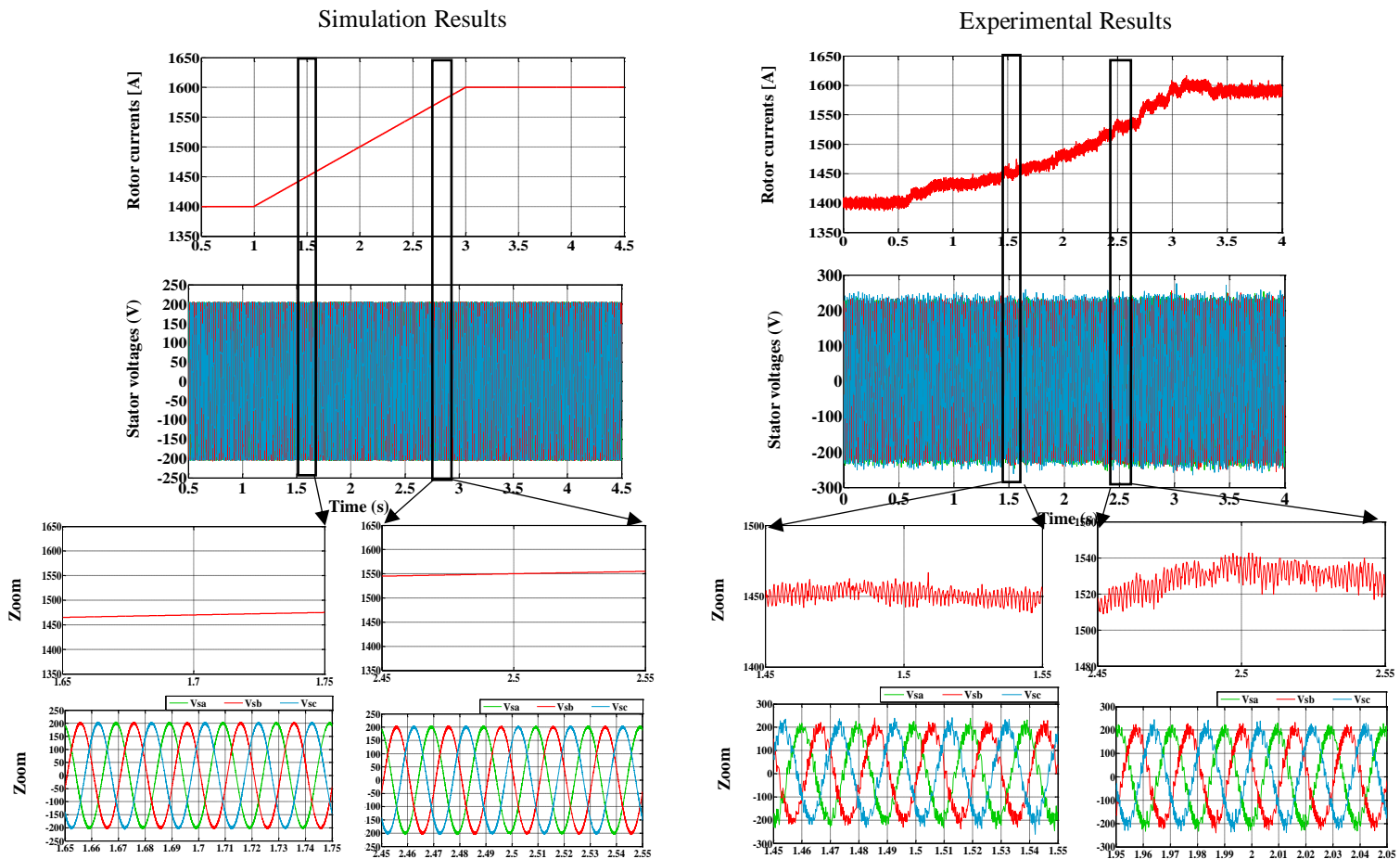
**Fig. 4.19.** Three phase stator voltage-waveforms during rotor speed change. From top to bottom: Stator voltage magnitude, stator frequency, rotor flux, stator current waveform. (Left) Simulation results. (Right) Experimental test.

At t = 2s when passing through the synchronous speed, the direction of rotor flux rotation is reversed which conduct to the change of the polarity of the rotor currents resulting in a phase shaft of 180◦. Moreover, it is possible to observe that the sector number, which represents the rotor-flux position at each time ascends in sub-synchronous speed operation, whereas, it is changed to descending in super-synchronous speed operation. This means that the direction of rotor-flux vector is reversed when the rotor-speed exceeds the synchronous-speed. Furthermore, the obtained results in Fig. 4.19. indicate that the stator voltage waveforms has the same controlled value of magnitude and frequency (200V-50Hz) at deferent of rotor speed as 1480 and 1550 rpm. In the same time, they are balance and clean from the harmonics frequency, which is an expected result since the control of stator voltage magnitude

and frequency, is the mean target of proposed control approach. Hence, these test results demonstrating the ability of proposed controller to assert the DFIG operate with constant stator voltage and frequency around synchronous-speed, and ensuring the stability of the generator in the full speed range. Looking to these results, a very good agreement between the simulation and experimental results is observable. At all operating conditions, the generator torque and rotor flux closely follow their desired reference with an acceptable ripple.

5. Chapter conclusion

This chapter incorporated the subtle element explanation of the traditional DRFVC and DTC methodology. This direct control methodology has many merits over field arranged regulation which is examined in this part additionally has a few demerits such as generation of torque and flux ripple and changing exchanging frequency. The torque and flux ripple is because of the hysteresis regulator which can moreover be diminished fundamentally by diminishing the sampling time. The changing switching frequency is because of the part variation of the rotor flux vector. This method controls the stator-voltage amplitude and frequency by controlling the rotor-flux magnitude and angle, respectively. Since the proposed method was completely performed in the rotor reference frame, neither rotor position/speed sensor nor any reference-frame transformation is required. The proposed method employed the same switching strategy for both the sub and supersynchronous speed operation modes, which was another outstanding feature of this controller design.

General conclusion

General conclusion

In this thesis, a control of standalone DFIG for autonomies systems based on stator voltage and frequency control has been developed, analyzed, designed and implemented. The simulation and experimental results show that effective control of the standalone DFIG has been achieved for generating modes. This study provides a high performance control solution for a standalone DFIG in the fixed voltage and frequency application, other than the widely applied stator flux oriented control scheme [16, 20, 24-26, 38] which is sensitive to the variation of machine parameters and requires accurate speed sensor signal for the flux orientation and decoupling. Considering the moist, direct control scheme is more reliable and attractive without involving many machine parameters and requiring speed sensor signal for the control of torque and rotor flux.

In summary, the contributions made in this thesis are:

- Review and investigation on classical control methods for standalone DFIG based FOC.
- Improved rotor current control schemes based indirect stator voltage magnitude and frequency control (Approach-1), via FS-PCC or HCC for standalone DFIG.
- Develop a new sensor-less control methods for standalone DFIG based direct stator voltage magnitude and frequency control (Approach-2), via DTC or DRFVC for standalone DFIG.
- Simulation and experimental verification of two proposed control approaches for RSC.

In this thesis, a satisfactory modeling and experimental results indicate the feasibility of the proposed control scheme for RSC. The proposed approach-1 control scheme has a simple structure with only one PI controller, and eliminates the PI current loop and PWM modulator successfully. The controller gives good stator-voltage and frequency control performance. The approach-2 control scheme of RSC employs a sensor-less control structure and is implemented to control the voltage magnitude and frequency adequately. By controlling and the rotor flux vector of the DFIG, the required dc bus voltage sensor is used for well generation of the rotor voltage vector. Table a.1 lists

general comparison of the control schemes for the RSC discussed in this thesis in terms of the control ability, structure, etc. The shadowed parts indicate the drawbacks of the schemes.

Table a.1 Comparison of different control schemes for the RSC.

	DTC	DRFVC	FS-PCC	HCC
Stator Voltage Sensors	required	required	required	required
Stator Current Sensors	not required	not required	required	required
Rotor Current Sensors	required	required	required	required
DC Bus Voltage Sensor	required	required	not required	not required
Rotor Speed Sensor	not required	not required	not required	not required
PI rotor currents controllers	not required	not required	not required	not required
PWM or SVM modulators	not required	required	not required	not required
DFIG parameters involved	R_r	R_r	R_r, R_s, L_s, L_m, L_r	L_s, L_m
Flux orientation and decoupling algorithm	not required	not required	required	required
Flux estimation	required	required	not required	not required
Torque control	directly	indirectly	indirectly	indirectly
Flux control	directly	directly	indirectly	indirectly
Switching frequency	variable	constant	variable	variable
Implementation Complexity	simplest	simplest	Medium	Medium

It can be concluded that both DTC and DRFVC schemes can effectively control the standalone DFIG for the fixed stator voltage and frequency applications. By considering the

parameters dependency, complexity of the structure and cost, it is clear that approach 2 is superior to FOC.

This thesis covers important subjects concerning the standalone DFIG systems. Nevertheless, there are more aspects that can be recommended for future research, listed as follows:

• Using other RSC converter topology like three-level converter, matrix converter…

• Using other doubly fed generator type as brushless DFIG, six phase rotor DFIG, dual stator DFIG.

• Experimental verification of back-to-back converter control including DTC techniques and DPC.

• DTC improvement to eliminate torque and rotor flux oscillation using DTC-SVM, Predictive DTC.

• Study of DTC with constant switching frequency by modification of the control algorithm.

References

References

References

[1]	A. Bocquel, J. Janning, Analysis of a 300 MW Variable Speed Drive for Pump-Storage Plant Applications, in : Eur. Conf. Power Electron. Appl., 2005: pp. 1–10

[2]	G. Abad, J. López, M.A. Rodríguez, L. Marroyo, G. Iwanski, Steady State of the Doubly Fed Induction Machine, in: Doubly Fed Induction Mach., John Wiley & Sons, Inc., 2011: pp. 155–208.

[3]	G. Abad, J. López, M.A. Rodríguez, L. Marroyo, G. Iwanski, Dynamic Modeling of the Doubly Fed Induction Machine, in: Doubly Fed Induction Mach., John Wiley & Sons, Inc., 2011: pp. 209–239.

[4]	B.K. Bose, Induction Motor Slip-Power Recovery Drives, in: Mod. Power Electron. AC Drives, Prentice Hall, 2002: pp. 301–332.

[5]	J. Pyrhönen, T. Jokinen, V. Hrabovcová, Design of Rotating Electrical Machines, John Wiley & Sons, Inc., 2008.

[6]	K. Protsenko, D. Xu, Modeling and Control of Brushless Doubly-Fed Induction Generators in Wind Energy Applications, Power Electron. IEEE Trans. 23 (2008) 1191–1197.

[7]	M.G. Jovanovic, R.E. Betz, J. Yu, The Use of Doubly Fed Reluctance Machines for Large Pumps and Wind Turbines, IEEE Trans. Ind. Appl. 38 (2002) 1508–1516.

[8]	S. Ademi, M. Jovanovic, Theoretical and Experimental Evaluation of Vector Control for Doubly-Fed Reluctance Generators, Proc. - 2014 Int. Conf. Electr. Mach. ICEM 2014. (2014) 936–942.

[9]	P. Zhan, W. Lin, J. Wen, M. Yao, N. Li, Design of LCL Filters for the Back-to-back Converter in a Doubly Fed Induction Generator, 2012 IEEE Innov. Smart Grid Technol. - Asia, ISGT Asia 2012. (2012) 1–6.

[10]	N. Flourentzou, V.G. Agelidis, G.D. Demetriades, VSC-Based HVDC Power Transmission Systems: An Overview, IEEE Trans. Power Electron. 24 (2009) 592– 602.

[11]	D.W. Hart, Introduction to Power Elctronics, Prentice Hall, 1997.

[12]	R. Pena, J.C. Clare, G.M. Asher, Doubly Fed Induction Generator Using Back-to-back PWM Converters and Its Application to Variable-Speed Wind-Energy Generation, IEE Proc. - Electr. Power Appl. 143 (1996) 231.

[13]	M. Malinowski, K. Gopakumar, J. Rodriguez, M.A. Perez, A Survey on Cascaded 125 Multilevel Inverters, IEEE Trans. Ind. Electron. 57 (2010) 2197–2206.

[14]	G. Abad, M.Á. Rodriguez, J. Poza, Three-Level NPC Converter-Based Predictive Direct Power Control of the Doubly Fed Induction Machine at Low Constant Switching Frequency, IEEE Trans. Ind. Electron. 55 (2008) 4417–4429.

[15]	M. Dybkowski, K. Szabat, Direct Torque Control of Induction Motor Drive System with Adaptive Sliding-Mode Neuro-Fuzzy Compensator, in: IEEE Int. Conf. Ind. Technol., 2015: pp. 714–719.

[16] R. Cárdenas, R. Peña, G. Tobar, Stability Analysis of a Wind Energy Conversion System Based on a Doubly Fed Induction Generator Fed by a Matrix Converter, Ind. Electron. IEEE Trans. 56 (2009) 4194–4206.

[17] G. Abad, J. López, M.A. Rodríguez, L. Marroyo, G. Iwanski, Introduction to A Wind Energy Generation System, in: Doubly Fed Induction Mach., John Wiley & Sons, Inc., 2011: pp. 1–85.

[18] M. Tsili, S. Papathanassiou, A Review of Grid Code Technical Requirements for Wind Farms, IET Renew. Power Gener. 3 (2009) 308.

[19] G. Iwanski, P. Pura, T. Luszczyk, M. Szypulski, Harmonics and Unbalance Compensation of the Generated Voltage in a Standalone DFIG, in: 2013 Eighth Int. Conf. Exhib. Ecol. Veh. Renew. Energies, IEEE, 2013: pp. 1–6.

[20] R. Cardenas, R. Pena, S. Alepuz, G. Asher, "Overview of control systems for the operation of DFIGs in wind energy applications," IEEE Transactions on Industrial Electronics , vol. 60, no. 7, pp. 2776–2798, July 2013.

[21] M. Stiebler, "Wind energy systems for electric power generation," Springer, Germany, pp. 30–53, 2008.

[22] I. Boldea, "Variable Speed Generators (The Electric Generators Handbook)," Taylor and Francis, Cha.4, pp-1– 46, 2006.

[23] P. Vas, "Vector control of AC machines," Clarendon press Oxford, 1990.

[24] J. A. Santisteban and R. M. Stephan, "Vector control methods for induction machines: An overview," IEEE Transactions Education., vol. 44, no. 2, pp. 170– 175, May 2001.

[25] L. Xu and P. Cartwright, "Direct active and reactive power control of in DFIG for wind energy generation," IEEE Transactions on Energy Conversion, vol. 21, no. 3, pp. 750–758, Sep. 2006.

[26] M. Depenbrock, "Direct self-control (DSC) of inverter-fed induction motors," IEEE Transactions on Power Electronics, vol. 3, no. 4, pp. 420–429, 1988.

[27] J. A. Santisteban and R. M. Stephan, "Vector control methods for induction machines: An overview," IEEE Transactions Education., vol. 44, no. 2, pp. 170– 175, May 2001.

[28] B. Hopfensperger, D. Atkinson, and R. A. Lakin, "Stator-flux-oriented control of a doubly-fed induction machine with and without position encoder," IEE Proceedings Electric Power Applications, vol. 146, No. 6, pp. 597–605, Nov. 1999.

[29] S. Pererada, A. Tilli, and A. Tonielli, "Indirect stator flux-oriented output feedback control of a doubly fed induction machine," IEEE Transactions on Control System Technology, vol. 2, no. 6, pp. 875–887, Nov. 2003.

[30] S. Muller, M. Deicke, and R. W. De Doncker, "Doubly fed induction generator systems for wind turbines, " IEEE Industrial Application Magazine, vol. 17, no. 1, pp. 26–33, May/June 2002.

[31] H. Akagi and H. Sato, "Control and performance of a doubly-fed induction machine intended for a flywheel energy storage system," IEEE Transactions Power Electronics, vol. 17, no. 1, pp. 109–116, Jan. 2002.

[32] Bimal K. Bose, "Modern Power Electronics and AC Drives," Chapter 10, pp. 535- 557, Prentice Hall PTR, 2002.

[33] Bose, B.K., "Expert system, fuzzy logic, and neural network applications in power electronics and motion control," In Proceedings of the IEEE , vol. 82, no. 8, pp.1303- 1323, Aug 1994.

[34] M. G. Simoes, B.K. Bose, Ronald J. Spiegel, "Design and performance evaluation of a fuzzy logic-based variable-speed wind generation system," In IEEE Transactions on Industry Applications , vol.33, no.4, pp.956–965, Jul/Aug 1997.

[35] Wang Jialong; Hyun Seung Ho, "ANN based pitch angle controller for variable speed variable pitch wind turbine generation system," In Strategic Technology (IFOST), 2011 6th International Forum on , vol. 1, pp. 443-447, 22-24 Aug. 2011.

[36] I. Takahashi, and T. Noguchi, "A new quick-response and high-efficiency control strategy of an induction motor," IEEE Transactions on Power Electronics, vol. 22, no. 5, pp. 820–827, 1986.

[37] S. Arnalte, J. C. Burgos, and J. L. Rodríguez-Amenedo, "Direct torque control of a doubly-fed induction generator for variable speed wind turbines," Electric Power Components and Systems, vol. 30, no. 2, pp. 199–216, 2002.

[38] M. Malinowski, M.P. Kazmierkowski, S. Hansen, F. Blaabjerg, G.D. Marques, "Virtual-flux-based direct power control of three-phase PWM rectifiers," IEEE Transactions on Industry Applications, vol. 37, no. 4, pp.1019–1027, Jul/Aug 2001.

[39] R. Datta, and V.T. Ranganathan, "Direct power control of grid-connected wound rotor induction machine without rotor position sensors," IEEE Transactions on Power Electronics, vol. 16, no. 3, pp.390–399, May 2001.

[40] L. Xu and P. Cartwright, "Direct active and reactive power control of in DFIG for wind energy generation," IEEE Transactions on Energy Conversion, vol. 21, no. 3, pp. 750–758, Sep. 2006.

[41] W. S. Kim, Su. Jou; K. Lee, and S. Watkins, "Direct power control of a doubly fed induction generator with a fixed switching frequency," IEEE Industry Applications Society Annual Meeting, 2008. IAS '08. pp.1–9, Oct. 2008.

[42] D. Zhi, L. Xu, and B.W. Williams, "Improved direct power control of grid-connected dc/ac converters," IEEE Transactions on Power Electronics , vol. 24, no. 5, pp. 1280–292, May 2009.

[43] M. Malinowski, M. Jasinski, and M.P. Kazmierkowski, "Simple direct power control of three-Phase PWM rectifier using space-vector modulation (DPC-SVM)," IEEE Transactions on Industrial Electronics, vol. 51, pp. 447 454, 2004.

[44] D. Casadei, G. Serra, A. Tani, "Improvement of direct torque control performance by using a discrete SVM technique," Power Electronics Specialists Conference (PESC) 98 Record Annual IEEE 29th, vol. 2, pp. 997–1003, May 1998.

[45] M.V. Kazemi, A.S. Yazdankhah, H.M. Kojabadi, "Direct power control of DFIG based on discrete space vector modulation," Journal of Renewable Energy, vol. 35, no. 5,pp. 1033–1042, 2010.

[46] A.L. Sergio, R. Angel, O. Estanis, "Predictive control strategy for DC/AC converters based on direct power control," IEEE Transactions on Industrial Electronics, vol. 54,pp. 1261–1271, 2007.

[47] D. Zhi, L. Xu, B.W. Williams, "Model-based predictive direct power control of doubly Fed induction generators," IEEE Transactions on Power Electronics, vol. 25, no. 2, pp. 341–351, Feb. 2010.

[48] G. Abad, M. A. Rodrıguez, and J. Poza, "Predictive direct power control of the doubly fed induction machine with reduced power ripple at low constant switching frequency," in Proceedings IEEE ISIE'07 Conference, 2007.

[49] L. Shang and J. Hu., "Sliding-mode-based direct power control of grid-connected wind-turbine-driven doubly fed induction generators under unbalanced grid voltage conditions," IEEE Transactions on Energy Conversion, vol. 27, no. 2, June 2012.

[50] R. D. Shukla, R. K. Tripathi, "A novel voltage and frequency controller for standalone DFIG based wind energy conversion system," Renewable and Sustainable Energy Review, vol. 37, pp. 69–89, 2014.

[51] R.S. Pena, G.M. Asher, J.C Clare, and R. Cardenas, "A constant frequency constant voltage variable speed stand-alone wound rotor induction generator," In International Conference on Opportunities and Advances in International Electric Power Generation, no. 419, pp.111–114, Mar 1996.

[52] R.S. Pena, R.J. Cardenas, G.M. Asher, J.C. Clare, "Vector controlled induction machines for stand-alone wind energy applications", Industry Application Conference, vol. 3, pp. 1409–1415, Oct. 2000.

[53] A.K. Jain, V.T. Ranganathan, "Wound rotor induction generator with sensorless control and integrated active filter for feeding nonlinear loads in a stand-alone grid," In IEEE Transactions on Industrial Electronics, vol.55, no.1, pp.218–228, Jan. 2008.

[54] G. Iwanski G, W. Koczara "Sensorless direct voltage control method for stand- alone slip-ring induction generator," Proceedings of 11th EPE, Dresden, Germany, 2005.

[55] G.Iwanski, W. Koczara,"DFIG-Based power generation system with UPS function for variable-speed applications," in Industrial Electronics, IEEE Transactions on, vol. 55, no. 8, pp.3047–3054, Aug. 2008.

[56] C. Schauder, Adaptive Speed Identification for Vector Control of Induction Motors Without Rotational Transducers, IEEE Trans. Ind. Appl. 28 (1992) 1054–1061.

[57] M. Dybkowski, T. Orlowska-Kowalska, Performance of the Speed Sensorless Induction Motor Drive for Traction Application with MRAS Type Speed and Flux 123 Estimator, Proc. Int. Conf. Optim. Electr. Electron. Equipment, OPTIM. (2012) 477– 481.

[58] M. Dybkowski, T. Orlowska-Kowalska, Speed Sensorless Induction Motor Drive System with MRAS type Speed and Flux Estimator and Additional Parameter Identification, IFAC, 2013.

[59] T. Orlowska-Kowalska, M. Dybkowski, Stator-Current-Based MRAS Estimator for a Wide Range Speed-Sensorless Induction-Motor Drive, IEEE Trans. Ind. Electron. 57 (2010) 1296–1308.

[60] R. Cárdenas, R. Peña, J. Proboste, G. Asher, J. Clare, MRAS Observer for Sensorless Control of Standalone Doubly Fed Induction Generators, IEEE Trans. Energy Convers. 20 (2005) 710–718.

[61] G. Yuan, J. Chai and Y. Li. "Vector control and synchronization of doubly fed induction wind generator system," IEEE 4th International Power Electronics and Motion Control Conference, pp. 886–890, 2004.

[62] A.G. Abo-Khalil, D.-C. Lee, and S.P. Ryu, "Synchronization of DFIG output voltage to utility grid," European Power and Energy Systems, pp. 1–6, 2006.

[63] X. Zhang, D. Xu, Y. Lang and H. Ma. "Study on stagewise control of connecting DFIG to the grid," IEEE 5th International Power Electronics and Motion Control Conference, pp. 1–5, 2006.

[64] S. A. Gomez and J. L. R. Amenedo. "Grid synchronization of doubly fed induction generators using direct torque control," IEEE 28th Annual Conference of the Industrial Electronics Society, pages 3338–3343, 2002.

[65] J. Arbi, M. J.-B. Ghorbal, I. Slama-Belkhodja, and L. Charaabi, "Direct virtual torque control for doubly fed induction generator grid connection," IEEE Transaction on Industrial Electronics, vol. 56, no. 10, pp. 4163–4173, Oct. 2009.

[66] H. Jiefeng, Z. Jianguo, Z. Yongchang,G. Platt,M. Qishuang and D.G. Dorrell, "Predictive direct virtual torque and power control of doubly fed induction generators for fast and smooth grid synchronization and flexible power regulation," IEEE Transaction on Power Electronics, vol. 28, no. 7, pp.3182–3194, July 2013.

[67] G. Abad, M. A. Rodriguez, and J. Poza, "Two-level VSC based predictive direct torque control of the doubly fed induction machine with reduced torque and flux ripples at low constant switching frequency, " IEEE Transactions on Power Electronics. vol. 23, no. 3, pp. 1050–1061, May 2008.

[68] R. Tirumala and N. Mohan, "Seamless transfer of a grid-connected PWM inverters between utility-interactive and stand-alone modes," in Proceedings Annual Power Electronic Conference, vol. 2, pp. 1081–1086, 2002.

[69] R. Teodorescu and F. Blaabjerg, "Flexible control of small wind turbines with grid failure detection operating in stand-alone and grid-connected mode," IEEE Transactions on Power Electronics, vol. 19, no. 5, pp. 1323–1332, Sep. 2004.

[70] J. Mohammadi, S. Vaez-zadeh, S. Afsharnia and E. Daryabeigi, "A combined vector and direct power control for DFIG-based wind turbines, " IEEE Transaction on Sustainable Energy, vol. 5, no. 3, pp. 767–775, July 2014.

[71] Y. Kumar et al., "Wind energy: Trends and enabling technologies," Renew. Sustain. Energy Rev., vol. 53, pp. 209–224, 2016.

[72] Barra, A., Ouadi, H., Giri, F. et al. Sensorless Nonlinear Control of Wind Energy Systems with Doubly Fed Induction Generator. J Control Autom Electr Syst 27, 562–578 (2016). https://doi.org/10.1007/s40313-016-0263-1.

[73] S. Soued, M. A. Ebrahim, H. S. Ramadan, and M. Becherif, "Optimal blade pitch control for enhancing the dynamic performance of wind power plants via metaheuristic optimisers," IET Electr. Power Appl., vol. 11, no. 8, pp. 1432–1440, 2017.

[74] B. B. M. El Amine, A. Ahmed, M. B. Houari, and D. Mouloud, "Modeling, simulation and control of a doubly-fed induction generator for wind energy conversion systems," Int. J. Power Electron. Drive Syst., vol. 11, no. 3, pp. 1197–1210, 2020.

[75] Jaladi, K.K., Sandhu, K.S. & Bommala, P. Real-Time Simulator of DTC–FOC-Based DFIG During Voltage Dip and LVRT. J Control Autom Electr Syst 31, 402–411 (2020).

[76] W. Slimane, M. T. Benchouia, A. Golea, and S. Drid, "Second order sliding mode maximum power point tracking of wind turbine systems based on double fed induction generator," Int. J. Syst. Assur. Eng. Manag., vol. 11, no. 3, pp. 716–727, 2020.

[77] A. Dida and D. Benattous, "Doubly-fed induction generator drive system based on maximum power curve searching using fuzzy logic controller," Int. J. Power Electron. Drive Syst., vol. 5, no. 4, pp. 583–594, 2015.

[78] N. El Ouanjli, A. Derouich, A. El Ghzizal, Y. El Mourabit, B. Bossoufi, and M. Taoussi, "Contribution to the performance improvement of doubly fed induction machine functioning in motor mode by the DTC control," Int. J. Power Electron. Drive Syst., vol. 8, no. 3, pp. 1117–1127, 2017.

[79] A. Dida and D. Benattous, "Modeling and Control of DFIG Through Back-to-Back Five Levels Converters Based on Neuro-Fuzzy Controller," J. Control. Autom. Electr. Syst., vol. 26, no. 5, pp. 506–520, 2015.

[80] S. Abdeddaim, A. Betka, S. Drid, and M. Becherif, "Implementation of MRAC controller of a DFIG based variable speed grid connected wind turbine," Energy Convers. Manag., vol. 79, pp. 281–288, 2014.

[81] S. Abdeddaim and A. Betka, "Optimal tracking and robust power control of the DFIG wind turbine," Int. J. Electr. Power Energy Syst., vol. 49, no. 1, pp. 234–242, 2013.

[82] A. Benamor, M. T. Benchouia, K. Srairi, and M. E. H. Benbouzid, "A new rooted tree optimization algorithm for indirect power control of wind turbine based on a doubly-fed induction generator," ISA Trans., vol. 88, pp. 296–306, 2019.

[83] N. Bouchiba, A. Barkia, S. Sallem, L. Chrifi-Alaoui, S. Drid, and M. B. A. Kammoun, "Implementation and comparative study of control strategies for an isolated DFIG based WECS," Eur. Phys. J. Plus, vol. 132, no. 10, 2017.

[84] S. Mensou, A. Essadki, I. Minka, T. Nasser, B. B. Idrissi, and L. Ben Tarla, "Performance of a vector control for dfig driven by wind turbine: Real time simulation using DS1104 controller board," Int. J. Power Electron. Drive Syst., vol. 10, no. 2, pp. 1003–1013, 2019.

[85] S. Mensou, A. Essadki, T. Nasser, B. B. Idrissi, and L. Ben Tarla, "Dspace DS1104 implementation of a robust nonlinear controller applied for DFIG driven by wind turbine," Renew. Energy, vol. 147, pp. 1759–1771, 2020.

[86] S. Soued et al., "Experimental behaviour analysis for optimally controlled standalone DFIG system," IET Electr. Power Appl., vol. 13, no. 10, pp. 1462–1473, 2019.

[87] Y. Bekakra and D. Ben Attous, "Optimal tuning of PI controller using PSO optimization for indirect power control for DFIG based wind turbine with MPPT," Int. J. Syst. Assur. Eng. Manag., vol. 5, no. 3, pp. 219–229, 2014.

[88] F. Amrane, A. Chaiba, B. E. Babes, and S. Mekhilef, "Design and implementation of high performance field oriented control for grid-connected doubly fed induction generator via hysteresis rotor current controller," Rev. Roum. des Sci. Tech. Ser. Electrotech. Energ., vol. 61, no. 4, pp. 319–324, 2016.

[89] R. R. Behera and A. Thakur, "Finite-control-set predictive current control based real and reactive power control of grid-connected hybrid modular multilevel converter," Int. J. Power Electron. Drive Syst., vol. 9, no. 2, pp. 660–667, 2018.

[90] M. Chebaani, A. Goléa, M. T. Benchouia, and N. Goléa, "Sliding Mode Predictive Control of Induction Motor Fed by Five-Leg AC–DC–AC Converter with DC-Link Voltages Offset Compensation," J. Control. Autom. Electr. Syst., vol. 28, no. 5, pp. 597–611, 2017.

[91] S. Vazquez, J. Rodriguez, M. Rivera, L. G. Franquelo, and M. Norambuena, "Model Predictive Control for Power Converters and Drives: Advances and Trends," IEEE Trans. Ind. Electron., vol. 64, no. 2, pp. 935–947, 2017.

[92] R. R. Behera and A. Thakur, "Finite-control-set predictive current control based real and reactive power control of grid-connected hybrid modular multilevel converter," Int. J. Power Electron. Drive Syst., vol. 9, no. 2, pp. 660–667, 2018.

[93] H. Mesloub, M. T. Benchouia, A. Goléa, N. Goléa, and M. E. H. Benbouzid, "Predictive DTC schemes with PI regulator and particle swarm optimization for PMSM drive: comparative simulation and experimental study," Int. J. Adv. Manuf. Technol., vol. 86, no. 9–12, pp. 3123–3134, 2016.

[94] S. Chikha and K. Barra, "Predictive control of variable speed wind energy conversion system with multi objective criterions," Period. Polytech. Electr. Eng. Comput. Sci., vol. 60, no. 2, pp. 96–106, 2016.

[95] G. Abad, J. López, M. A. Rodríguez, L. Marroyo, and G. Iwanski, Doubly Fed Induction Machine: Modeling and Control for Wind Energy Generation. 2011.

[96] M. Ahmed, M. K. Metwaly, and N. Elkalashy, "Performance investigation of multi-level inverter for DFIG during grid autoreclosure operation," Int. J. Power Electron. Drive Syst., vol. 10, no. 1, p. 454, 2019.

[97] R. G. Kanojiya, "Method for Speed Control of DC Motor," Int. Conf. Adv. Eng. Sci. Manag., pp. 117–122, 2012.

[98] Mohammed Saci. Chabani, M. T. Benchouia, A. Golea, R. Boumaaraf. "Implementation of direct stator voltage control of stand-alone DFIGbased wind energy conversion system", 2017 5th International Conference on Electrical Engineering - Boumerdes (ICEE-B), 2017.

Appendix

Appendix

Real Time Implementation of the DFIG Control

A. 1. General description of the experimental setup:

The experimental setup of the induction machine electrical drives has been designed and constructed in order to check and validate the simulation results of the presented theory. The real-time control was conducted in the LGEB laboratory of Biskra/ Algeria which equipped by DSPACE 1104 board. The implementation ground of induction machine drive is shown in Fig. A. 1.
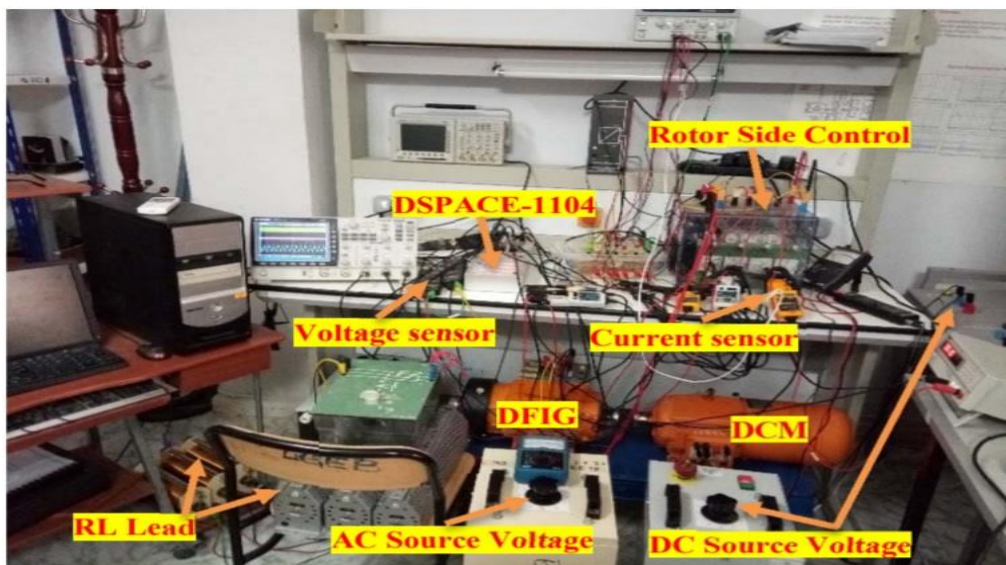

Fig. A.1. Presentation of the experimental setup.

The experimental setup is essentially composed of:
1. DFIG of 3 kW.
2. DC motor
3. Power electronics Semikron converter composed of a rectifier and an IGBT inverter.
4. Position and speed sensor (incremental encoder).
5. DSPACE DS 1104 signal card.
6. Control desk/Matlab/Simulink software plugged in personnel computer.
7. Magnetic powder brake with load control unit.
8. Current sensors.

9. Voltage sensors
10. RL load
11. DC source Voltage.
12. AC source Voltage
13. Numerical oscilloscopes.

A .2 Digital control implementation DSPACE 1104 controller and interface board

The DSPACE 1104 board is an input-output (I/O) interface between the power electronics and the software part which is MATLAB/Simulink/Control desk [Dsp12]. For each sampling period, the dS1104 receives the input signals from sensors (currents, voltages from ADC ports and speed from encoder through INC ports) and generates the digital control signals. These signals are provided by MATLAB/Simulink program with real-time interface (RTI), where the I/O ports of dS1104 are accessible in Simulink's library.

The DSPACE DS1104 controller board is shown in Figure A.5.2. The main processor of DS1104 is MPC8240 with PowerPC 603e core of 250 MHz. It has a memory of 32 Mbyte synchronous DRAM (SDRAM) and 8 MByte boot flash for applications.

Fig. A.2. DSPACE DS1104 Controller.

It is characterized by 8 analog-to-digital converters (ADCs) (4 in 16 bits, 4 in 12 bits), 8 digital-to- analog converters (DACs) with 16 bits which can deliver an analog voltage between −10V and +10V, a serial link, 2 incremental encoders, 20 digital inputs/outputs, a slave DSP (TMS320F240) and 3 independent 32-bit timers. The architecture of DS1104 is presented in Fig. A.3.
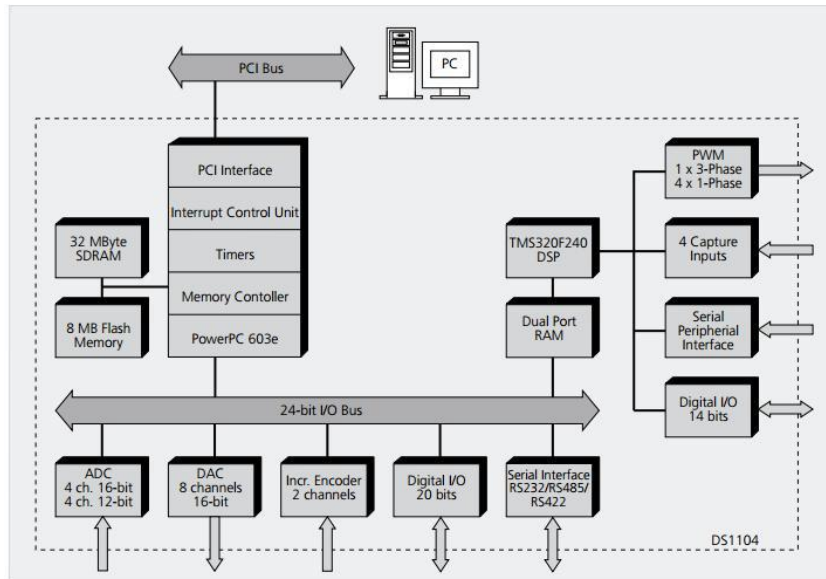
Fig. A.3. Architecture of DS1104.

The real-time interface of DSPACE 1104 board which linked to the power converter is shown in Fig A.4.
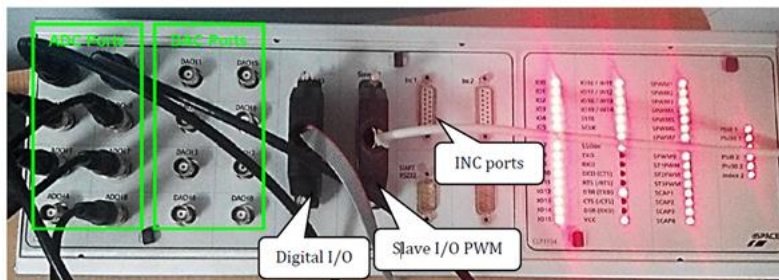

Fig. A.4. DSPACE 1104 interface board.

The execution of the program inside the DSP of dS1104 board converts it into a real time system on the hardware (DSPACE 1104 RTI) after it was in the software (Simulink). In addition, it gives us the access to adjust all Simulink variables in real time in order to obtain a satisfied control behavior. The sampling frequency of DSPACE 1104 can reach to 20 kHz. The suitable choice of sampling frequency has an apparent influence on quality of signals, especially the phase current and the produced electromagnetic torque.

Fig. A.5. shows a descriptive diagram of experimental setup and software/hardware linkage.

Table 2. DFIG main parameters

Parameters	value	unit
Nominal Power	3	kW
Stator Voltage	325.26	V
Stator frequency	50	Hz
Number of pairs poles	2	
Nominal speed	1450	rpm
Stator resistance	1.6000	Ω
Rotor resistance	2.6200	Ω
Stator inductance	0.1950	H
Rotor inductance	0.1950	H
Mutual inductance	0.1770	H

Table 3. PI regulator parameters for HCC.
Table 3. PI regulator parameters for FS-PCC.

K_p	K_i
0.07	
1.4	

K_p	K_i
0.07	
3.4	

Table 3. PI regulator parameters for DRFVC.

	k_p	k_i
Voltage regulator	0.2	3
Frequency regulator	2	120

Table 3. PI regulator parameters for DTC.

	k_p	k_i
Voltage regulator	0.02	0.5
Frequency regulator	2	120